PREPARATION AND CHARACTERIZATION OF RARE EARTH IONS-DOPED TiO_2 PHOTOCATALYST FILM BY RF-MAGNETRON SPUTTERING

Mr. Suthin Yuenyaw

A Thesis Submitted in Partial Fulfillment of the Requirements

for the Degree of Master of Science Program in Ceramic Technology

Department of Materials Science

Faculty of Science

Chulalongkorn University

Academic Year 2010

การเตรียมและลักษณะสมบัติของฟิล์มโฟโตคะตะลิสต์ไทเทเนียมไดออกไซด์ที่โดปแรร์เอิร์ทไอออนโดยอาร์เอฟแมกนีตรอนสปัตเตอริง

นาย สุทิน ยืนยาว

วิทยานิพนธ์นี้เป็นส่วนหนึ่งของการศึกษาตามหลักสูตรปริญญาวิทยาศาสตรมหาบัณฑิต
สาขาวิชาเทคโนโลยีเซรามิก ภาควิชาวัสดุศาสตร์
คณะวิทยาศาสตร์ จุฬาลงกรณ์มหาวิทยาลัย
ปีการศึกษา 2553

Thesis Title	PREPARATION AND CHARACTERIZATION OF RARE EARTH IONS-DOPED TiO_2PHOTOCATALYST FILM BY RF-MAGNETRON SPUTTERING
By	Mr. Suthin Yuenyaw
Field study	Ceramics Technology
Thesis Advisor	Assistant Professor Pornapa Sudjaridwarakun, D.Eng.
Thesis Co-Advisor	Professor Kazuya Saito, D.Sci.

Accepted by the Faculty of Science, Chulalongkorn University in Partial Fulfillment of the Requirements for the Master's Degree

……..Dean of the Faculty of Science
(Professor Supot Hannongbua, Dr.rer.nat.)

THESIS COMMITTEE

…… Chairman
(Assistant Professor Sirithun Jiemsirilers, Ph.D.)

…….. Thesis Advisor
(Assistant Professor Pornapa Sujaridworakun, D.Eng)

…… Thesis Co-Advisor
(Professor Kazuya Saito, D.Sci)

…… Examiner
(Assistant Professor Thanakorn Wasanapiarnpong, D.Eng)

…… External Examiner
(Siriporn Larpkiatthaworn, Ph.D.)

สุทิน ยืนยาว : การเตรียมและลักษณะสมบัติของฟิล์มโฟโตคะตะลิสต์ไทเทเนียมไดออกไซด์ที่โดปแรร์เอิร์ทไอออนโดยอาร์เอฟแมกนีตรอนสปัตเตอริง (PREPARATION AND CHARACTERIZATION OF RARE EARTH IONS-DOPED TiO_2 PHOTOCATALYST FILM BY RF-MAGNETRON SPUTTERING) อ. ที่ปรึกษาวิทยานิพนธ์หลัก: ผศ. ดร. พรนภา สุจริตวรกุล, อ. ที่ปรึกษาวิทยานิพนธ์ร่วม: Prof. Kazuya Saito, D. Sci, 92 หน้า.

งานวิจัยนี้ได้ทำการศึกษาการเตรียมและผลของการโดปด้วย Yb_2O_3 และ Er_2O_3 ต่อโครงสร้างจุลภาคพื้นผิว สมบัติทางแสง และสมบัติโฟโตคะตะลิสต์ภายใต้แสงยูวีและฟูลออเรสเซนต์ของฟิล์มบางที่เตรียมโดยวิธีอาร์เอฟแมกนีตรอนสปัตเตอริง การเตรียมฟิล์มถูกกำหนดโดยให้ แหล่งกำเนิดไฟฟ้า ระยะระหว่างเป้ากับซับสเตรต และอุณหภูมิของซับสเตรตคงที่ที่ 150 วัตต์ 5.0 เซนติเมตร และ 500 องศาเซลเซียส ตามลำดับ และในงานวิจัยนี้กำหนดให้ฟิล์มมีความหนาประมาณ 1.0 ไมโครเมตร จากผลการทดลองพบว่าฟิล์มไทเทเนียมไดออกไซด์ที่เตรียมได้เป็นเฟสอะนาเทสเพียงเฟสเดียว ผลของความดันในการสปัตเตอริง และสปัตเตอริงแก๊ส เป็นตัวแปรที่มีความสำคัญ ที่ส่งผลต่อการเกิดโครงสร้างของฟิล์ม ซึ่งฟิล์มที่เตรียมที่ความดันสูง (3 พาสคัล) ในบรรยากาศของแก๊สอาร์กอนอย่างเดียว ฟิล์มที่ได้มีความพรุนตัวและความขรุขระพื้นผิวสูงซึ่งส่งผลให้มีสมบัติโฟโตคะตะลิสต์ที่สูง ในขณะที่ฟิล์มที่เตรียมในบรรยากาศของแก๊สผสมระหว่างอาร์กอนกับออกซิเจน (Ar/O_2:8/2) มีความพรุนตัวและค่าความขรุขระพื้นผิวต่ำจึงส่งผลให้ประสิทธิภาพโฟโตคะตะลิสต์ต่ำเมื่อเทียบกับฟิล์มที่เตรียมภายใต้บรรยากาศแก๊สอาร์กอนอย่างเดียว ในกรณีของฟิล์มที่เตรียมด้วยการโดปด้วย Yb_2O_3 และ Er_2O_3 พบว่าฟิล์มที่ถูกเตรียมภายใต้แก๊สผสมระหว่างอาร์กอนกับออกซิเจน เมื่อปริมาณความเข้มข้นของ Yb_2O_3 และ Er_2O_3 ในเป้าเซรามิกเพิ่มขึ้นจาก 0.5 เป็น 1 เปอร์เซ็นต์โดยโมล ส่งผลทำให้ฟิล์มมีค่าความขรุขระพื้นผิวเพิ่มขึ้นและค่าการส่งผ่านของแสงลดลง นอกจากนี้ค่าการดูดกลืนแสงยังเลื่อนไปยังความยาวคลื่นที่สูงขึ้นทำให้ค่าแถบช่องว่างพลังงานลดลง และสมบัติโฟโตคะตะลิสต์มีค่าเพิ่มขึ้นภายใต้การฉายแสงยูวีและฟูลออเรสเซนต์ ในขณะที่ฟิล์มที่เตรียมภายใต้แก๊สอาร์กอนเพียงอย่างเดียวเมื่อมีการเพิ่มปริมาณการโดป ค่าการดูดกลืนแสงและแถบช่องว่างพลังงาน มีแนวโน้มเช่นเดียวกับฟิล์มที่เตรียมได้ภายใต้แก๊สผสม แต่ไม่ส่งผลต่อค่าความขรุขระพื้นผิวอย่างชัดเจน และยังให้สมบัติโฟโตคะตะลิสต์ที่ต่ำกว่าเมื่อเทียบกับฟิล์มที่เตรียมด้วยแก๊สผสมระหว่างอาร์กอนกับออกซิเจน

ภาควิชา วัสดุศาสตร์ ..... ลายมือชื่อนิสิต .....

สาขาวิชา เทคโนโลยีเซรามิก ..... ลายมือชื่อ อ.ที่ปรึกษาวิทยานิพนธ์หลัก .....

ปีการศึกษา 2553 ..... ลายมือชื่อ อ.ที่ปรึกษาวิทยานิพนธ์ร่วม .....

5172504323 : MAJOR CERAMIC TECHNOLOGY

KEYWORDS : TITANIUM DIOXIDE / RARE EARTH / PHOTOCATALYTIC/ RF-MAGNETRON SPUTTERING

SUTHIN YUENYAW: PREARATION AND CHARACTERIZATION OF RARE EARTH IONS-DOPED TiO_2 PHOTOCATALYST FILM BY RF MAGNETRON SPUTTERING. THESIS ADVISOR: ASST. PROF. PRONAPA SUDJARIDWARAKUN, D. Eng, THESIS CO-ADVISOR: PROF. KAZUYA SAITO, D. Sci, 92 pp.

This research studied on the preparation and the effect of Yb_2O_3 and Er_2O_3 doped TiO_2 on the surface morphology, optical and photocatalyst properties under UV and fluorescent irradiation of thin films via RF-magnetron sputtering method. The preparation conditions were fixed for applied power, distance between target-substrate and substrate heating temperature at 150 W, 5.0 cm and 500 ^{o}C, respectively. All deposited films were controlled the thickness at about 1.0 μm by varying deposition time. As the results, all of prepared films showed only pure anatase phase. The sputtering pressure and sputtering gas had significantly affected on the microstructure of TiO_2 film. The films prepared under high pressure (3 Pa) and pure Ar gas displayed porous structure and high surface roughness, resulted in high photocatalytic activity. While the TiO_2 films prepared under gas mixture Ar/O_2 (8/2) showed porous structure with lower surface roughness resulted in lower photocatalytic activity than that of film prepared under pure Ar gas. In case of TiO_2 films doping with Yb_2O_3 and Er_2O_3, the increasing in surface roughness and the decreasing in transmittance of the films prepared under gas mixture of Ar/O_2 (8/2) when concentration of Yb_2O_3 and Er_2O_3 target increased from 0.5 to 1.0 mol% was observed. Moreover, the absorption thresholds slightly shifted to longer wavelength which was attributed to the decreases in band gap energy. And higher photocatalytic activity under UV and Fluorescent irradiation was obtained. The similar result of absorption and band gap energy of the films prepared under pure Ar was also observed. But the difference in surface roughness was not significantly affected as the concentration of dopant increased. In addition, the doped films prepared under gas mixture had better photocatalytic activity than that of films prepared under pure Ar gas.

Department : Materials Science ..... Student's Signature .....

Field of Study : Ceramic Technology ..... Advisor's Signature .....

Academic Year : 2010 ..... Co-Advisor's Signature .....

ACKNOWLEDGEMENT

I would like to express my sincere appreciation to my thesis advisor, Asst. Prof. Dr. Pornapa sudjaridworakun and Prof. Dr. Kazuya Saito, my co-advisor for encouragement, in valuable support, including their kindness and guidance and to opportunity to pursue throughout my research freely. Their comments and suggestions not merely provide valuable knowledge but broaden perspective in practical applications as well.

Special gratitude goes to the chairman to the committee, Asst. Prof. Dr. Sirithun Jiemsirilers for providing invaluable advice and examining my final work. I would also like to thank other committee members, Dr.Siriporn Larbkiattaworn and Asst. Prof. Dr Thanakorn Wasanapiarnpong members of thesis committee for many valuable comments and their perceptive suggestions.

My sincerely thanks Dr. Edson H. Sekiya and Mr. Masaki Tada for the help with RF-magnetron sputtering process while living in Japan.

Thank you Prof. Masammichi Yoshimura, Mr.Matsuoka Yuki for FE-SEM, Mr. Seiya Suzuki for AFM characterization, Mr. Fukuzawa Jun for EPMA, Dr. Kojima Nobuaki for XPS and Miss Laksana Kreethawate for FE-SEM.

I would like to thanks Department of Materials Science, Faculty of Science, Chulalongkorn University and Frontier Materials Laboratory, Research Center for Advanced Photon Technology, Toyota Technological Institute, Japan for providing laboratory facilities and support.

Finally, I am eternally grateful to my beloved family for their forever support, love and encouragement throughout my life.

This research was supported by Center for Petroleum, Petrochemicals and Advance Materials, Chulalongkorn University, Japan Student Services Organization (JASSO) scholarship and Conference Grant for Master degree.

CONTENTS

Page

Page

Page

LIST OF TABLES

Page

LIST OF FIGURES

Page

Page

Page

Page

CHAPTER I

INTRODUCTIONS

1.1 Background and Motivations

In recently there is an increased awareness for the exhaustion of natural energy sources and severe environmental pollution problems. Semiconductor photocatalysis using sunlight to break down harmful organic pollutants is one of the promising approaches to solve these pollution problems. Up to date, research of photocatalyst materials has been focused on TiO_2 due to its high refractive index, high transparency in the visible and near-infrared wavelength region, high dielectric constant, very good wear resistance, low cost, chemical satiability, non- toxicity and good durability in hostile environmental. Thus have been widely used for many applications such as optical thin films device, anti-bacteria, self-cleaning, water purify [1]. However, a major drawback of TiO_2 photocatalyst is its large band gap value (ca.3.0, 3.2 eV for rutile and anatase, respectively), making it can only be excited by the light in UV range (λ<390 nm) which is only 4-5 % in the sunlight has the required energy to activate the catalyst [2]. In comparison to the other crystalline phase of TiO_2, such as rutile and brookite, the most photoactive phase of TiO_2 is anatase.

Generally, a good photocatalyst must process a large catalytic surface in which the size of the primary catalyst particles is related to the surface area available for the adsorption and decomposition of the organic pollutants. The high surface to bulk ratio of the ultrafine particles should favor the transfer of photogenerated charge carriers, and enhance the photocatalytic activity. For this reason, most of the studies were focused on the preparation of nanosized powder of the transition metal ions or rare earth ions doped TiO_2 photocatalyst. However, there are some drawbacks of the practical use of powder during the photocatalytic process: separation powder TiO_2 from water is difficult, and the suspended powder TiO_2 tends to aggregate especially at the high concentrations.

Therefore, the immobilize TiO_2 onto various supports in order to overcome these problems has been developed.

The thin films of titanium dioxide are prepared by several of deposition methods for examples, sol-gel, precipitation-dipping, chemical vapor deposition, evaporation, plasma sputtering depositions, ion beam-assisted process etc. It is known that the method of doping and preparing the film strongly determine the properties of the resulting catalyst films, thus many controversial results of doping transition metal into TiO_2 using different techniques were obtained in the literatures. Wet process as sol-gel has been widely performed at present, but their mechanical durability is less stable. Among those deposition techniques, RF-magnetron sputtering is suggested as the most promising technique because of it provides large area coating with good thickness uniformity, film quality, mechanical durability, and friendly environmental industrial process.

Many studies have been performed on the properties of TiO_2 films that are influenced by growth parameters such as substrate temperature, discharge voltage and oxygen partial pressure, etc [3-6]. It has been recently reported that impurity doping could improve the properties of composite thin films. For example, doping transition metal ions such as Fe^{3+}, Ru^{3+}, Os^{3+}, Re^{5+},Cr^{3+}, Ni^{2+} etc., in to the lattice of TiO_2 was reported to be the proficient way due to the fact that the overlap of the conduction band of Ti (d) of TiO_2 and the metal (d) orbital of the implanted metal ions can decrease the band gap of TiO_2 [7-8]. Some studies indicated that the photocatalytic activity of TiO_2 catalyst depends on adsorption behavior and the separation efficiency of electron-hole pairs. It was found that the photocatlytic activity of TiO_2 can be significantly enhanced by doping with lanthanide ions/oxides with 4f electron configurations for examples Ce^{3+}, as lanthanide ions have ability to form complexes with various Lewis bases including organic acid, amines, aldehydes, alcohols, and thiols by the interaction of the functional groups with their f-orbital [9-10]. Moreover, the formation of two sub-energy levels

(defect level and Ce 4f level) in Ce^{3+}-TiO_2 might be a key reason to eliminate the recombination of electron-hole pairs and to enhance the photocatalytic activity was proposed.

However, some ions such as Er and Yb which had attracted more attention in TiO_2-based optical materials, but less report had studied on their photocatalytic activity for degradation of organic pollutants [11].

In this work we focus on the study of effect of sputtering condition on the physical and photocatalytic activity of TiO_2 and Yb_2O_3/Er_2O_3 doped TiO_2 film.

1.2 The objective of this research

To study effects of deposition parameters and Yb_2O_3/Er_2O_3 doping on physical properties and photocatalytic activity of TiO_2 thin films prepared by RF-magnetron sputtering.

1.3 Expected results

Obtain the high efficiency UV and visible light responsible Yb_2O_3/Er_2O_3 doped photocatalyst films.

1.4 Thesis organization

This work is divided into 5 chapters as follow:

CHAPTER I presents the background and motivations.

CHAPTER II presents literature reviews of previous works related to this research.

CHAPTER III presents experimental procedure.

CHAPTER IV presents result and discussions.

CHAPTER V presents overall conclusions of this research and recommendations for future work.

CHAPTER II

LITERATURE REVIEW

2.1 Titanium dioxide

This section discusses properties and applications of titanium dioxide. These materials were employed to coat on silica glass substrates to be treated for photocatalytic activity.

2.1.1 Physical and Chemical properties[1,12-13]

Titanium dioxide may take on any of the following three crystal structure: anatase, which tends to be more stable at low temperature; brookite, which is usually found only minerals; and rutile, which tends to be more stable at higher temperatures and thus is sometimes found in igneous rock.

Anatase generally shows a higher photocatalytic activity then the other types of titanium dioxide. Comparison of same physical properties of rutile, anatase and brookite are shown in table 2.1.

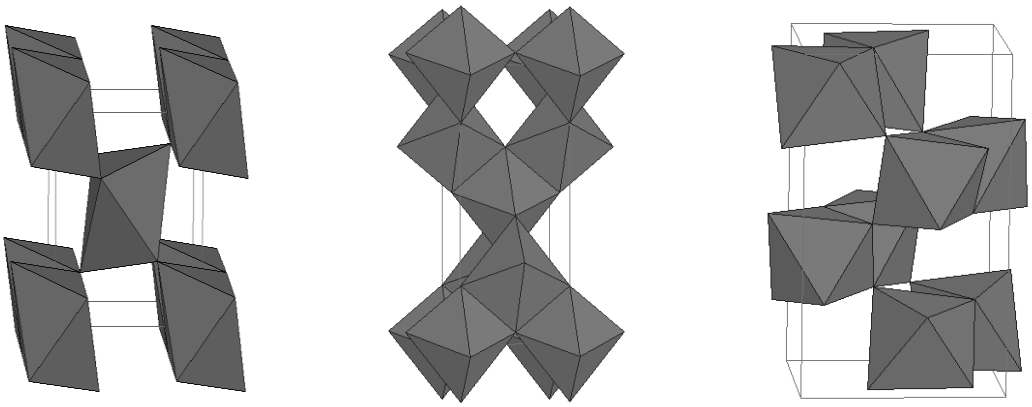

A B C

Figure 2.1 Structure of titanium dioxide anatase (A) rutile (B) and brookite (C)

Table 2.1 Comparision properties of anatase, brookite and rutile [1, 12,14]

Properties	Anatase	Rutile	Brookite
Crystal structure	Tetragonal system	Tetragonal system	Orthorhombic system
Optical	Uniaxial, negative	Uniaxial, negative	Biaxial, positive
Density, g/cm^3	3.9	4.23	4.0
Harness, Mohs scale	$5^{1/2}$-6	7-$7^{1/2}$	$5^{1/2}$-6
Dimension, nm			
a	0.3758	0.4584	0.9166
b	-	-	0.5436
c	0.9514	2.953	0.5135
Refractive index	2.52	2.52	-
Band gap energy	3.2	3.0	3.1
Permittivity	31	114	78
Melting point	Changes to rutile at high temperature	1858 ^{o}C	-

The reason that anatase is more photocatalytic active than rutile may lie in the differences in their so called energy band structure. The band gap energy of a semiconductor is the minimum energy of light required to make the material electrically conductive or in other words, to get the electrons excited enough to get moving. The band gap energy of anatase is 3.2 eV, which corresponds to UV light with wavelength of 388 nanometers, while the band gap energy for the rutile type is 3.0 eV which corresponding to UV light that has a wavelength of 413 nanometers [12,15]. The level of the conduction band for anatase is 0.2 eV higher than that for rutile. In more technical terminology, the band gap energy for a semiconductor indicates the minimum energy of light necessary to produce electrons in the conduction band (CB) and give rise to

electrical conductivity and hole, which are actually the absence of electrons, in the valence band (VB). These holes can react with water to produce the highly reactive hydroxyl radical (OH^-). Both holes and hydroxyl radicals can oxidize most organic materials.

The VB energies for both anatase and rutile are very low in the energy. Consequently, the VB holes (and the hydroxyl radicals) have great oxidizing power. The CB energy for rutile is close to the potential required to electrolytically reduce water to hydrogen gas, but that for anatase is higher in the energy, meaning that it has higher reducing power. Therefore, anatase can drive the very important reaction involving the electrolytic reduction of molecular oxygen (O_2) to superoxide (O_2^-)

Although anatase and rutile are both tetragonal, they don't have the same crystal structures. Anatase exists in near-regular octahedral and rutile forms slend prismatic crystal. Rutile is the thermally stable form and is one of the two most important ores of titanium.

The three forms of titanium (IV) oxide have been prepared in laboratories but only rutile, the thermally stable form, has been obtained in the form of transparent large single crystal. The transformation from anatase to rutile is accompanied by the evolution of ca 12.6 kJ/mol (3.01 kcal/mol), but the rate of transformation is greatly affected by temperature and by the presence of other substance which may either catalyze or inhibit the reaction. The lowest temperature at which conversion of anatase to rutile take place at a measurable rate is around 700 $^{\circ}C$, but this is not a transition temperature. The change is not reversible since ΔG for the change from anatase to rutile is away negative.

Brookite has been produced by heating amorphous titanium (IV) oxide, which is prepared from and alkyl titanate or sodium titanate, with sodium or potassium hydroxide in and autocave at 200 to 600 $^{\circ}C$ for several days. The important commercial forms of titanium (IV) oxide are anatase and rutile, and they can readily be distinguished by X-ray diffraction spectrometry.

Since both anatase and rutile are tetragonal, they are both anisotropic, and their physical properties, e.g. refractive index, very according to the direction relative to the crystal axes. In the most applications of these substances, the distinction between crystallographic directions is lost because of the random orientation of large number of small particles, and only average values of the properties are significant.

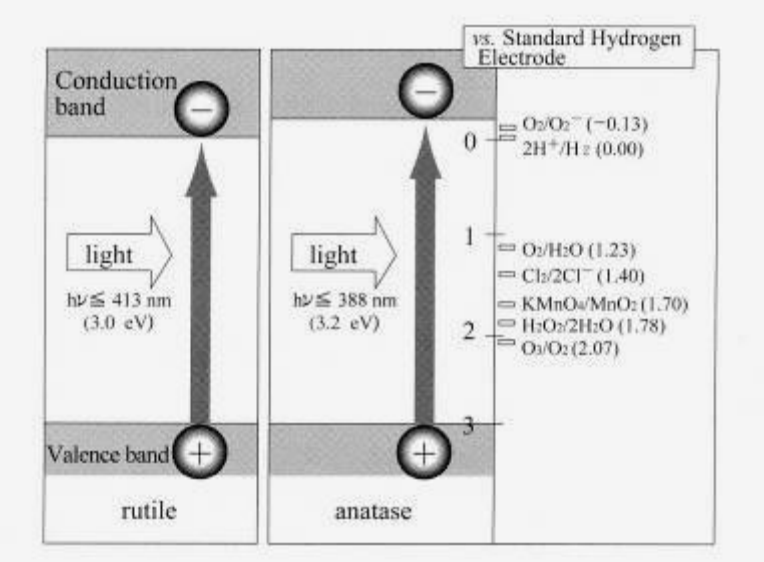

Figure 2.2 Show relationship between energy diagram of TiO_2 and redox potentials [12,16].

2.1.2 The photocatalytic process[12,17]

Photocatalyst process is discovered by Fujishima in 1972 year ago, which is using electrode together with light for reducing water for purpose hydrogen and oxygen molecular, that process of oxidations (Advanced Oxidation Technologies, AOTs).

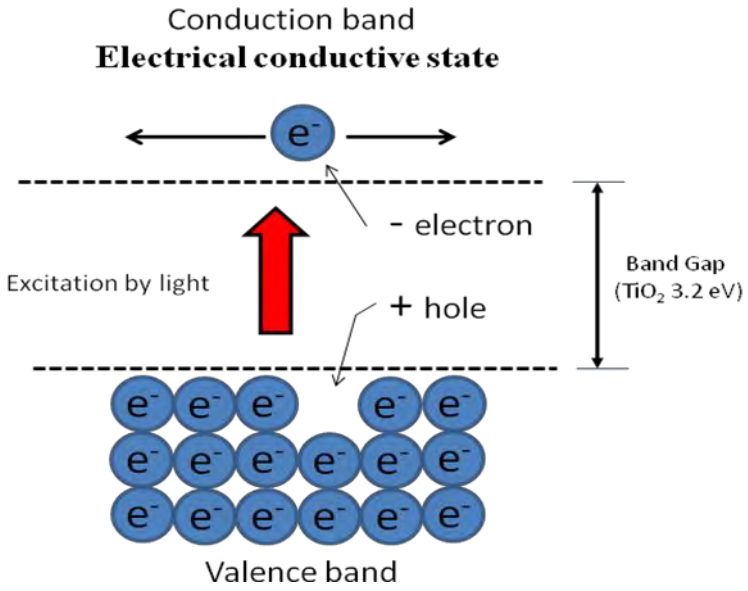

Figure 2.3 Process at titanium dioxide surface of semiconductor when it had activated by UV light [18].

The photocatalyst process is the systems supported by photon energy, which was affected to reaction. The photon energy (E) can be calculated from Equation 2.1[12].

$$E = h\nu = \frac{hc}{\lambda} \qquad \text{(Equation 2.1)}$$

When: E is photon energy, eV

h is Planck's Constant = 6.625×10^{-34} , Js

ν is frequency , s^{-1}

λ is wavelength , nm

c is light velocity $c=2.997X10^{8}$ m/s

Therefore, basic of photocatalyst process is electron moved from valance band (VB) to conduction band (CB) of semiconductor and holes in the valence band. These can be excited by ultraviolet light source (band gap energy = 3.0, 3.2 eV for rutile and

anatase, respectively). Then a reaction of photocatalytic of semiconductor is both electron hole pair (e^- -h^+) shown in Equation 2.2.

$$TiO_2 \text{ (semiconductor)} + h\nu \longrightarrow TiO_2 (e_{cb}^- + h_{vb}^+) \quad \text{(Equeation 2.2)}$$

Hole (h^+) can be reacted with water (H_2O) and hydroxyl group (OH^-) converting into hydroxyl radical ($OH^\bullet$) show in Equation 2.3-2.4.

$$h_{vb}^+ + H_2O \longrightarrow OH^\bullet + H^+ \quad \text{(Equation 2.3)}$$

$$h_{vb}^+ + OH^- \longrightarrow OH^\bullet \quad \text{(Equation 2.4)}$$

Electron (e^-) can be reacted with oxygen (O_2) to create super oxide anion (O_2^-) it was changed to hydrogenperoxide when it reacts with water. Then hydrogen peroxide can be changed to super hydroxyl radical. (Equation 2.5-2.7)

$$e_{cb}^- + O_2 \longrightarrow O_2^- \quad \text{(Equation 2.5)}$$

$$O_2^- + 2H_2O \longrightarrow 2H_2O_2 \quad \text{(Equation 2.6)}$$

$$H_2O_2 \longrightarrow 2OH^- \quad \text{(Equation 2.7)}$$

But electron and hole can be recombined without the electron donor or the electron accepter is shown in Equation 2.8.

$$e_{cb}^- + h_{vb}^+ \longrightarrow TiO_2 + \text{heat} \quad \text{(Equation 2.8)}$$

Therefore, photocatalyst process was occurring on the surface of semiconductor. The titanium dioxide was absorbed photons in UV light, these energy greater than or equal to energy band gap ($h\nu \geq E_{bg}$) that the overall process as shown in fig 2.4.

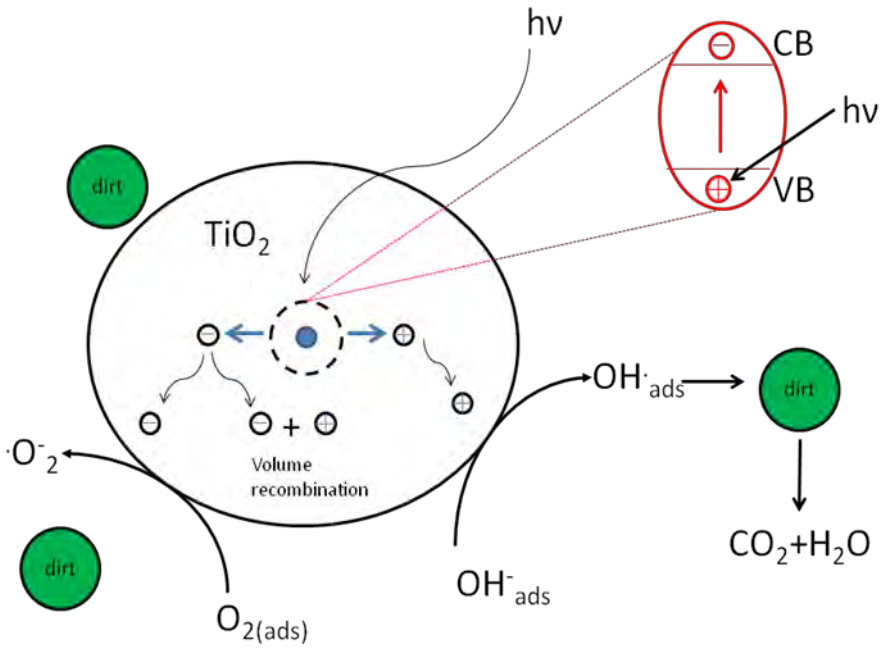

Figure 2.4 Schematic of the photocatalytic process [8]

The photocatalysis process is dependent on the two ability of the catalyst to adsorb both pollutants on the surfaces and absorb light with an appropriate wavelength. Various type of semiconductor (Table 2.2), such as TiO_2, ZnO, CdS, WO_3, ZnS, $SrTiO_3$, CdSe, $BaTiO_3$ and Fe_2O_3, has been used as the catalysts in photocatalysis process. From the available semiconductor, ZnO is generally unstable with respect to inconsistent dissolution yielding $Zn(OH)_2$ on the ZnO particle surface, and WO_3, although useful in the visible range, is less photocatalytically active than TiO_2. It has been indicated that TiO_2 is the most useful material due to its interesting qualities of high stability, high photocatalytic activity, non-toxicity and inexpensive.

Form Table 2.2 and fig 2.5 show band gap energy of semiconductor, which were excited in difference wavelength. At wavelength less than 390 nm, it has enough to create a strong oxidant hydroxide mineral for TiO_2.

Table 2.2 Band gap energy of semiconductors [19]

Semiconductor	Band gap energy (eV)	Wavelength (nm)
TiO_2 (anatase)	3.2	390
TiO_2 (rutile)	3.0	413
WO_3	2.8	443
$SrTiO_3$	3.4	365
Fe_2O_3	2.2	565
ZnO	3.2	390
ZnS	3.7	336
CdSe	1.7	730
CdS	2.5	497
$BaTiO_3$	3.3	375

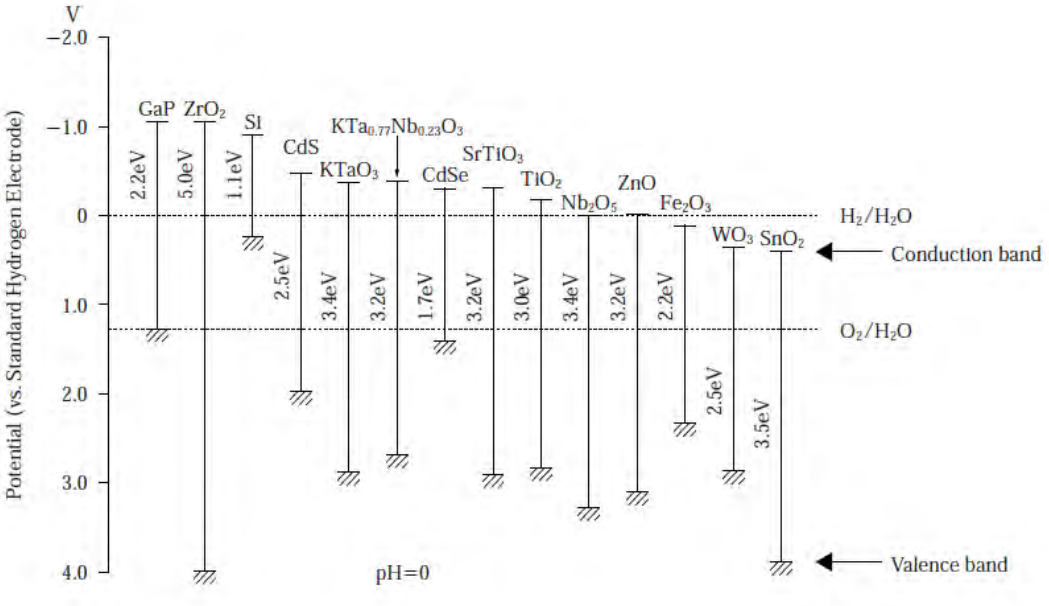

Figure 2.5 Band gap energy of semiconductors [12, 20]

2.2 Applications of titanium dioxide

Titanium dioxide is one of the most basic materials in our daily life. Titanium dioxide has been widely used in a variety of paints, plastics, paper, inks, fiber, cosmetics, sunscreens and foodstuffs because titanium dioxide has been known as a material with a high refractive index, high transparency in the visible and near-infrared wavelength region, high dielectric constant, very good wear resistance, low cost, chemical satiability and non-toxicity. Naturally, the type of titanium dioxide that is used as a pigment is different from that used as a photocatalyst. The photocatalytic technology is becoming more and more attractive to industries today because environmental pollution has been recognized as a serious problem that needs to be addressed immediately. Various applications in which research and development activities involving titanium dioxide have been investigated see in the table 2.3.

Table 2.3 Application of Titanium dioxide photocatalytic [1,12,14]

Properties	Applications
Self-cleaning	1. Exterior tiles, kitchen and bathroom components, interior furnishings, plastic surfaces, aluminum siding, building stone and curtains, paper window blinds. 2. Translucent paper for indoor lamp covers, coatings on fluorescent lamps and highway tunnel lamp cover glass. 3. Tunnel wall, soundproofed wall, traffic signs and reflectors. 4. Tent material, cloth for hospital garments and uniforms and spray coatings for cars.
Air cleaning	1. Room air cleaner, photocatalyst-equipped air conditioners and interior air cleaner for factories. 2. Concrete for highways, roadways and footpaths, tunnel walls, soundproof walls and building walls.
Water purification	1. River water, ground water, lakes and water-storage tanks. 2.Fish feeding tanks, drainage water and industrial wastewater
Antitumor activity	Cancer therapy, Endoscopic-like instruments.
Self-sterilizing	1. Tiles to cover the floor and walls of operating rooms, silicone rubber for medical catheters and hospital garments and uniforms. 2. Public rest rooms, bathrooms and rat breeding rooms.

2.3 Magnetron sputtering system

Thin films are the subject of matter for many applications and have got significant importance in physical sciences and engineering. A number of methods and techniques are used to deposit thin films. Sputtering is one important technique used for thin films deposition. Sputter deposition is a physical vapor deposition process for depositing thin films, sputtering means ejecting material from a target and depositing it on a substrate such as a Quartz glass and silicon wafer.

Sputtering is extensively used in the semiconductor industry to deposit thin films of various materials in integrated circuits processing. Thin anti-reflection coatings on glass, which are useful for optical applications are also deposited by sputtering. Because of the low substrate temperatures were used, sputtering is an ideal method to deposit contact metals for thin film transistors. This technique is also used to fabricate thin film sensors, photovoltaic thin films (solar cells), metal cantilevers and interconnects etc.

Anelva Corp L-332S-FS sputtering system, shown in fig 2.9 is equipped with three 3-inch diameter planar magnetron cathode to facilitate multi layer with target shutter and pre-sputtering shutter and with a rotatable substrate holder shown in fig 2.10. The substrate can be heated up to 800 ^{o}C (maximum of Anelva Corp L-332S-FS sputtering system can be used) to improve the film adhesion to the substrate. Magnetron sputtering can be done either in DC or RF modes.

2.3.1 Direct current (DC) sputtering mode

The dc sputtering is a basic sputtering technique using a DC power supply. This technique is only applicable to deposit conductive materials. The schematic of this system is shown in fig 2.6.

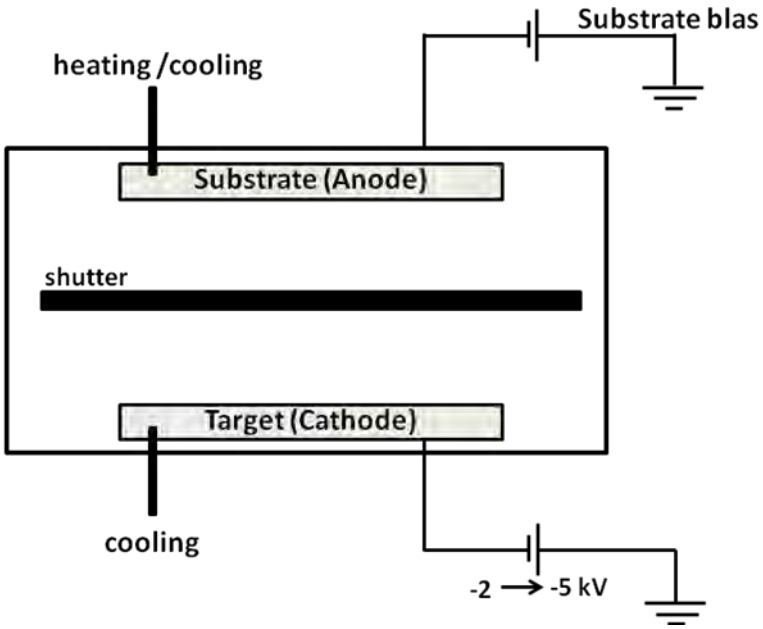

Figure 2.6 Schematic of DC sputtering [21]

Advantages of DC sputtering.

1. DC sputtering is done with conducting materials.
2. If target is non-conducting material, the positive charge will built up on target material and stops sputtering

2.3.2 Radio frequency (RF) sputtering mode

RF sputtering technique can be used to deposit both conductive and non-conductive films. The schematic of RF sputtering is given in fig 2.7.

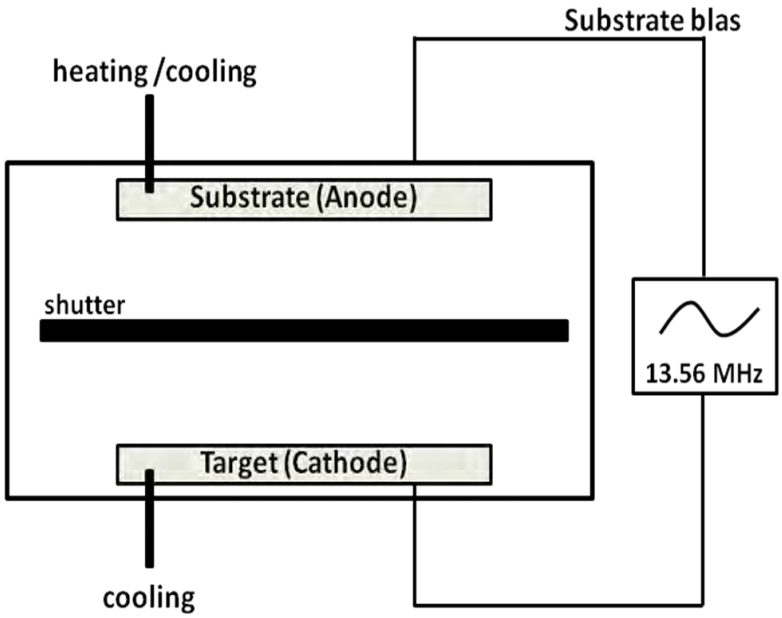

Figure 2.7 Schematic of RF sputtering [21]

Advantages of RF sputtering.

1. Both conducting and non-conducting materials can be sputtered.
2. Higher sputter rate at lower pressure.

The deposition of thin films by sputtering involves the acceleration of positive ions in many cases form gaseous (inert gas) plasma to bombard a target material that is negatively biased. Sputtering starts when a negative charge is applied to the target material causing a plasma or glow discharge. Positive charged gas ions generated in the plasma region are attracted to the negatively biased target plate at a very high speed. The commonly radio frequency (RF) electromagnetic radiations are used. This collision creates a momentum transfer and ejects atomic size particles from the target. These particles are deposited as a thin film into the surface of the substrates [22].

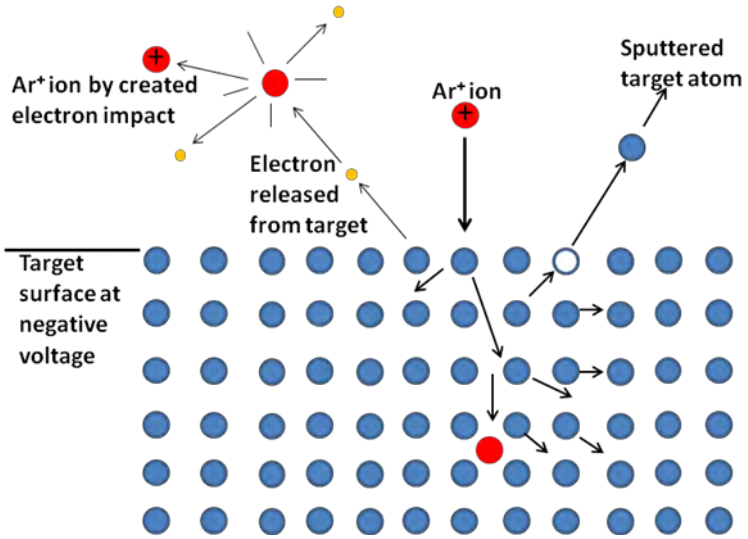

Figure 2.8 Show mechanism of sputtering process [23]

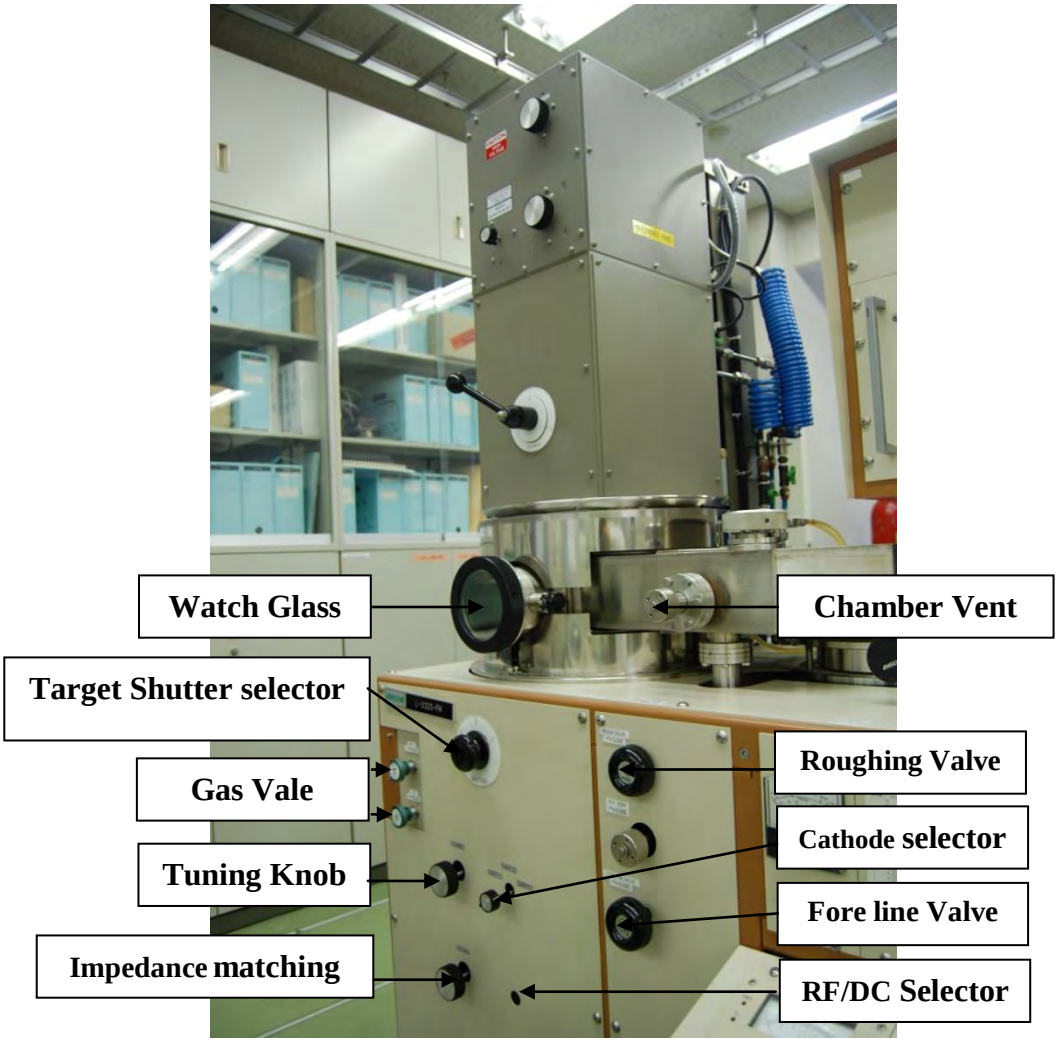

Figure 2.9 Schematic of L-332S-FS, Anelva Corp sputtering system

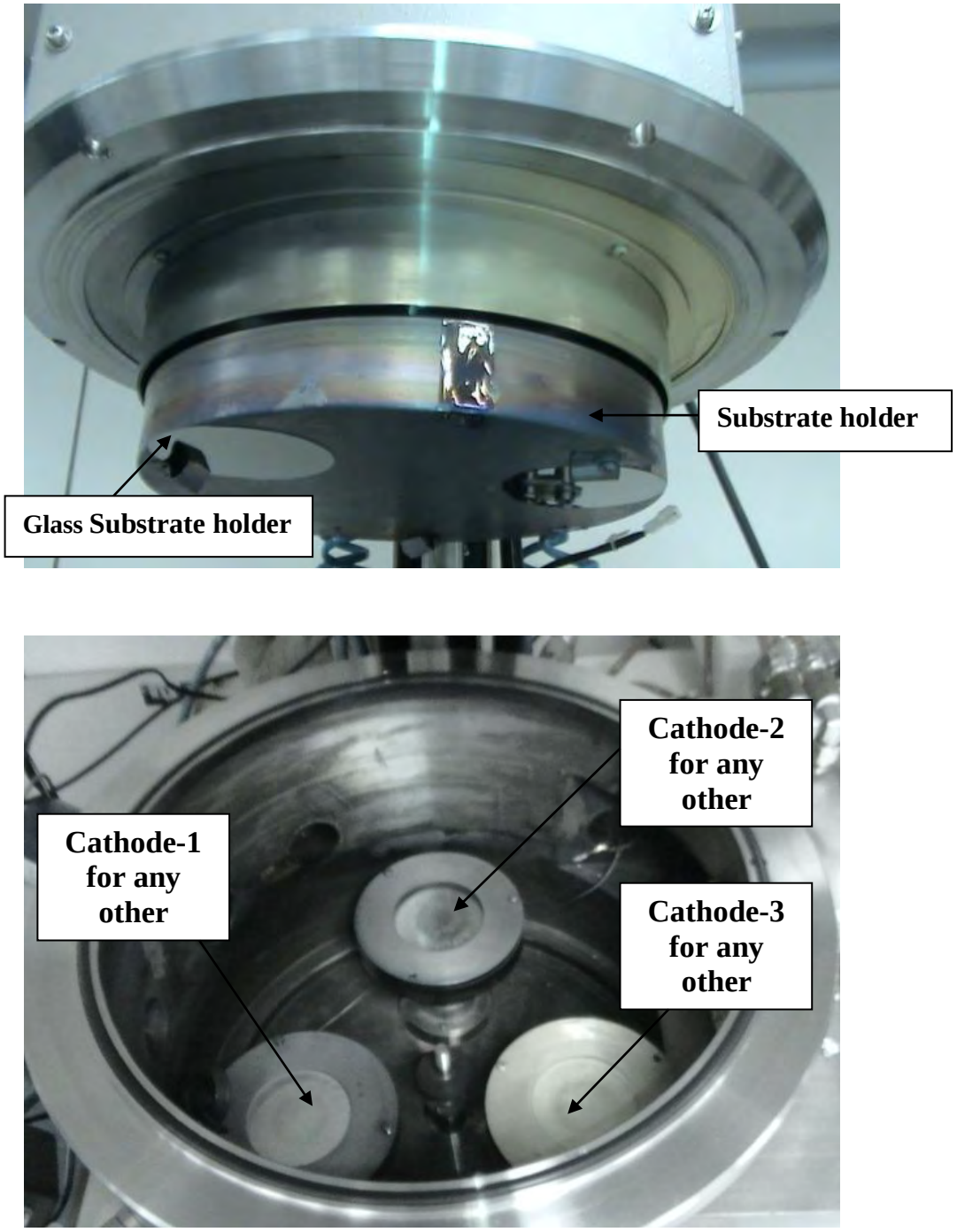

Figure 2.10 Top and side views of L-332S-FS, Anelva Corp sputtering chamber system

Advantages of magnetron sputtering

1. The magnets are used to increase the percentage of electrons that take part in ionization events, increase probability of electrons striking Argon, increase electron path length, so the ionization efficiency is increased significantly.

2. Other reasons to use magnets:

    2.1 Lower voltage needed to strike plasma.

    2.2 Controls uniformity.

    2.3 Reduce wafer heating from electron bombardment.

3. Increased deposition rate

2.4 Parameter in the sputtering system

2.4.1 Target Materials

Ceramic is a generally multi-component solid that is chemically bonding by ionic or covalent bonding such that there is no free electron. Therefore, the electrical conductivity and thermal conductivity are low and the material is brittle.

The purity of the sputtering target material should be as high as is needed to achieve the desired purity in the deposited material, but not any higher, since the price of the target generally goes up rapidly with purity. In many cases, the supplier does not specify some impurities such as oxygen in the form of oxides, hydrogen such as are found in chromium, etc. The target purity and allowable impurities should be specified in the initial purchase of the target material. As a minimum, there should be a purity certification from the supplier.

2.4.2 Substrate Temperature

Substrate temperature is an important for controlling phase structure and morphology of the film. The crystallinity and dense of films can be improved by increasing the substrate temperature. Moreover, the temperature of substrate substantially affects the atom mobility and the rate of chemical reaction on the substrate.

2.4.3 Total sputtering pressure

The properties of sputter-deposited films can be very dependent on the gas pressure. At low pressure, there is less gas molecule collision taking place. Moreover, gas molecules can directly get though the surface of film on substrate. On the other hand, at high pressure, there are collision can slow down the gas movement and also reduce the energy of the gas molecules, which affect the deposition rate and properties of the films.

2.4.4 Gas flow rate

In reactive sputter deposition the gas flow is an important processing variable and in the non-reactive deposition, gas flow is important in clean contaminants from the processing chamber. Generally, Argon (Ar) gas is usually option of sputtering because of Ar gas can be injected at high flow rate in order to generate plasma.

2.4.5 RF power

The ion bombardment energy and the discharge current strongly depend on rf power. As a result, the sputter rate strongly depends on the rf power. The sputtering yield is proportional to the ion bombardment energy. Therefore, the sputter rate increases with increasing rf power.

2.4.6 Reactive sputtering

When a reactive gas is intentionally included to the sputtering system then the sputtering process is call reactive sputtering. Argon is used as reactive gas in the present work. Reactive gas in the sputter atmosphere enables one to alter or control the properties of the deposit. Depending on the pressure of the reactive gas, a reaction may occur during the deposition of the films either at the cathode or at the surface. In most cases, the composition of the film may be altered by simply varying the quantity of reactive gas or the proportion of reactive to inert gases in the discharge.

2.5 Rare earth type of lanthanide [10]

Rare earth ions also referred to as lanthanides group; show an important role in modern technology as the active component of many optical materials. In the lanthanides it is the 4f electrons that account for the magnetism. As in the iron-group 3d electrons, a significant number of them can have unpaired spins, with a resultant atomic magnetic moment. In neutral rare earth atoms the number of 4f electrons ranges from 0

(La) to 14 (Yb and Lu), and the number of unpaired spins can be as large as 7. Specific applications may use the rare earths' atomic-like $4f^N$ to $4f^{N-1}$ optical transitions when long lifetimes, sharp absorption lines, and excellent coherence properties are required, while others may employ the $4f^N$ to $4f^{N-1}5d$ transitions when large oscillator strengths, broad absorption bands, and shorter lifetimes are desirable. The lanthanides always form trivalent ions by discarding their two 6s electrons and one 4f electron. The remaining 4f electrons are shielded from intracrystalline electric fields by a dense cloud of 5s and 5p electrons, so that, unlike the iron-group elements, their orbital moments are not quenched. Thus both spin and orbital components are significant in rare earth magnetism, and the behavior of these elements in compounds more closely resembles that of free ions than is the case with iron.

2.6 Literature review of TiO_2 and rare-earth doped TiO_2

S. Takabayashi *et al* [24] (2002) studied effects of total and oxygen partial pressure on structure of photocatalytic TiO_2 films deposited by reactive rf magnetron sputtering on glass substrates under with and without additional external heating. The results showed that the crystalline anatase, anatase/rutile or rutile films can be successfully deposited on unheated substrate and their formation is dependent on the total pressure and the oxygen partial pressure. A schematic phase diagram was constructed. The surface morphology is strongly influenced by the total pressure, the anatase TiO_2 films with a more open surface, a higher surface roughness and a larger surface area are formed at higher total pressures. The anatase films with such surface morphology deposited in the reactive sputtering mode exhibit the best photocatalytic activity.

M. Yamagishi *et al* [25] (2003) studied TiO_2 films deposited by RF reactive magnetron sputtering on non-alkali glass at 200 ^{o}C under total pressure of 0.3, 1.0 and 3 Pa with Argon and Oxygen ratio. The TiO_2 films with high photocatalytic activities and

photoinduced hydrophilicity were successfully deposited by reactive rf magnetron sputtering at p_{tot} as high as 3.0 Pa. The film was confirmed to be anatase polycrystalline with characteristic substructures. The photocatalytic activity showed the clear tendency to decrease with the decrease in *p*tot during the deposition. Such dependence of the photocatalytic activity on p_{tot} was correlated with the transport processes of the high-energy particles of Ar^0 or O^- between the target and the substrate. TiO_2 films deposited at the lower p_{tot} of 0.3 or 1.0 Pa, showed poor photocatalytic activities because of the defect level generation caused by the bombardment of the high-energy particles on the growing film surface.

P. Zemen *et al* [26] (2003) studied of nano scaled photocatalytic TiO_2 thin films prepared by reactive RF magnetron sputtering using PVD method deposited on glass substrate. They were found that the photocatalytic activity increases with increasing films thickness only if the films are prepared at higher sputtering pressure. Moreover, 65 nm thicknesses of TiO_2 films were deposited on rotating substrate and the relationship between the deposition parameters, such as the substrate temperature and the total pressure, the structure and the photocatalytic activity was studied. These thin films showed a very good photocatalytic activity when an appropriate substrate temperature (>100 ^{o}C) and/or total pressure (>1Pa) are selected.

K. Takamura *et al* [27] (2004) studied effect of oxygen flow ratio on the oxidation of Ti target and the formation process of TiO_2 films by RF reactive sputtering. The TiO_2 films were found to be formed at oxygen flow ratios above 7%. At the critical O_2 flow ratio, the amount of supplied Ti atoms was found to agree with that of O_2 molecules. Above the critical O_2 flow ratios, the amount of sopplied O_2 molecules exceeded the getting effect of the sputtering Ti atoms and oxygen density in the plasma began to increase.

In recently, metals and rare earth ions doped TiO_2 have been widely studied in order to improve the photocatalytic activity of TiO_2 films.

S.C. Kim *et al* [28] (2005) studied on the photocatalytic activity of Pd-doped TiO_2 films prepared by RF magnetron co-sputtering method. They were found that the crystallite sizes of Pd/TiO_2 thin films were slightly larger than those of the TiO_2 thin films. The secondary particle sizes of Pd/TiO_2 thin films at 600 ^{o}C were about 20 – 60 nm, and the secondary particles were more uniform and less agglomerated. The deposited films calcined at 300 – 600 ^{o}C had high transparency in the visible range. The transmittances of the films calcined at 900 ^{o}C were significantly reduced in the wavelength range of 300 – 800 nm due to the absorption and the scattering of light resulting from agglomerates of the primary particles. The Pd/TiO_2 thin films showed better photocatalytic activity than the TiO_2 thin films.

F Meng *et al* [29] (2009) studied on photocatalytic activity of Ag nanoparticles modified TiO_2 films by RF magnetron sputtering. It was found that silver content influences microstructure of TiO_2 thin films, and silver in the films is metallic Ag (Ag^0). Photocatalytic activity of the films increases with increasing silver content up to 5 vol.% Ag, and then decreases to values significantly still bigger than that of pure TiO_2 thin films. Silver nanoparticles significantly enhance the photocatalytic activity of TiO_2 films. The better separation between electrons and holes on silver modified TiO_2 thin films surface allowed more efficiency for the oxidation and reduction reactions. The enhanced photocatalytic activity was mainly attributed to the decrease of energy gap of the films and the increase of oxygen anion radicals O_2^- and reactive center of surface Ti^{3+} on silver modified TiO_2 thin films surface.

A.D. Paola *et al* [30] (2010) studied on pure and Sm-loaded brookite nanoparticles and thin films were prepared using $TiCl_4$ as precursor of TiO_2. At the results of Sm loading, significant improvement of the photocatalytic of brookite and beneficial effect was attributed to an increased separation efficiency of the photogenerated electron-hole pares. The content of Sm was an important factor affecting the photocatalytic activity. The optimum amount of Sm was 1% for the powders

and 0.1% for the films. There is a relationship between PL spectra and photocatalytic, namely, the lower the PL intensity the higher the photocatalytic activity.

V. Stengl *et al* [31] (2009) studied on rare earth doped TiO_2 nanopaticles prepared by a one-step, a one-pot, no post-synthesis calcinations and no sol-gel synthesis. As a results, the rare earth (La, Ce, Pr, Nd, Sm, Eu, Dy, Gd) for doped titanium were used, the best photocatalytic properties in visible light have samples doped with Nd^{3+} ions ($k=0.0272\ min^{-1}$ for UV and $0.0143\ min^{-1}$ for visible light)

W. Chen *et al* [32] (2006) studied on the photocatalytic activity enhancing for TiO_2 photocatalyst by doping with La by sol-gel method. The results show that the crystallinity of anatase is improved by La doping. Moreover, La not only suppresses phase transition from anatase to rutile but also exhibits an absorption in the $\lambda \geq$ 400 nm rage. The photocatalytic activity of La-doped TiO_2 photocatalysts excessds that of pure TiO_2 photocatalyst prepared by the same method when the molar ratio of La to Ti is kept at 0.3 %.

Thus, numerous studies had paid their attention on doping TiO_2 with various rare earth ions. Some ions such as Er^{3+} and Yb^{3+} which had attracted more attention in TiO_2-based optical materials, but less report had studied on their photocatalytic activity for degradation of organic pollutants via RF magnetron sputtering technique.

H.Q. Jiang *et al* [33] (2006) studied of the nanoparticles of Yb^{3+}-doped (0.125 wt %) and pure TiO_2 were prepared by an acid catalyzed sol-gel method. The results showed that the photocatalytic activity of Yb^{3+}/TiO_2 composite nanoparticles is much higher than that of pure TiO_2. A low amount of Yb^{3+} in TiO_2 can inhibit the anatase-rutile phase transformation of TiO_2, prevent grain growth, increasing the specific surface area, and favor the high temperature stabilization of the pores. According to the surface voltage spectroscopy data, Yb^{3+}-doping prevents recombination of photoinduced electrons and holes and improves the light absorption capacity of the particle surface.

M. Pal *et al* [34] (2008) studied on topic of synthesis and photocatalytic activity of Yb doped TiO_2 nanoparticles under visible light which were prepared by hydrolysis method. Average size of the nanoparticles was found to decrease with the increase of Yb doping concentration. The photocatalytic activity of Yb doped TiO_2 was evaluated by measuring the degration rates of methylene blue (MB) under UV and Visible lights. Doping with ytterbium ion enhanced significantly the photocatalytic activity of TiO_2 nanoparticles for MB oxidation under visible light.

C.H. Liang *et al* [10] (2008) studied on rare earth ions doped TiO_2 (RE^{3+}-doped TiO_2) catalyst prepared by the sol-gel method. They were found that the absorption equilibrium constant and the saturated adsorption amount of RE^{3+}-TiO_2 would increase with the increase of dosage. The photocatalytic activity of RE^{3+}-TiO_2 for Orange I degradation under both UV and visible light irradiations were higher than that of TiO_2. The optimal dosage was 1.5% for Orange I degradation under UV light and 1.0% under visible light. They were suggested that the higher photocatalytic activity effect of the transitions (4f electrons of RE^{3+}).

Y. Yang *et al* [35] (2010) studied on TiO_2 nanofibrous films with variable amounts of erbium were prepared by electrospinning technique. The results demonstrated that the doping of erbium inhibited the phase transformation and the crystallite growth of TiO_2. The doped samples were more efficient for degradation of methylene blue than TiO_2, and an optimal dosage of erbium at 0.5 mol% activated at 773 K achieved the highest degradation rate. The higher photoactivity might be attributable to the transition of 4f electrons of erbium, particle size, phase composition and the increase of the separating rate of photogenerated charges by erbium doping.

CHAPTER III

EXPERIMENTAL PROCEDURE

3.1 Preparation of TiO_2 and Yb_2O_3/Er_2O_3-doped TiO_2 thin film

Radio-frequency magnetron sputtering system (L-332S-FS, Anelva Corp) was used to produce thin films in this work. TiO_2, TiO_2-Yb_2O_3 (0.5-1mol%) or TiO_2-Er_2O_3(0.5-1mol%) (Toshima Manufacturing Co, Ltd.) ceramic disc with a 76.2 mm in diameter and 5 mm thickness was used as a sputtering target. The vacuum chamber was evacuated to a pressure lower than 10^{-4} Pa before the film deposition in order to avoid the contaminations. All samples were sputtered in a mixture of high purified Argon and Oxygen gas at ratio of 8/2 and 10/0 on a pre-cleaned silica glass substrate (ED-H; Tosoh Quartz Inc.). Deposited films were produced at a constant substrate-to-target distance at 50 cm, and the substrate was heated at temperature 500°C during deposition without further annealing after sputtering. In order to study the effect of deposition condition, applied powers were fixed at 150W. The sputtering conditions for deposition thin films were shown in table 3.1. After that, the crystalline structure of the deposited films was characterized by X-ray diffraction (XRD with Mo radiation: λ = 0.7093 nm). A typical thickness of films was controlled at approximately 1.0-1.2 μm measured by Dektak3 ST. The optical properties of produced films were investigated by UV-Vis spectrophotometer (Lambda 950). FE-SEM (Hitachi S-4700) was used to study the morphology of deposited films. Surface morphology and roughness was investigated by SPM. Photocatalytic activity of sputtered films, 20x20x2 mm in size, was evaluated through the degradation of methylene blue solution with initial concentration of $5x10^{-3}$ mM under UV (Toshiba FL10BLB-A) and white light (Fluorescent lamp FSL T8 10W) irradiation.

Table 3.1 Sputtering conditions for deposition thin films.

Deposition Parameters	conditions
Target-to-substrate distance (cm)	5
Base pressure (Pa)	$<10^{-4}$
Applied power (W)	150
Ar/O_2 ratios (sccm)	8/2, 10/0
Total sputtering pressures (Pa)	0.5, 1, 3
Substrate heating temperatures (^{o}C)	500
Times (min)	60-240
Film thickness (μm)	~1.0

3.2 Characterizations of sputtered thin films

3.2.1 X-ray diffraction (XRD)

Phase structure of deposited films were characterized by XRD using Mo-K_α (λ = 0.7093 nm) source with 40 kV, 25 mA. Scanning rate is 0.2 degree/min from 2θ at 5 to 50 degree. The obtained peaks were matched with JCPDS (Joint Committee on Powder Diffraction Standard file) No. 211272. The cryatallinity size was estimated via Debye-Scherrer equation:

Debye-Scherrer equation: $D_c = \frac{K\lambda}{\beta \cos\theta}$ (Equation 3.1)

When D_c is average grain size (nm).

K is Debye-Scherrer constant (usually taken as 0.89).

λ is wavelength of the X-ray radiation (MoKα = 0.7093 nm).

β is line width at half-maximum height of the broadened peak (full width at half-maximum (FWHM))

θ is the half diffraction angle of the centroid of the peak(degree)

3.2.2 Dekktak 3 ST Surface Profiler [36]

The Dektak3ST is a surface profiling system capable of measuring surface textures and variations in the submicro-inch range to a sample thickness of 131 microns. By way of a diamond-tipped stylus, samples are analyzed under it on a moving stage according to parameters set by the user (scan length and time). As the stylus traverses the pre-determined length of the sample surface, surface variations are recorded. The data recorded can then be analyzed (up to 30 functions per scan) depending on user interests. These parameter capabilities include: roughness, waviness, step height and geometry (area, radius, slope, etc.). The graphic screen display exhibits data plot and live video imaging.

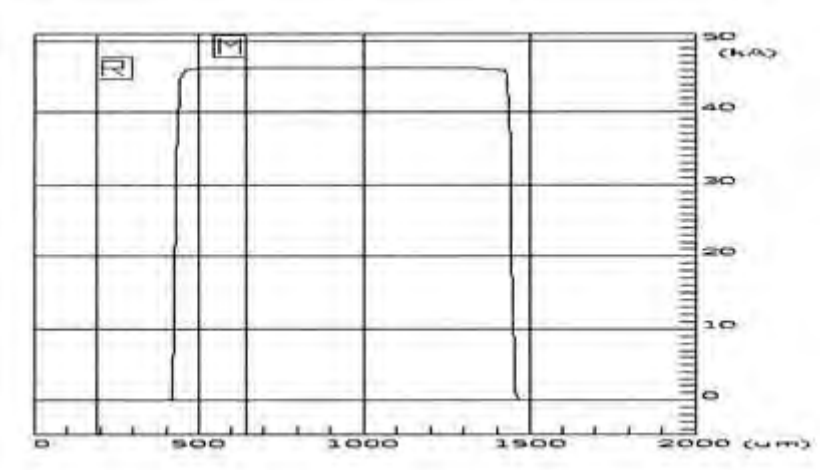

Figure 3.1 Profile of 46.250 KÂ NIST Certified Calibration Standard

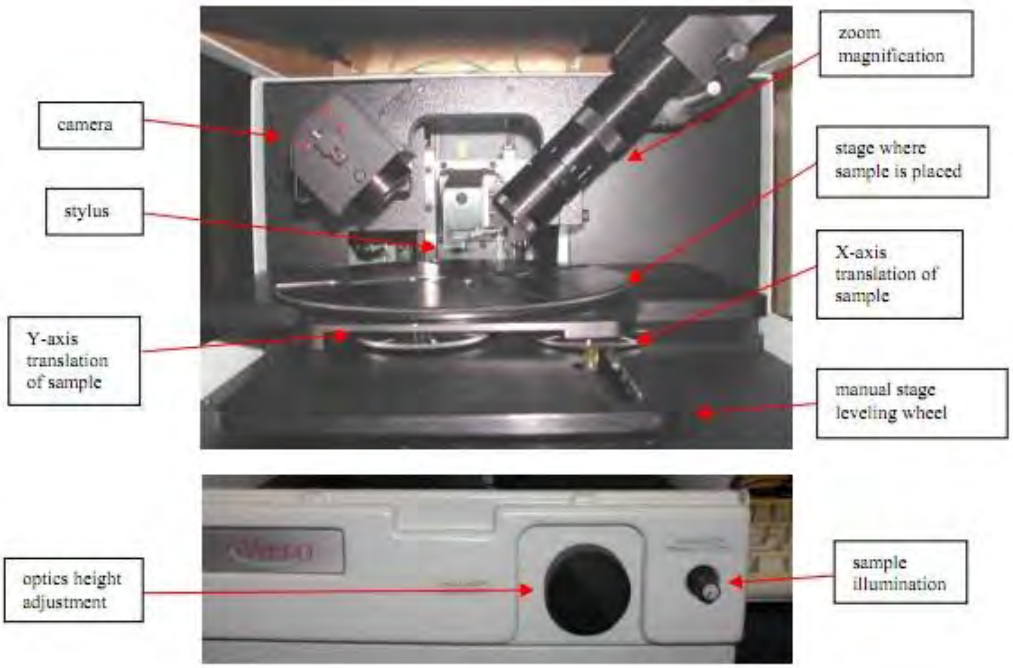

Figure 3.2 Veeco Dektak 3 ST model

3.2.3 Field Emission Scanning Electron Microscopy (FE-SEM)[37]

Structure, surface morphology and thickness of thin films were observed by Field Emission Scanning Electron Microscopy (Hitachi S-4700). With this microscope tiny structure as small as 1 nanometer can be visualized in small objects.

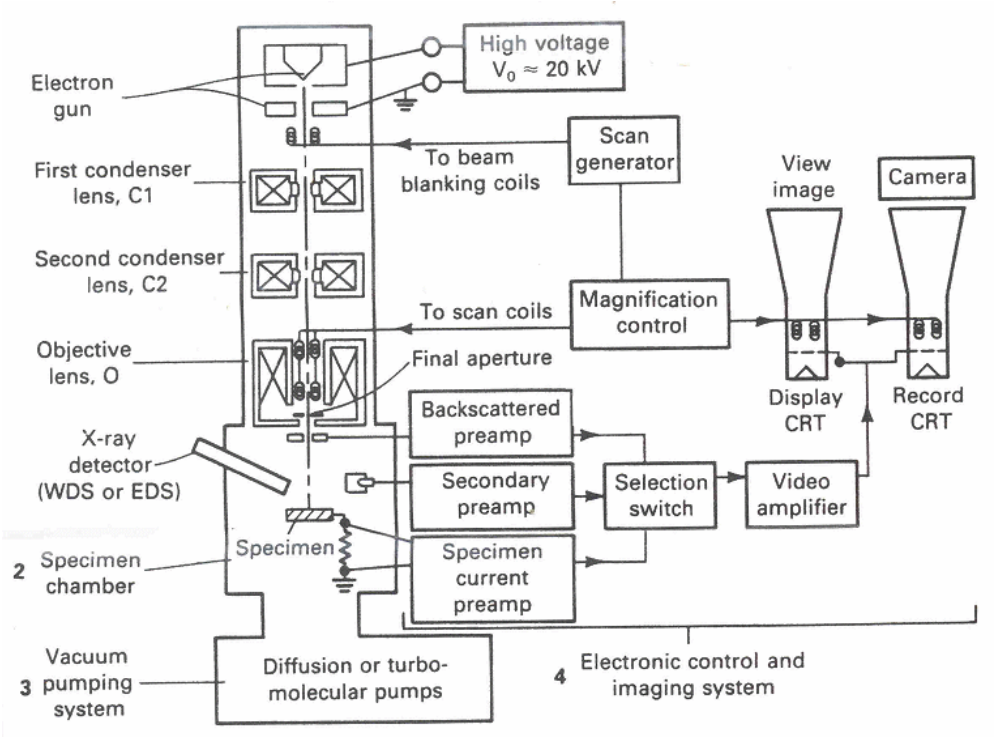

Figure 3.3 Shows the basic components of the scanning electron microscope. The various components of the microscope can be categorized as (1) the electron column, (2) the specimen chamber, (3) the vacuum pumping system and (4) the electron control and imaging system.

Like the name FE-SEM already indicates, this microscope does not work with light (photons) but with electrons. Electrons are generated in a 'source' (Emission) and accelerated under influence of a strong electrical voltage gradient (Field). With electromagnetic coils an electron beam is formed that scans the object (Scan) and secondary electrons are produced by interaction with the atoms at the surface of the sample. These electrons contain valuable information that is employed to reconstruct a very detailed image of the topography of the surface of the specimen.

3.2.4 Scanning Probe Microscopy (SPM) [38]

Surface roughness of Rare earth-doped TiO_2 films were observed by Scanning Probe Microscopy (SPM). These techniques are based upon scanning a probe just above a surface whilst monitoring some interaction between the probe and the surface.

Scanning Probe Microscopy has enabled researchers to image surfaces at the nanometer scale. Rather than using a beam of light or electrons, SPM uses a fine probe that is scanned over a surface (or the surface is scanned under the probe). By using such a probe, researchers are no longer restrained by the wavelength of light or electrons. The resolution obtainable with this technique can resolve atoms, and true 3-D maps of surfaces are possible. Scanning Probe Microscopy is a general term, used to describe a growing number of techniques that use a sharp probe to scan over a surface and measure some property of that surface. Some examples are STM (scanning tunneling microscopy), AFM (atomic force microscopy), and NSOM (Near-Field Scanning Optical Microscopy).

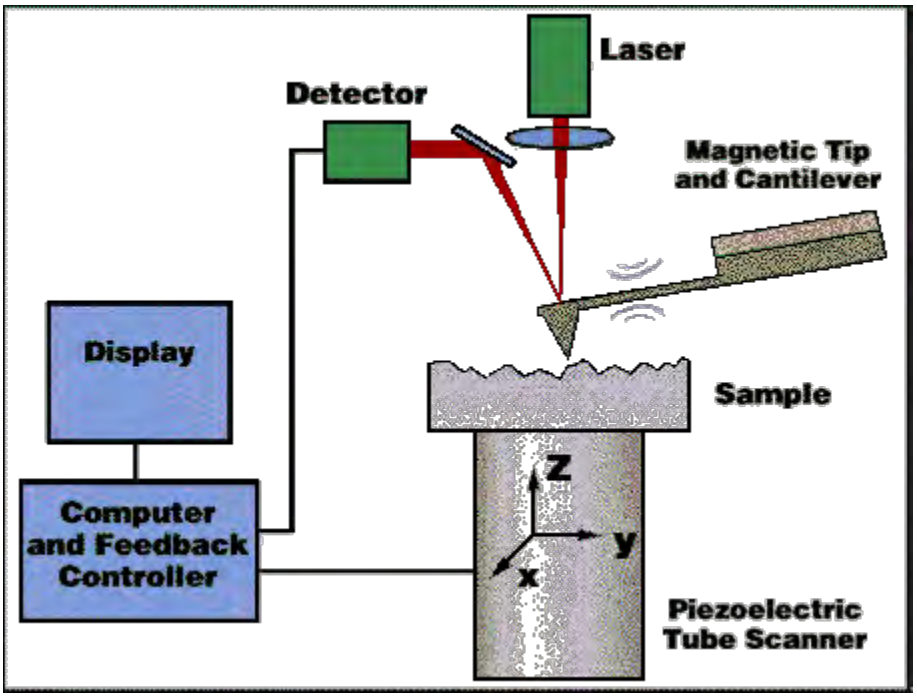

Figure 3.4 Basic idea of scanned probe techniques

The number of techniques is constantly growing, as the tip can be modified in many ways to investigate surface properties. In addition, the uses of a tunneling current, simple force feedback or light through an aperture in the probe enable different ways to interact with the surface.

3.2.5 Transmittance by UV-vis spectrophotometer (Lambda 950) [39]

Transparency of thin films was observed by UV-Vis spectrophotometer (Lambda 950) from 200 to 800 nm.

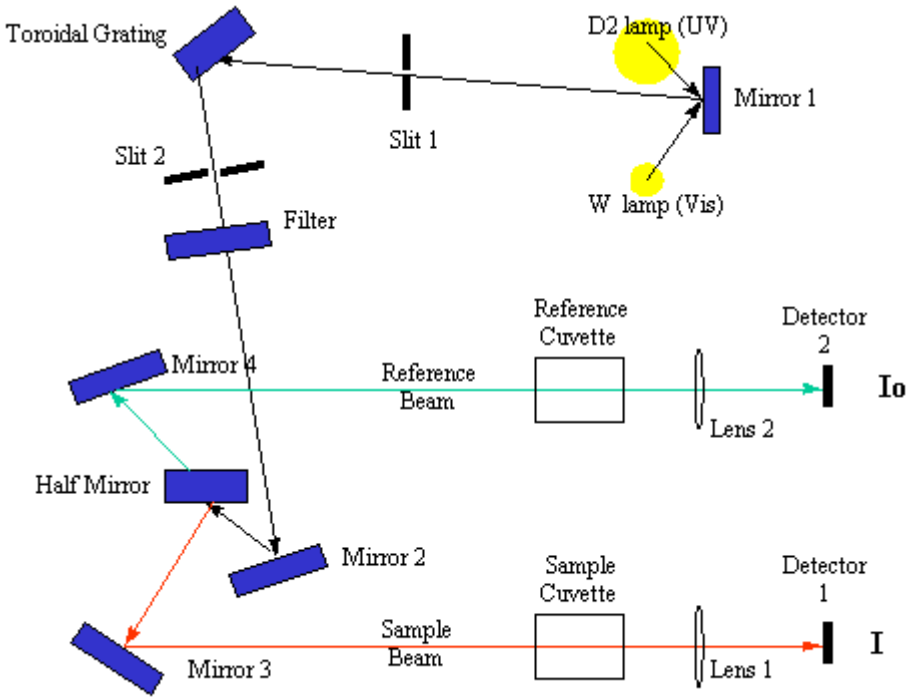

Figure 3.5 Flow chart of beam UV-vis spectrophotometer

The UV-Visible spectrophotometer uses two light sources, a deuterium (D2) lamp for ultraviolet light and a tungsten (W) lamp for visible light. After bouncing off a mirror (mirror 1), the light beam passes through a slit and hits a diffraction grating. The grating can be rotated allowing for a specific wavelength to be selected. At any specific orientation of the grating, only monochromatic (single wavelength) successfully passes

through a slit. A filter is used to remove unwanted higher orders of diffraction. The light beam hits a second mirror before it gets split by a half mirror (half of the light is reflected, the other half passes through). One of the beams is allowed to pass through a reference cuvette (which contains the solvent only), the other passes through the sample cuvette. The intensities of the light beams are then measured at the end.

3.2.6 Optical band gap energy [40-44]

The absorption coefficient (α), which can be derived from Equation 3.2.

$$T = \frac{(1-R)^2 \exp(-\alpha d)}{1-R^2 \exp(-2\alpha d)} \qquad \text{(Equation 3.2)}$$

Where *T* is optical transmittance, *R* is reflectance, and *d* is film thickness. However, at the short wavelength close to the optical band gap, the scattering losses are dominated by the fundamental absorption, and the absorption coefficient is given by Equation 3.3.

$$\alpha = -\frac{\ln T}{d} \qquad \text{(Equeation 3.3)}$$

Over the optical absorption edge, the indirect-allowed transitions dominate and above the threshold of fundamental adsorption, the following expression can be written:

$$(\alpha h\nu)^{\frac{1}{2}} = \alpha_0 (h\nu - E_g) \qquad \text{(Equation 3.4)}$$

Where $h\nu$ is photon energy, E_g is energy gap, and α_0 is a constant which does not depend on photon energy. From the linear part of $(\alpha h\nu)^{\frac{1}{2}} = f(h\nu)$ dependence, the extrapolated energy gap, E_g, can be obtained, for $\alpha = 0$. The energy gap is determined by plotting $(\alpha h\nu)^{\frac{1}{2}}$ versus equivalent energy at the wavelength λ, as shown in fig 3.6. This is called ‘‘Tauc plot’’

Form the ‘‘Tauc plot’’, the tangential at high α region of $h\nu$ and $(\alpha E)^{1/2}$ cure is extrapolated to intercept the $h\nu$ axis. This intercept value is defined as the optical band gap energy.

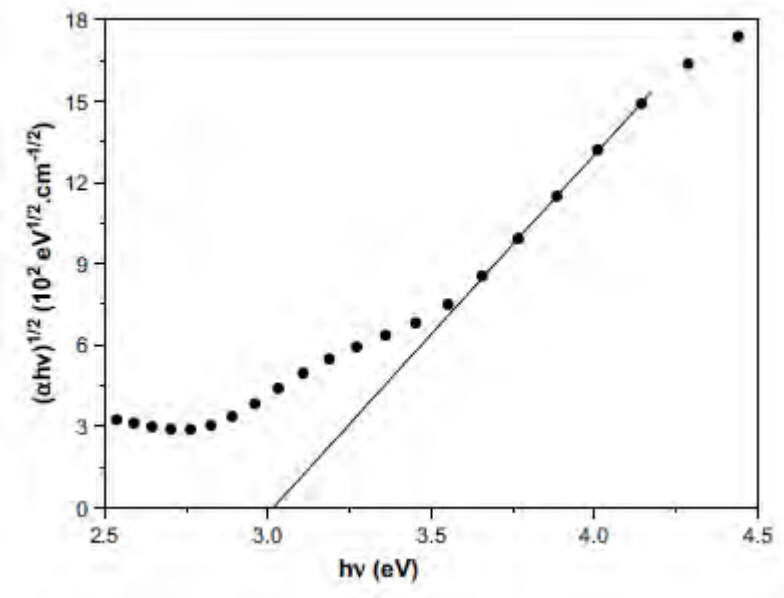

Figure 3.6 Determination of energy of TiO_2 films deposited on glass substrate by "Tauc's plot" [41]

3.2.7 Photocatalytic activity

Photocatalytic activity of sputtered films, 20x20x2 mm^3 in size, was evaluated through the degradation of methylene blue $(C_{16}H_{18}N_3S.Cl.3H_2O)$ solution with initial concentration of methylene blue of $5x10^{-3}$ mM under UV (Toshiba FL10BLB-A) Fluorescent lamp (FSL T8 10W). At first, films were vibrated in the dark for 1 hour to measure the absorbance of methylene blue onto the TiO_2 thin films before irradiation. After that, these films were irradiated under a black lamp and Fluorescent lamp at intensity of 2 and 5 mW/cm^2, respectively. To evaluate the photocatalytic activity. The absorptions of methylene blue were measured by UV-Vis spectrophotometer (Lambda 950) at wavelength 644 nm.

Photocatalytic activity was presented by kinetic energy (k). The kinetic energy of TiO_2 and RE-doped TiO_2 films prepared under difference deposition conditions was calculated using the following equation 3.5:

$$\ln\left(\frac{C_0}{C_t}\right) = kt \qquad \text{(Equation 3.5)}$$

Where C_0 = initial concentration of methylene blue

C_t = concentration measured at the irradiation time

t = time (minute)

k= kinetic energy

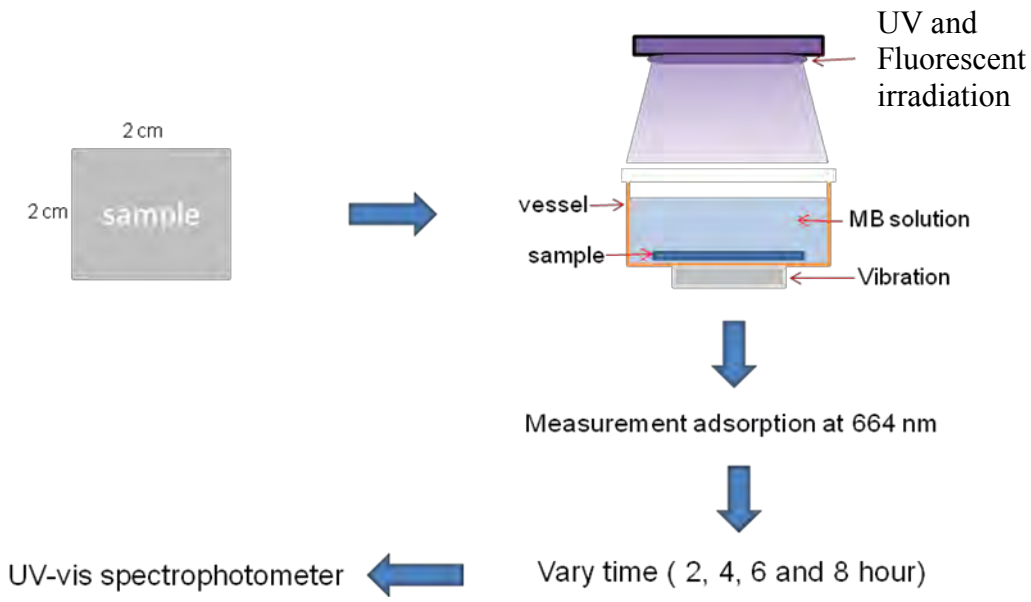

Figure 3.7 Photocatalytic activity characterization and equipment

3.2.8 Electron probe micro-analyyzer (EPMA) [45]

An electron probe micro-analyzer is a micro beam instrument used primarily for the in situ non-destructive chemical analysis of minute solid samples. EPMA is also informally called an electron microprobe, or just probe. It is fundamentally the same as an SEM, with the added capability of chemical analysis. The primary importance of an EPMA is the ability to acquire precise, quantitative elemental analyses at very small "spot" sizes (as little as 1-2 microns), primarily by wavelength-dispersive spectroscopy (WDS). The spatial scale of analysis, combined with the ability to create detailed images of the sample, makes it possible to analyze geological materials in situ and to resolve complex chemical variation within single phases (in geology, mostly glasses and minerals). The electron optics of an SEM or EPMA allow much higher resolution images to be obtained than can be seen using visible-light optics, so features that are irresolvable under a light microscope can be readily imaged to study detailed microtextures or provide the fine-scale context of an individual spot analysis.

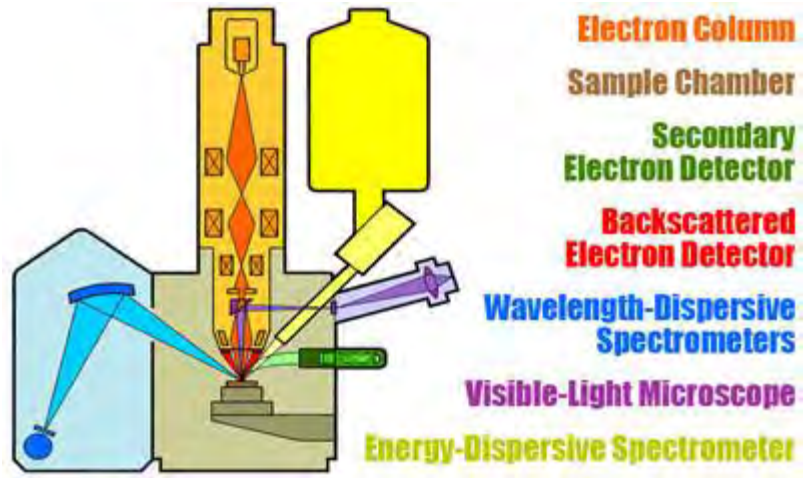

Figure 3.8 Schematic cut-away diagram of a typical microprobe.

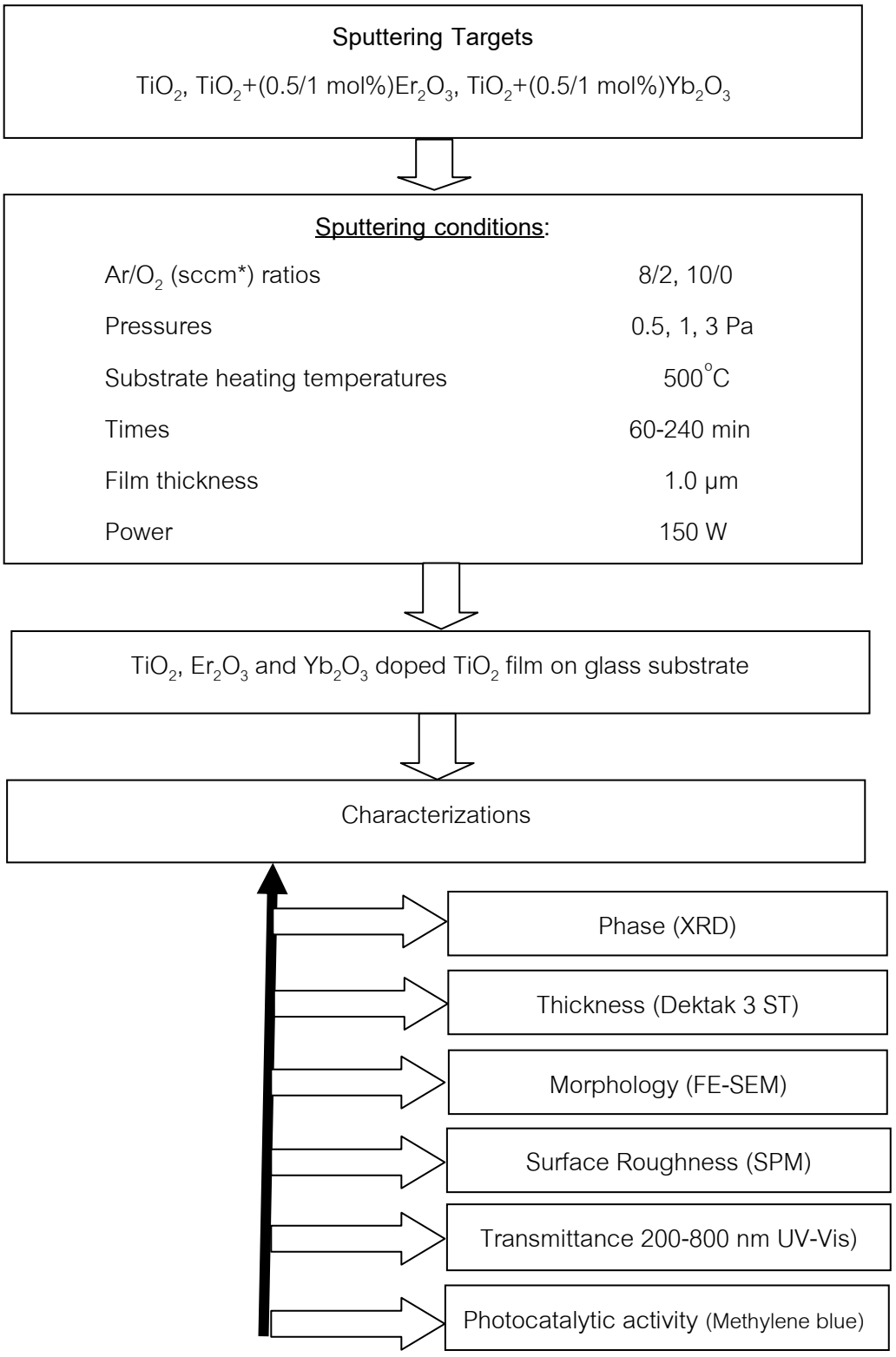

Figure 3.9 Flow chart of sputtering conditions and characterizations of thin films.

(* **sccm** : standard cubic centimeters per minute)

CHAPTER IV

RESULTS AND DIDCUSSIONS

In this research, preparation of pure TiO_2, Yb_2O_3-doped TiO_2 and Er_2O_3-doped TiO_2 thin films on glass substrate by RF-magnetron sputtering technique were studied. The effect of sputtering parameters on the phase structure, surface morphology and roughness, optical properties of deposited films were investigated. Moreover, the photocatalytic activity of prepared films was examined under UV and fluorescent lamp. The results were divided into 3 parts as follows:

4.1 TiO_2 thin films

4.1.1 Deposition rate

The deposition rate of TiO_2 thin films on glass substrate prepared by RF-magnetron sputtering technique was shown in fig 4.1.

Form fig 4.1, the average deposition rate of TiO_2 films prepared under pure Ar and mixture of Ar and O_2 (8/2) gas are 8.33 nm/min and 4.16 nm/min, respectively. The deposition rate of films prepared under pure Ar gas was about two times higher than that of films deposited under gas mixture.

In the sputtering process, there are several kinds of the high energy gas particles, such as high energy neutrals (Ar^o) recoiled from the target or high energy negative ions (O^-) accelerate by the cathode toward the growing films surface. The bombardments by such high films particle should have heavy influence on the films structure and properties [46]. The main reason of different deposition rate is that it is different in Ar/O_2 flow ratio, when low O_2 there are more Ar ions to bombard the pure TiO_2 target, so the deposition rate is higher while high O_2 lower the deposition rate due to it impeded Ar ions bombardment at TiO_2 target, so the deposition rate is lower [49].

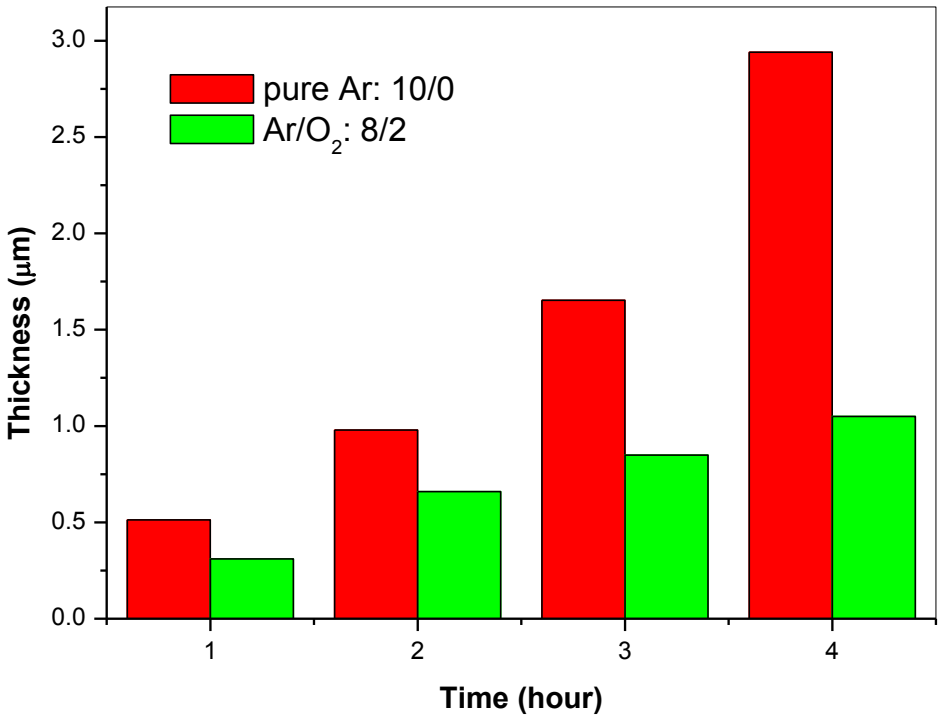

Figure 4.1 Graph of relation between sputtering time and thickness of TiO_2 films prepared by RF-magnetron sputtering under pure Ar (10/0) and mixed Ar/O_2 (8/2), at total sputtering pressure 3 Pa.

Since, the thickness of film has a significant influence on the characteristics of deposited film. Thus the thickness of all films sputtered under pure Ar (10/0) and Ar/O_2 (8/2) was controlled at about 1.0 μm for further characterizations by adjusting deposition time. According to the deposition rate, the deposition time for film prepared under pure Ar and Ar/O_2 (8/2) are 2 h and 4 h, respectively.

4.1.2 Phase structure

This section show effects of sputtering gas and total sputtering pressure on phase structure of TiO_2 thin films characterized by X-ray diffraction (XRD).

4.1.2.1 Effect of sputtering gas on phase structure of TiO_2 films

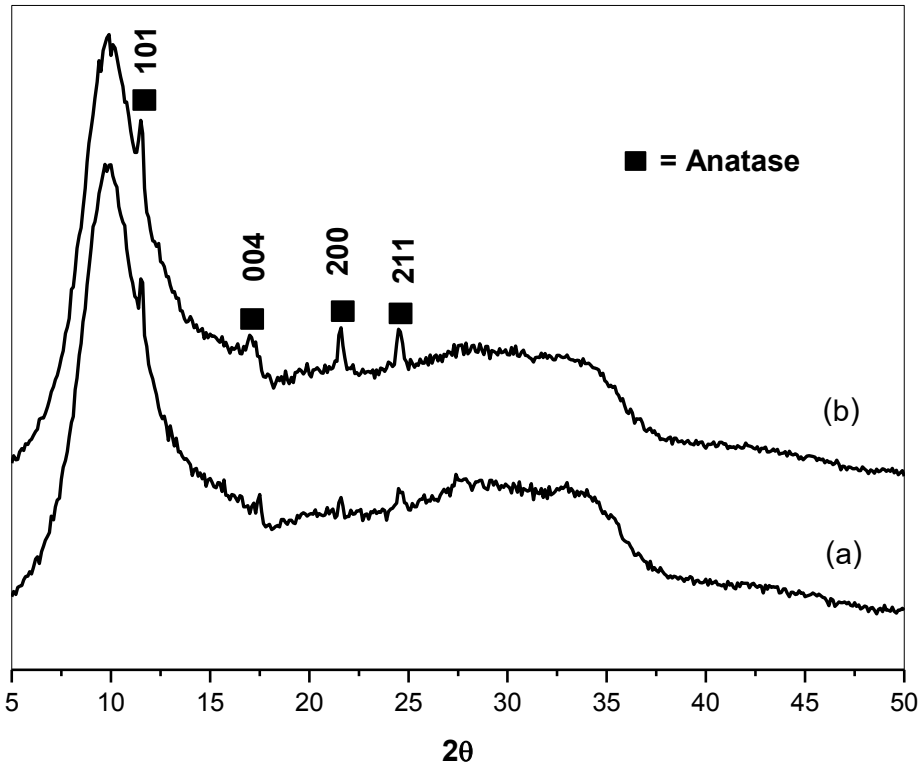

Figure 4.2 XRD patterns of TiO_2 thin films prepared under (a) Ar/O_2; 8/2 and (b) pure Ar 10/0, under 3 Pa and substrate heating temperature at 500 °C.

From XRD results (fig 4.2), the peaks were found at 2θ ; 11.5°, 17.1°, 21.6° and 24.5° corresponding to the 101, 004, 200 and 211 diffraction planes of anatase phase (JCPDS No. 211272) respectively. The ratio of gas mixture Ar/O_2 significantly affected on the deposition rate of films. Moreover, the film deposited under pure Ar (b) has higher crystallinity, which can be seen clearly the high intensity of diffraction peaks at 2θ 21.6° and 24.5 ° comparing to the films prepared under gas mixture (a).

4.1.2.2 Effect of sputtering pressure on phase structure of TiO_2 films

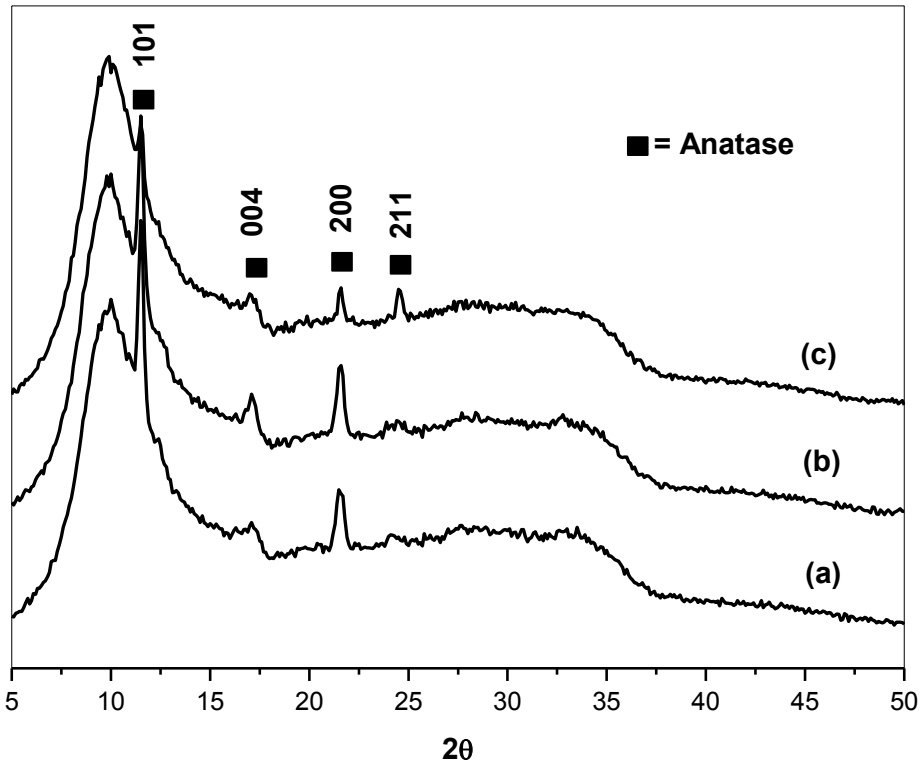

Figure 4.3 XRD patterns of TiO_2 film prepared under pure Ar at different total sputtering pressure, (a) 0.5 Pa, (b) 1 Pa and (c) 3 Pa.

The XRD patterns of TiO_2 films sputtered under different total sputtering pressure were shown in fig 4.3. In order to study effect of total sputtering pressure on TiO_2 films, heating temperature and applied power were fixed at 500 ^{o}C and 150 w, respectively. It was demonstrated that all of the deposited films consisted of the peaks at 2θ ; 11.5^{o}, 17.1^{o}, 21.6^{o} and 24.5^{o} corresponding to the 101, 004, 200 and 211 planes of anatase structure (JCPDS No. 211272), respectively. Peak intensity decreased with increasing sputtering pressure from 0.5 Pa to 3 Pa. However, the half width value remained nearly unchanged at different total sputtering pressure. Since no new peaks were observed, it can be concluded that the decrease in peak intensity does not indicate any deterioration in crystallinity, but rather that it is associated with the porous surface condition and, as a

result, the effective film thickness was seemingly smaller than it was when the surface was in a gap-free state [50].

4.1.3 Surface morphology and roughness

The effect of sputtering gas and total sputtering pressure on the surface morphology and roughness of deposited films were examined by Field Emission Scanning Electron Microscopy and Scanning Probe Microscopy (SPM).

4.1.3.1 Field Emission Scanning Electron Microscopy (FE-SEM)

The surface morphology is an important factor affecting on the photocatalytic activity of TiO_2 films, thus they were investigated by FE-SEM. The FE-SEM images in fig 4.4, 4.5 show effect of Ar/O_2 ratio and total sputtering pressure on the morphology of TiO_2 films. The different in morphology between TiO_2 films prepared under with and without O_2 flow was clearly demonstrated via FE-SEM (fig 4.4). It was found that the TiO_2 film prepared under pure Ar consisted of porous and pyramid grain structure with the grain size approximately 100 nm while the films prepared under Ar/O_2 gas mixtures displayed a porous structure with small subgrains approximately 10 nm in size which grouped together to form large grain of 120 nm.

Fig 4.5 shows the effect of total sputtering pressure on the morphology of films observed by FE-SEM. It was noticed that the films sputtered under low pressure (0.5-1 Pa) composed of dense packed grains, whereas, the film prepared at higher pressure (3 Pa) displayed porous and pyramid grain structure in which voids between grain boundary were created.

The creation of films structure could be explained in terms of total sputtering pressure. At the low pressure, there are fewer gas molecule collisions taking place. Therefore, high energy gas molecule can directly get through the surface of films. As a result, films grow to be dense. While at high pressure, due to higher number of gas molecules contained in the chamber, there is more probability for gas molecule collision

with each other. This collision can slow down the gas movement and also reduce the energy of the high energy gas molecules then the films grow to be porous [21].

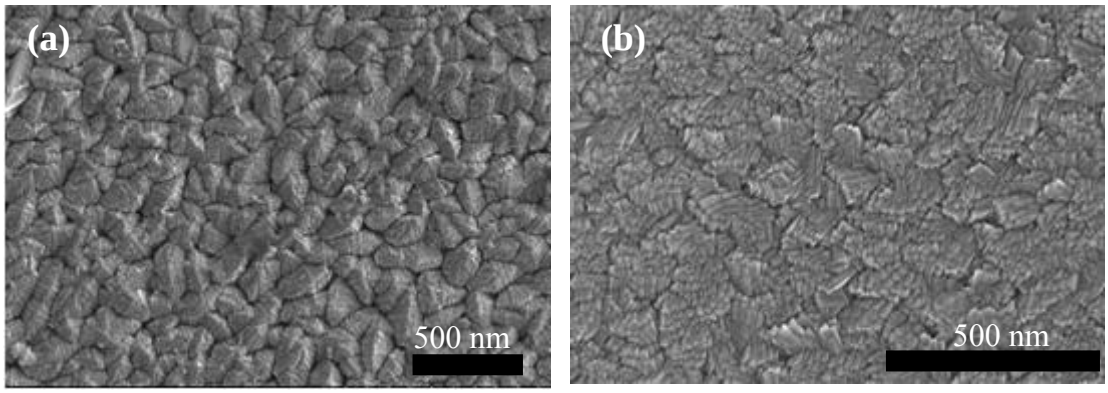

Figure 4.4 FE-SEM images of TiO_2 thin films prepared under (a) pure Ar (10/0) and (b) Ar/O_2 (8/2) at total sputtering pressure 3 Pa.

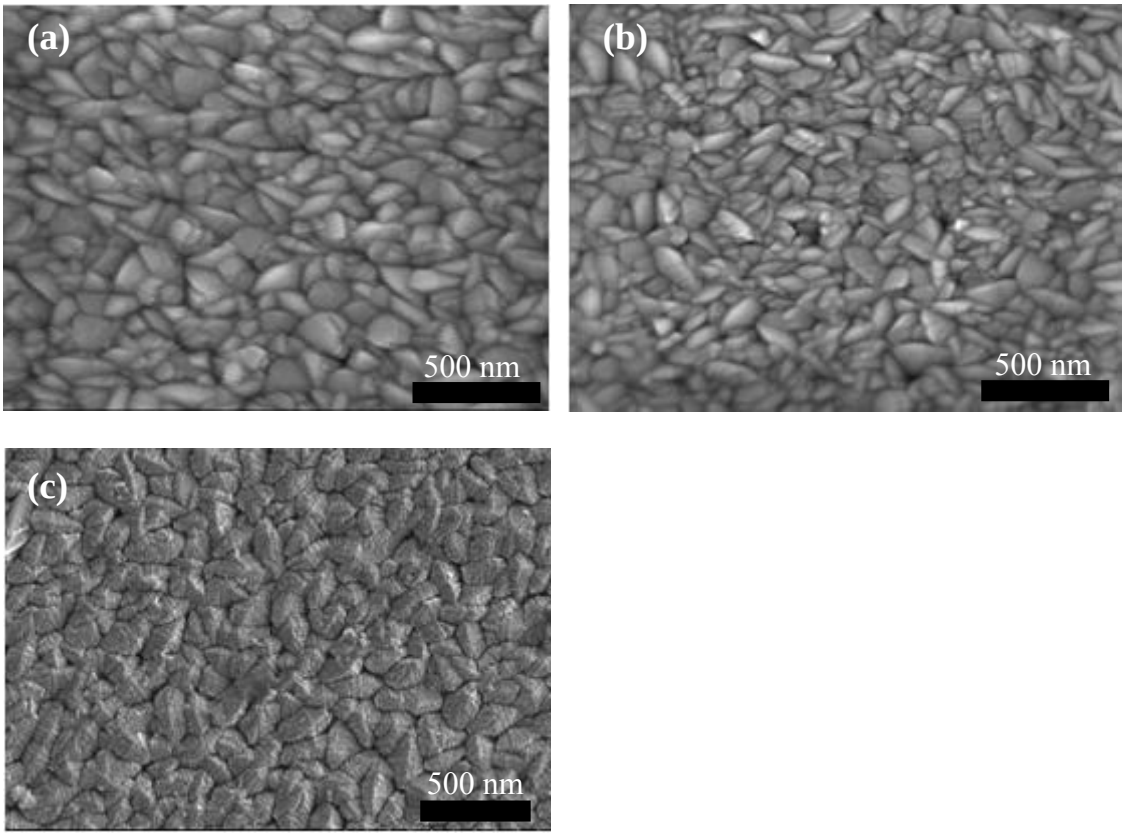

Figure 4.5 FE-SEM images of TiO_2 thin films prepared under pure Ar (10/0) at different total sputtering pressure (a) 0.5 Pa (b) 1 Pa (c) 3 Pa.

4.1.3.2 Scanning Probe Microscopy (SPM)

From fig 4.6, SPM images show the two-dimentions and three-dimentions of pure TiO_2 films prepared on glass substrate under different sputtering gas and total sputtering pressure. The surface roughness of TiO_2 films displayed in root mean square roughness (R_{rms}) were 6.37 and 12.58 nm of films deposition at 1 and 3 Pa under without O_2 gas, respectively. It suggested that the surface roughness of TiO_2 films was much increased when the film was sputtered under higher pressure (3 Pa) because the surface roughness developed during the films growth was controlled by the energy of deposited particles. When the energy of depositing particles decreased due to low pressure, the surface mobility decrease and the coalescence of crystals is limited. The depositing particles growing surface receive more deposited materials than valleys resulting in the formation of a more surface roughness. The difference in surface roughness between the film prepared under with and without O_2 gas flow was clearly observed through SPM (fig 4.6 (a, c)). The surface roughness of TiO_2 films prepared under with and without O_2 at 3 Pa were 5.63 and 12.58 nm, respectively. This indicated that the total sputtering pressure had a significant influence on creation of surface roughness of film sputtered under pure Ar (10/0). On the other hand, the surface roughness of films deposited under gas mixture (Ar/O_2) was not affected by total sputtering pressure.

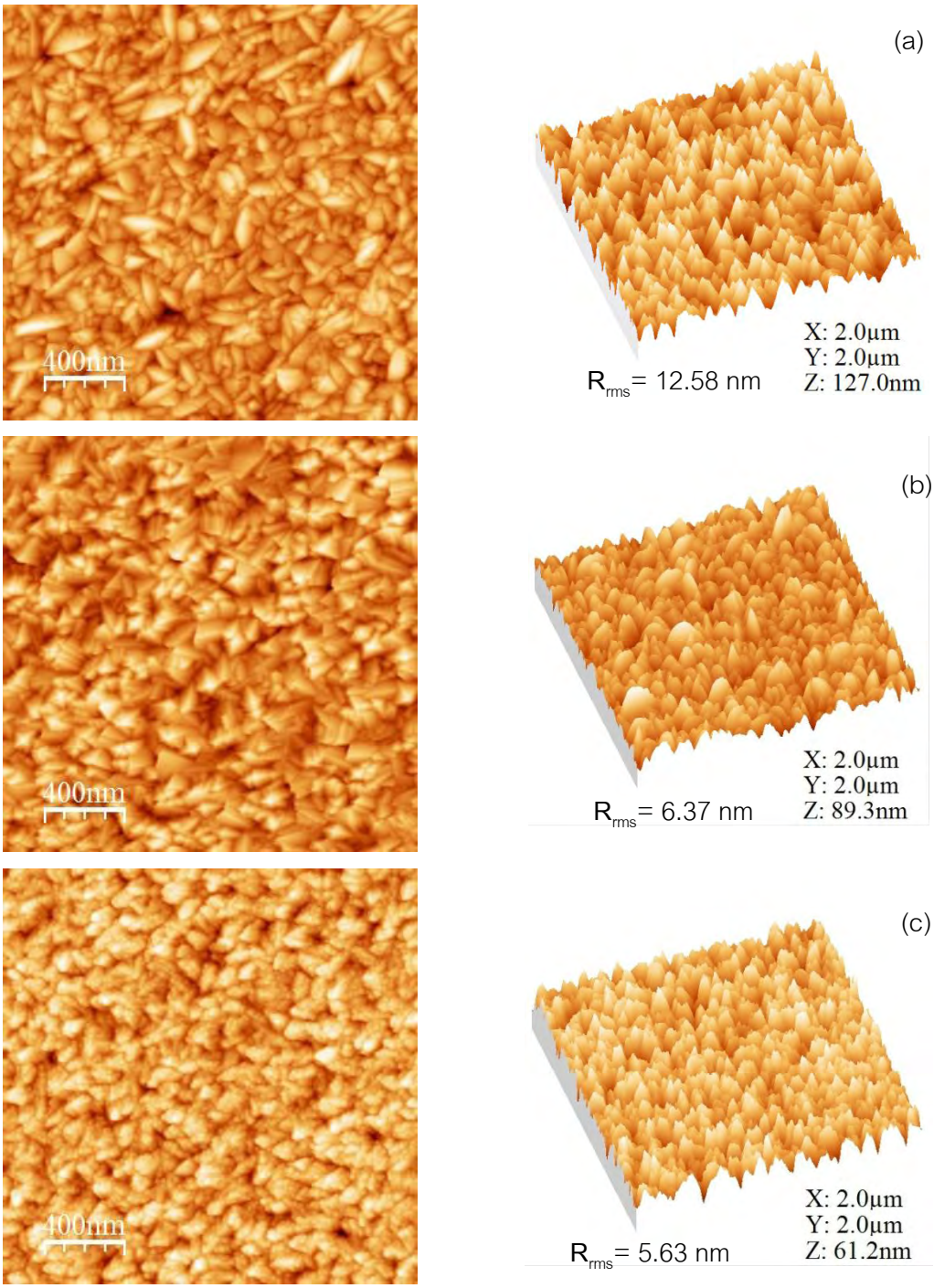

Figure 4.6 SPM images of TiO_2 films deposited under different sputtering conditions. (a) pure Ar, 3 Pa (b) pure Ar,1 Pa and (c) Ar/O_2, (8/2), 3 Pa.

4.1.4 Transmittance

This section presents transmittance of TiO_2 thin films sputtered under difference conditions, which can be seen in fig 4.7.

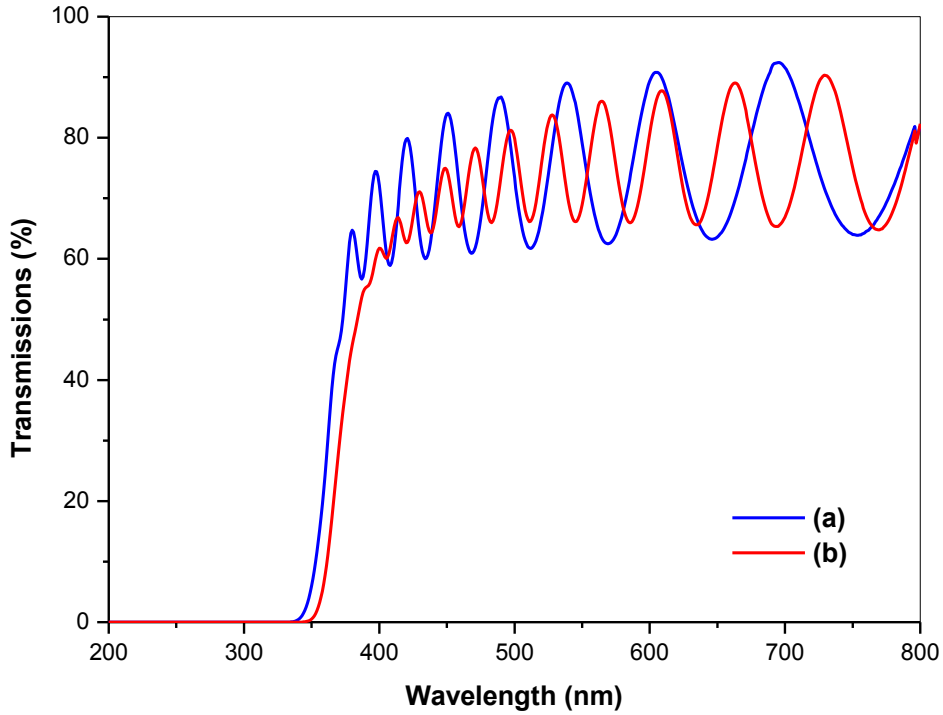

Figure 4.7 Transmittance spectra of TiO_2 thin films prepared under sputtering pressure at 3 Pa and different sputtering gas. (a) Ar/O_2 (8/2) and (b) pure Ar (10/0).

The transmittance spectra of TiO_2 thin films deposited under pure Ar and mixture of Ar/O_2 (8/2) were shown in fig 4.7. It was seen that all films show the usual light interference pattern in visible region (400-800 nm). The TiO_2 film deposited under Ar/O_2 gas mixtures has high transparency more than that of film prepared under pure Ar gas. The averages transmittance of TiO_2 films in the visible region (show in fig 4.7) is about 80 %. Also, the TiO_2 films prepared at pure Ar gas displayed markedly decrease in transmittance of films with red shift to longer wavelength. A decrease in optical transmittance of TiO_2 prepared under pure Ar (10/0) is resulted from its large grain size

and higher surface roughness. Corresponding to the XRD FE-SEM and SPM image results which were demonstrated above.

4.1.5 Optical band gap

Optical transmission spectra of pure TiO_2 measured at room temperature with an excitation wavelength of 200-800 nm by a UV-Vis spectrophotometer are shown in fig 4.7. Determination of the absorption edge or energy band gap has been described in chapter 3. The tangential line at high α region of the $h\nu$ *vs* $(\alpha E)^{1/2}$ curve is extrapolated to intercept the $h\nu$ axis as shown in fig 4.8. This intercept value is defined as the energy band gap, it was found that the energy band gap of films prepared under with and without O_2 gas are 3.20±0.01 eV and 3.17 ±0.01 eV, respectively.

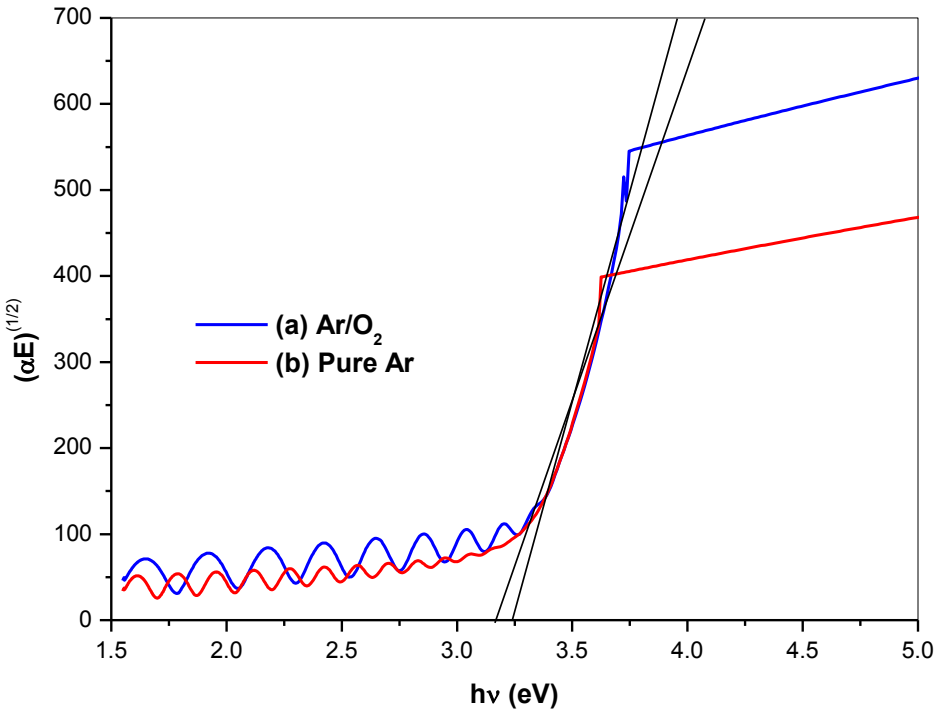

Figure 4.8 Graphs of $(\alpha E)^{1/2}$ versus photon energy, E ($h\nu$), for TiO_2 films prepared under pure Ar (10/0) and Ar/O_2 (8/2).

4.1.6 Photocatalytic activity

Photocatalytic activity was presented by kinetic energy; *k*. Determination of the kinetic energy (k) has been described in chapter 3. The kinetic energy of TiO_2 thin films prepared at different sputtering gas under UV irradiation was shown in fig 4.9-4.10.

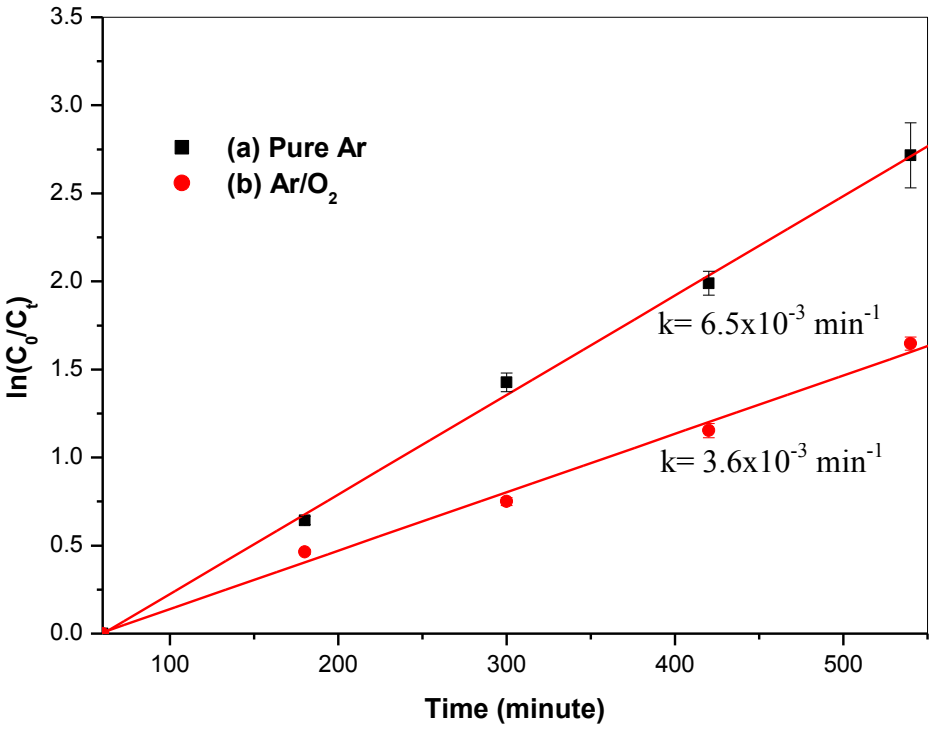

Figure 4.9 Photocatalytic degradation of methylene blue solution as a function of UV irradiation time of films prepared under (a) pure Ar (10/0) and (b) Ar/O_2 (8/2) at total sputtering pressure 3 Pa.

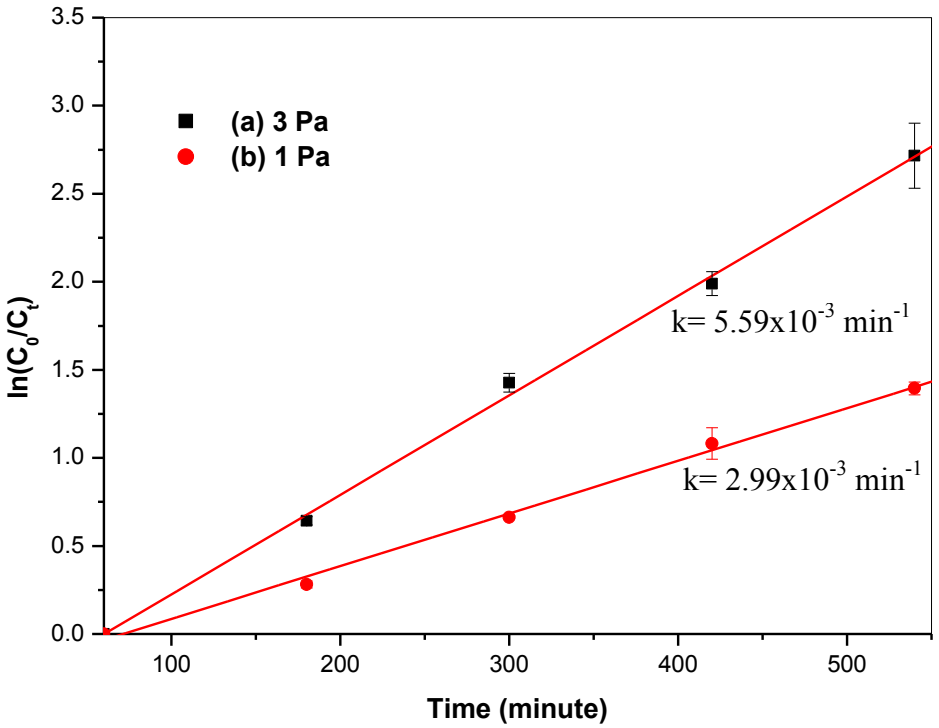

Figure 4.10 Photocatalytic degradation of methylene blue solution as a function of UV irradiation time of TiO_2 films prepared under pure Ar at total sputtering pressure (a) 3 Pa and (b) 1 Pa.

In this work, the TiO_2 thin film coated on glass substrate was repeatedly used for five times in degradation 0.05 mM of methylene blue under UV irradiation. The *k* value, which obtained by linear fitted from fig 4.9 are $6.5\mathbf{x}10^{-3}$, $3.6\ \mathbf{x}10^{-3}min^{-1}$ for films without and with O_2 flow gas under UV irradiation, respectively. The *k* values of TiO_2 under UV irradiation, which obtained by linear fitted for films prepared at different total sputtering pressure were shown in fig 4.10. It was found that the TiO_2 films prepared under pure Ar gas showed higher photocatalytic activity than that of films prepared under flowing O_2 gas. It can be explained in this study that, due to the films prepared under without O_2 showed high crystallinity and high surface roughness compared with films prepared under gas mixture. In general, the surface area and crystallinity play an

important role in photocatalytic activity. A higher surface area enhances the photocatalytic efficiency due to their being more active sites (e^- and h^+) for the reaction.

In addition, the effect of total sputtering pressure on the photocatalytic activity was shown in fig 4.10. The dramatic increase in photocatalytic activity of TiO_2 film when sputtering pressure increased from 1 to 3 Pa was demonstrated. As described in the previous section that films growth under high sputtering pressure has porous structure and rougher surface. The photocatalytic values of films prepared under 1 and 3 Pa are 2.99 **X**10^{-3}, 5.59 **X**10^{-3} min^{-1}, respectively.

4.2 Yb_2O_3-doped TiO_2 thin films

4.2.1 Phase structure

This section shows effect of sputtering gas and amount of Yb_2O_3 doping on phase structure characterized by X-ray diffraction (XRD).

4.2.1.1 Effects of sputtering gas and Yb_2O_3 concentrations on Yb_2O_3-doped TiO_2 films

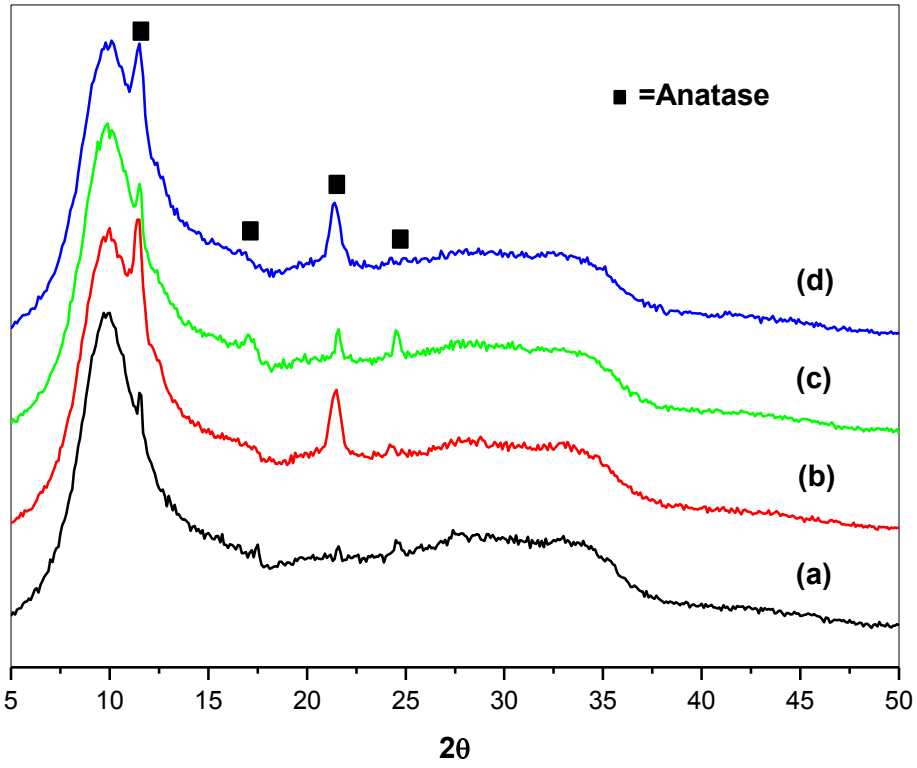

Figure 4.11 XRD patterns of TiO_2 and 1mol%Yb_2O_3doped TiO_2 (YbT) films prepared under different sputtering gas. (a) TiO_2 8/2; 3 Pa (b) YbT 8/2; 3 Pa (c) TiO_2 10/0; 3 Pa (d) YbT 10/0; 3 Pa.

From XRD results, the peaks were found at 2θ ; 11.5°, 17.1°, 21.6° and 24.5° corresponding to the 101, 004, 200 and 211 diffraction planes of anatase phase (JCPDS No. 211272) under all deposition conditions. The effect of doping concentrations of

Yb_2O_3 on Yb_2O_3-doped TiO_2 film was shown as in fig 4.12. It was indicated that all films consisted of reflection planes according to anatase phase. But the difference in their crystallinity was shown, in that the film deposited by 1mol% Yb_2O_3-doping displayed higher crystallinity with preferred orientation growth.

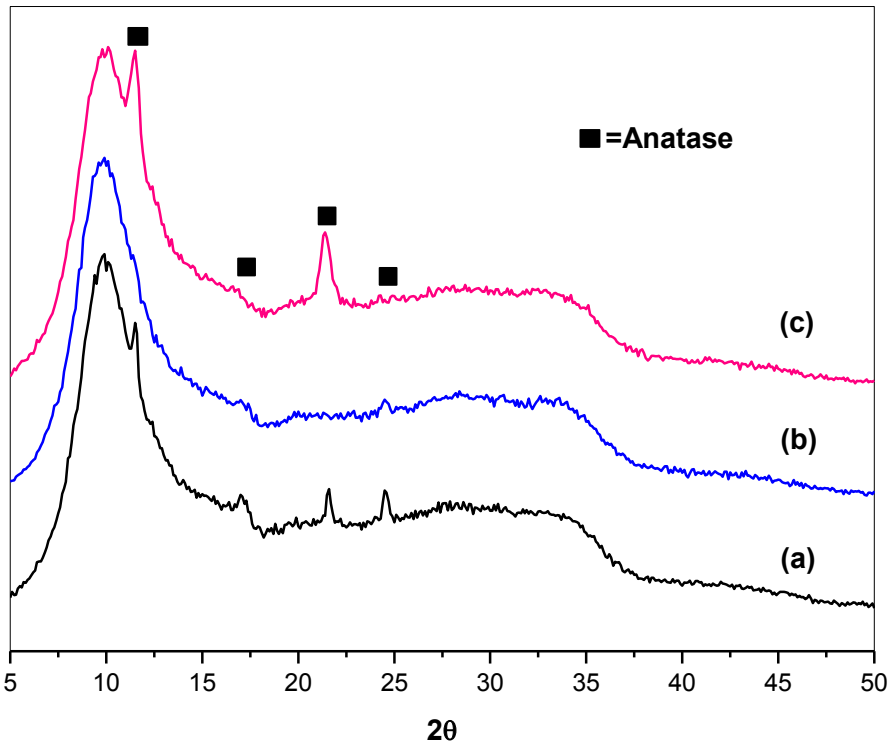

Figure 4.12 XRD patterns of TiO_2 and Yb_2O_3-doped TiO_2 films prepared under Ar/O_2 at 8/2. (a) pure TiO_2 (b) TiO_2-0.5 mol% Yb_2O_3 and (c) TiO_2-1 mol% Yb_2O_3

4.2.2 Surface morphology

4.2.2.1 Field Emission Scanning Electron Microscopy (FE-SEM)

From FE-SEM images in fig 4.13 shows the morphologies of Yb_2O_3-doped TiO_2 thin films prepared under difference Yb_2O_3 concentrations and sputtering gas. It was found that the films prepared under gas mixture displayed porous structure with smaller subgrain approximately 10 nm in size, grouped together to form large grain of 120 nm.

The similar microstructure of 1mol% Yb_2O_3-doped TiO_2 prepared under the same condition was observed. While, the Yb_2O_3-doped TiO_2 films prepared under pure Ar gas composed of dense packed grain with no gap between them and grain size about 120-150 nm. At the same time, the grain size of Yb_2O_3-doped TiO_2 increased as the amount of doping increased.

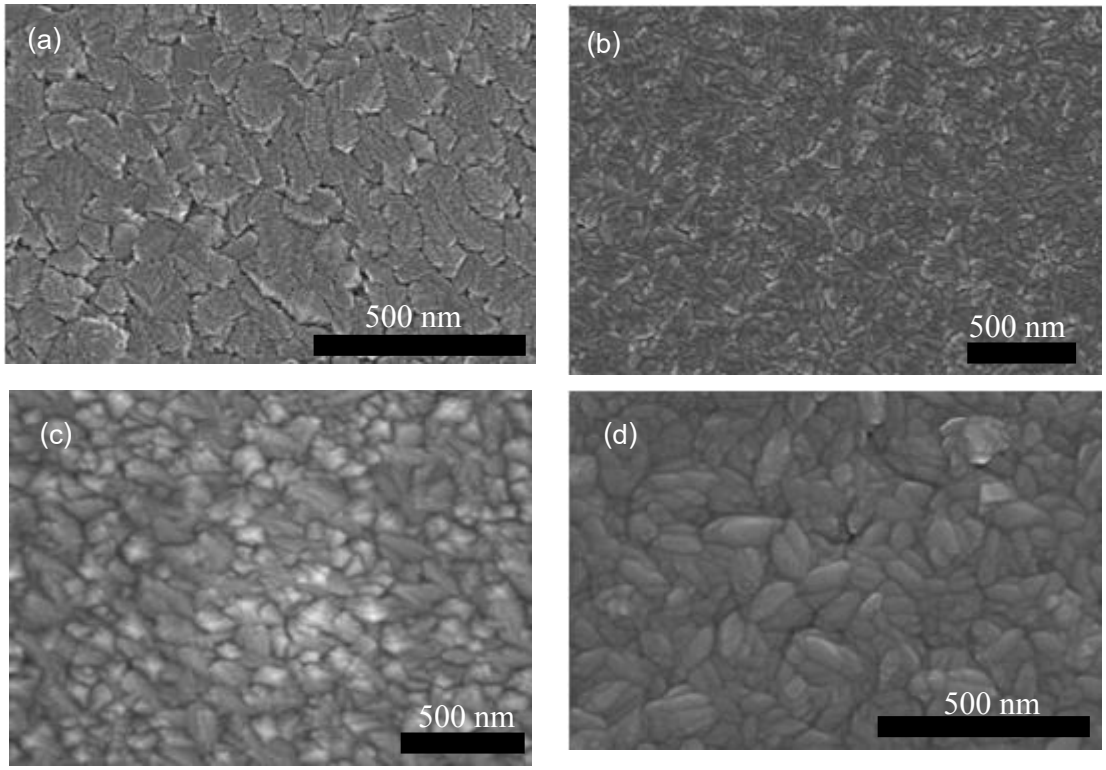

Figure 4.13 FE-SEM images of the films deposited under different Yb_2O_3 concentrations and sputtering gas. (a) 0.5mol% Yb_2O_3: 8/2, (b) 1mol% Yb_2O_3: 8/2, (c) 0.5mol% Yb_2O_3: 10/0 (d) 1mol% Yb_2O_3: 10/0

Form the results, effects of total sputtering pressure was observed. At high total sputtering pressure, the density of gas particles molecules in the chamber is increased, influence the probability of collisions and accelerate the particles. Consequently, the particle energy is decreased. The surface mobility decreases and the coalescence of crystal are limited, when the energy of depositing particle decreases. This results in the formation of rough microstructure with high surface [47].

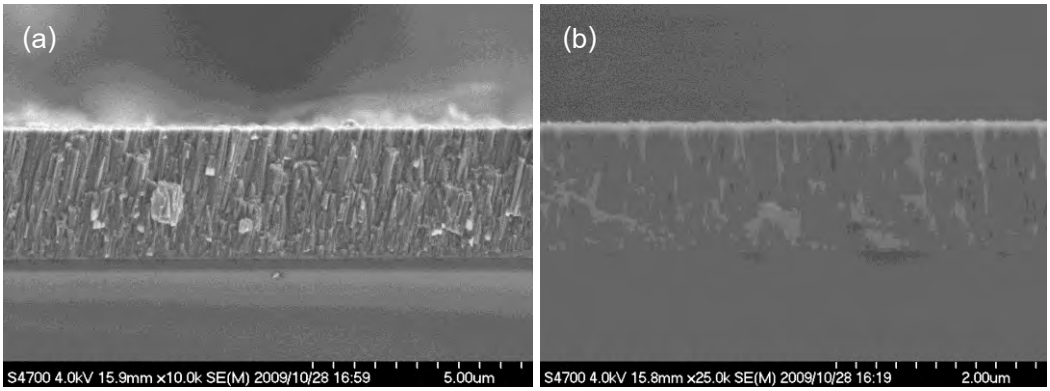

Figure 4.14 FE-SEM images from cross-section of Yb_2O_3-doped TiO_2 films deposited under different sputtering gas. (a) Ar/O_2; 10/0 and (b) Ar/O_2; 8/2, deposition time 4 hours.

From fig 4.14, FE-SEM images show the cross-section of Yb_2O_3-doped TiO_2 thin films formed at total sputtering pressure of 3 Pa under pure Ar (10/0) and Ar/O_2 (8/2) gas. The crystalline grains exhibit a columnar structure, which can be explained by shadowing model, that is, particles with various incident angles can deposit only on the top each dome because of the shadowing effect [48]. FE-SEM confirmed that the films have porous structure, due to gap were not only formed on the surface, but also in the bulk of the films.

4.2.2.2 Scanning Probe Microscopy (SPM)

Form fig 4.15 presents SPM images of Yb_2O_3-doped TiO_2 thin films prepared on glass substrate under different Yb_2O_3 concentrations at Ar/O_2 of 8/2. It was found that the surface roughness (present by root mean square roughness, R_{rms}) of the films were

5.63, 15.53 and 10.25 nm for pure TiO_2, 0.5 and 1 mol% Yb_2O_3-doped TiO_2, respectively. It was indicated that the surface roughness of films increased when doping with Yb_2O_3, but increasing in doping amount of Yb_2O_3 from 0.5 to 1 mol% slightly decreased the surface roughness. In case of Yb_2O_3 doped TiO_2 films prepared under pure Ar, the slightly decrease in surface roughness when doped with Yb_2O_3 was observed as shown in fig 4.16. The surface roughness values of films doped with 0.5 and 1 mol% of Yb_2O_3 and pure TiO_2 under pure Ar gas are 10.25, 10.97 and 12.58 nm, respectively.

Generally, in the sputtering process, the microstructure and the surface morphology develop during the film growth is controlled mainly by the energy of depositing particles which is affected by pressure. There are several kinds of the high energy gas particles, such as high energy neutrals (Ar^o) recoiled from the target, high energy of sputtering atom or high energy negative ions (O^-) accelerate by the cathode toward the growing films surface [47]. When the energy of depositing particles decreases, the surface mobility decreases and the coalescence of crystals is limited. The depositing particles are incorporated in the growing film at their impinging sites, high points on the growing surface receive more deposited material than valleys resulting in the formation of surface roughness.

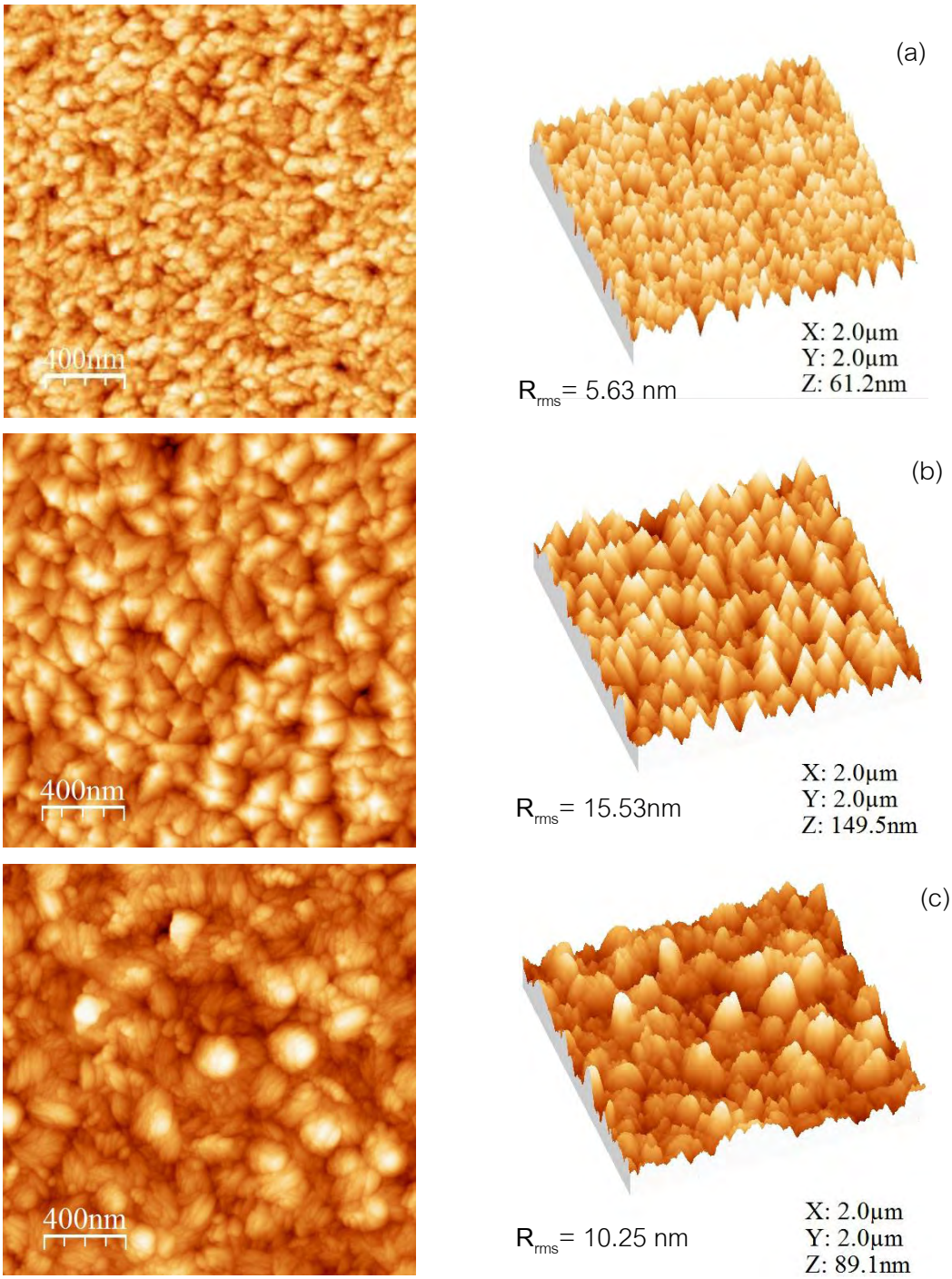

Figure 4.15 Two-dimensional and three-dimensional SPM images of (a) Pure TiO_2 (b) TiO_2-0.5mol% Yb_2O_3 and (c) TiO_2-1mol% Yb_2O_3 films prepared on glass substrate under Ar/O_2 at 8/2, heated at 500 $^{\circ}C$ and total sputtering pressure 3 Pa.

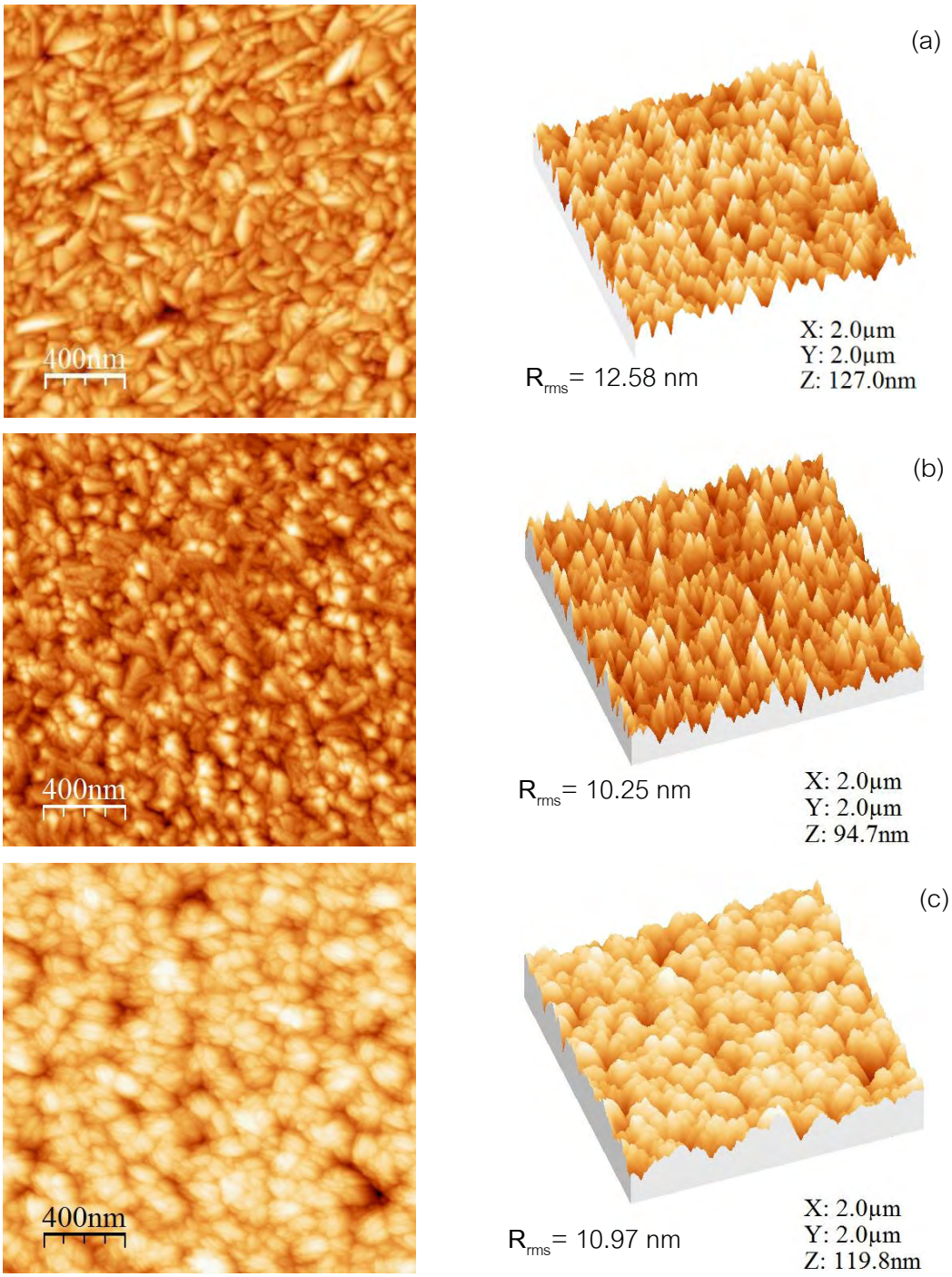

Figure 4.16 Two-dimensional and three-dimensional SPM images of (a) Pure TiO_2 (b) TiO_2-0.5mol% Yb_2O_3 and (c) TiO_2-1mol% Yb_2O_3 films prepared on glass substrate under pure Ar, heated at 500 $^{\circ}$C and total sputtering pressure 3 Pa.

4.2.3 Optical properties

This section show effects of Yb_2O_3 doping on transmittance of TiO_2 film observed via UV-vis spectrophotometer and optical band gap energy determined from Tauc's plot method

4.2.3.1 Transmittance

The effect of Yb_2O_3 doping on the optical transmittance of deposited films was shown in fig 4.17. It was seen that the TiO_2 film has high transparency in the visible range of 400-800 nm. The average transmittance of films in the visible region is about 80 %. The transmittance of films slightly decreased with Yb_2O_3 doping. This could be attributed to light scattering loss effect resulting from the increased crystallite size and surface roughness of the films. Besides, the Yb_2O_3-doped TiO_2 films showed rather lower transmittance at 350-400 nm when it was compared with pure TiO_2 film. It is observed that the absorption edges of Yb_2O_3-doped TiO_2 thin films are red-shift. This shift is ascribed to the variation of the optical band gap energy of TiO_2 and Yb_2O_3-doped TiO_2.

Moreover, the Ar/O_2 ratio and Yb_2O_3 doping had played an important role on the transparency together with the shift of absorption edge of films. It was found that the absorption edge of films prepared under mixture gas (Ar/O_2:8/2) shifts to longer wavelength with markedly dropped in transmittance.

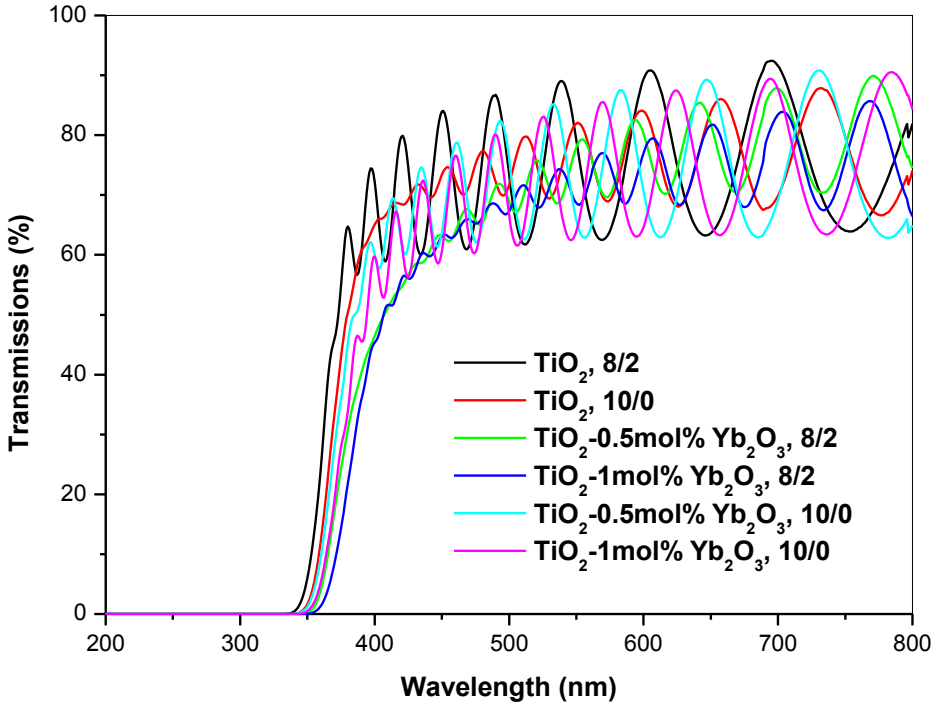

Figure 4.17 Transmittance spectra of TiO_2 and Yb_2O_3-doped TiO_2thin films prepared under different sputtering gas and doping amount of Yb_2O_3 at total sputtering pressure 3 Pa.

4.2.3.2 Optical band gap energy

Optical transmission spectra of Yb_2O_3-doped TiO_2 measured at room temperature with an excitation wavelength of 200-800 nm by a UV-Vis spectrophotometer is shown in fig 4.17. Determination of the absorption edge or energy band gap has been described in chapter 3. The tangential line at high α region of the $h\nu$ *vs* $(\alpha E)^{1/2}$ curve is extrapolated to intercept the $h\nu$ axis as shown in fig 4.18. This intercept value is defined as the energy band gap.

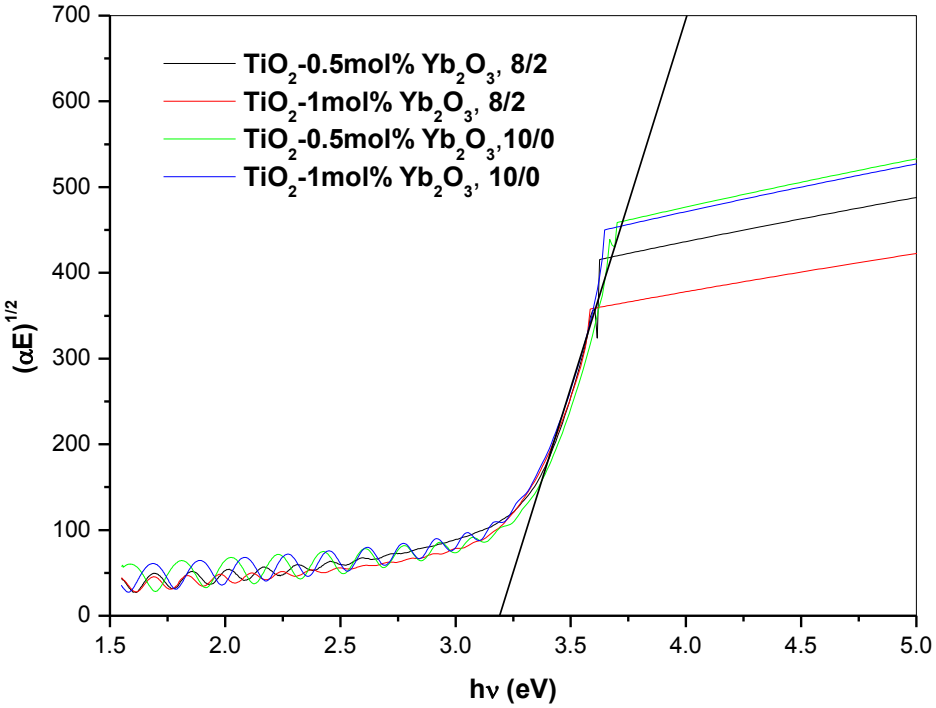

Figure 4.18 Graphs of $(\alpha E)^{1/2}$ versus photon energy, E ($h\nu$), for Yb_2O_3-doped TiO_2 films.

The energy band gap values of Yb_2O_3-doped TiO_2 thin films prepared under different Yb_2O_3 concentrations, with and without O_2 gas flow were shown in Table 4.1. The optical band gap of TiO_2 obtained in this work is about 3.19 ± 0.01 which is corresponded with general of the optical band gap of TiO_2 anatase (3.2 eV). However, the optical band gap energy of films decreased as concentration of Yb_2O_3 doping increased. Moreover, the optical band gap energy of Yb_2O_3-doped TiO_2 film was decreased when sputtered under O_2 gas flow.

Table 4.1 Band gap energy values (E_{bg}) of TiO_2 and Yb_2O_3-doped TiO_2 films

Target	Yb_2O_3 Concentrations (mol%)	Ar/O_2 ratio	Pressure	E_{bg}
TiO_2	-	10/0	3	3.20±0.01
		8/2	3	3.18±0.01
TiO_2-Yb_2O_3	0.5	10/0	3	3.17±0.02
		8/2	3	3.15±0.02
	1	10/0	3	3.15±0.01
		8/2	3	3.13±0.02

4.2.4 Photocatalytic activity

Photocatalytic activity was presented by kinetic energy; *k*. Determination of the kinetic energy (k) has been described in chapter 3. The kinetic energy of Yb_2O_3-doped TiO_2 thin films under UV and fluorescent irradiation was shown in fig 4.19-4.20, respectively.

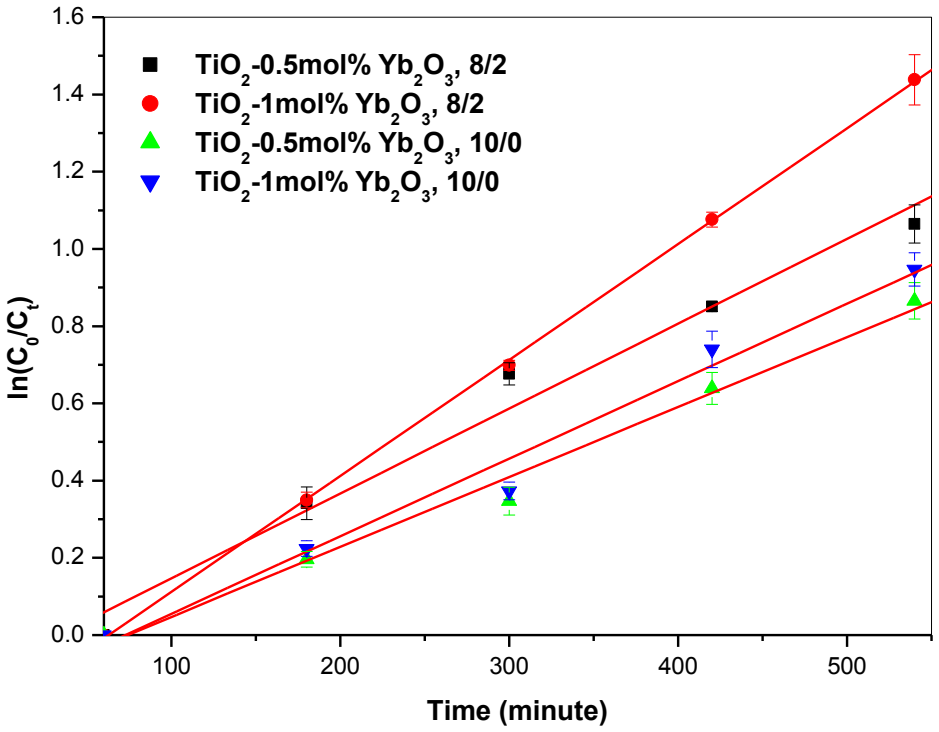

Figure 4.19 Photocatalytic degradation of methylene blue solution as a function of UV irradiation time of Yb_2O_3-doped TiO_2films prepared under different sputtering gas (Ar/O_2 and concentrations of Yb_2O_3. (■) 0.5mol%Yb_2O_3-8/2, (●) 1mol%Yb_2O_3-8/2, (▲) 0.5mol%Yb_2O_3-10/0 and (▼) 1mol%Yb_2O_3-10/0.

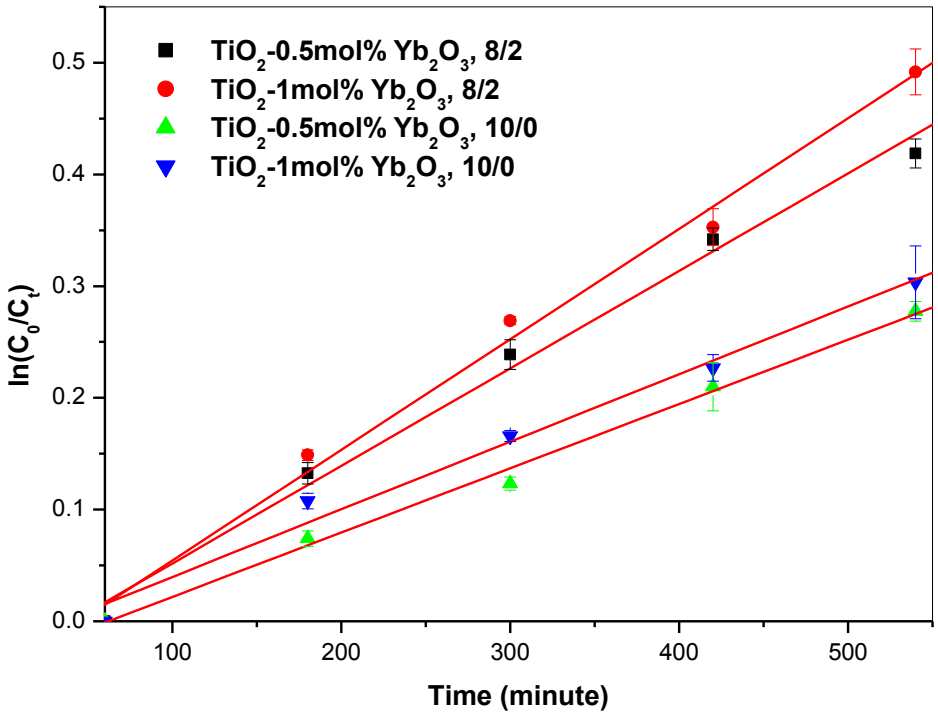

Figure 4.20 Photocatalytic degradation of methylene blue solution as a function of fluorescent irradiation time of Yb_2O_3-doped TiO_2films prepared under different sputtering gas (Ar/O_2) and concentrations of Yb_2O_3. (■) 0.5mol%Yb_2O_3-8/2, (●) 1mol%Yb_2O_3-8/2, (▲) 0.5mol%Yb_2O_3-10/0 and (▼) 1mol%Yb_2O_3-10/0.

As a result, the Yb_2O_3-doped TiO_2 films prepared with O_2 flow showed higher photocatalytic efficiency than that of film prepared under pure Ar under both UV and fluorescent irradiation. Moreover, the photocatalytic activity increased as the concentration of Yb_2O_3 increased from 0.5 to 1 mol%.

This can be suggested that the surface roughness and crystallinity had played a significant parameter influencing the photocatalytic activity. The films with high crystallinity and high surface roughness resulted in high photocatalytic activity. Because of a low degree of crystallinity would imply a great amount imperfections and defects in TiO_2 structure which could act as a recombination center for electron-hole pairs and led to lower efficiency of photocatatytic activity. While the film with higher open structure

and surface roughness would promote more number of active center for the catalytic activity.

Table 4.2 Kinetic energy of the Yb_2O_3-doped TiO_2 thin films under UV and fluorescent irradiation.

Target	Concentrations (mol%)	Ar/O_2 ratio	Pressure	*k* under UV irradiation	*k* under Fluorescent irradiation
TiO_2-Yb_2O_3	0.5	10/0	3	18.2 **X**10^{-4}	6.38 **X**10^{-4}
		8/2	3	21.5 **X**10^{-4}	8.81 **X**10^{-4}
	1	10/0	3	19.6 **X**10^{-4}	6.01 **X**10^{-4}
		8/2	3	30.5 **X**10^{-4}	9.68 **X**10^{-4}

4.3 Er_2O_3-doped TiO_2 thin films

This section shows effects of sputtering gas and amount of Er_2O_3 doping on phase structure, morphology, surface roughness, transmittance and photocatalytic activity of Er_2O_3-doped TiO_2 film.

4.3.1 Phase structure

4.1.3.3 Effects of sputtering gas, total sputtering pressure and target concentration on Er_2O_3-doped TiO_2 films

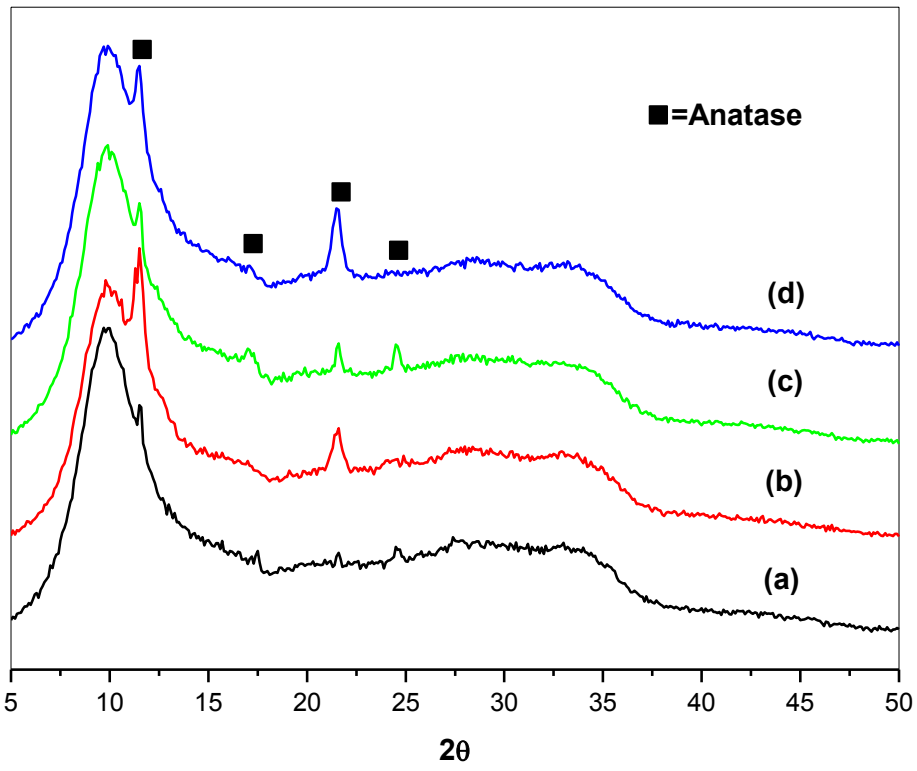

Figure 4.21 XRD patterns of TiO_2 and 1mol%Er_2O_3-doped TiO_2 (ErT) films prepared under different sputtering gas and Er_2O_3 doping. (a) TiO_2 8/2; 3 Pa (b) ErT 8/2;3 Pa (c) TiO_2 10/0;3 Pa (d) ErT 10/0; 3 Pa.

XRD patterns of Er_2O_3-doped TiO_2 thin films prepared on glass substrate under various sputtering gas and pressure, were shown in fig 4.21. It was confirmed that all of the deposited films composed of only reflection planes of anatase structure (JCPDS No. 211272) which was also observed the same results in case of using TiO_2 and TiO_2-Yb_2O_3 target. But, an apparent change in preferred orientation grown occurred when the film was sputtered at high pressure (3 Pa). For effect of Er_2O_3 concentrations, it was demonstrated that when concentration of Er_2O_3 doping in TiO_2 target increased, the crystallinity slightly decreased (fig 4.22).

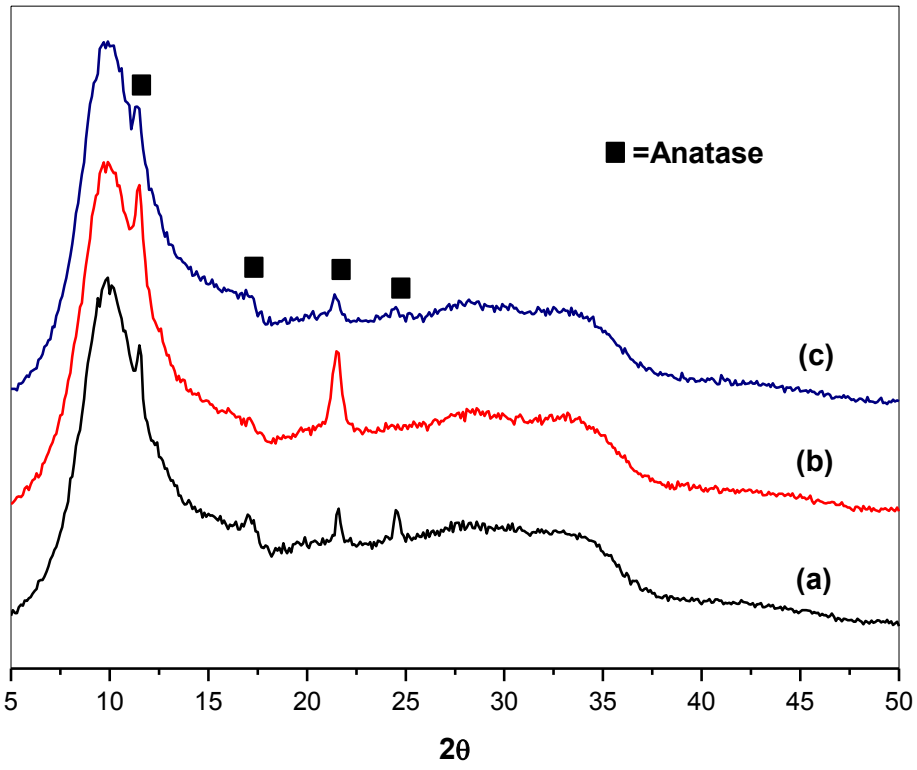

Figure 4.22 XRD patterns of TiO_2 and Er_2O_3-doped TiO_2 films prepared under Ar/O_2 at 8/2; (a) TiO_2 (b) TiO_2-0.5 mol% Er_2O_3 (c) TiO_2-1 mol% Er_2O_3.

4.3.2 Surface morphology

4.3.2.1 Filed Emission Scanning Electron Microscopy (FE-SEM).

FE-SEM images in fig 4.23 show the morphologies of Er_2O_3-doped TiO_2 thin films deposited under different Er_2O_3 concentrations and sputtering gas. It was found that the films prepared under gas mixture displayed porous structure with smaller subgrain approximately 10 nm in size, grouped together to form one large grain of 120-150 nm. The similar microstructure of 1mol% Er_2O_3-doped TiO_2 prepared under the same condition was observed. At the same time, the Er_2O_3-doped TiO_2 films prepared under pure Ar gas consisted of dense packed polycystalline grain with no gap between them and their grain size is about 120-150 nm, which is similar to that of films prepared from Yb_2O_3 –doped TiO_2 target under the same condition. Moreover, the grain size of Er_2O_3-doped TiO_2 films slightly increased with the amount of doping Er_2O_3 increased.

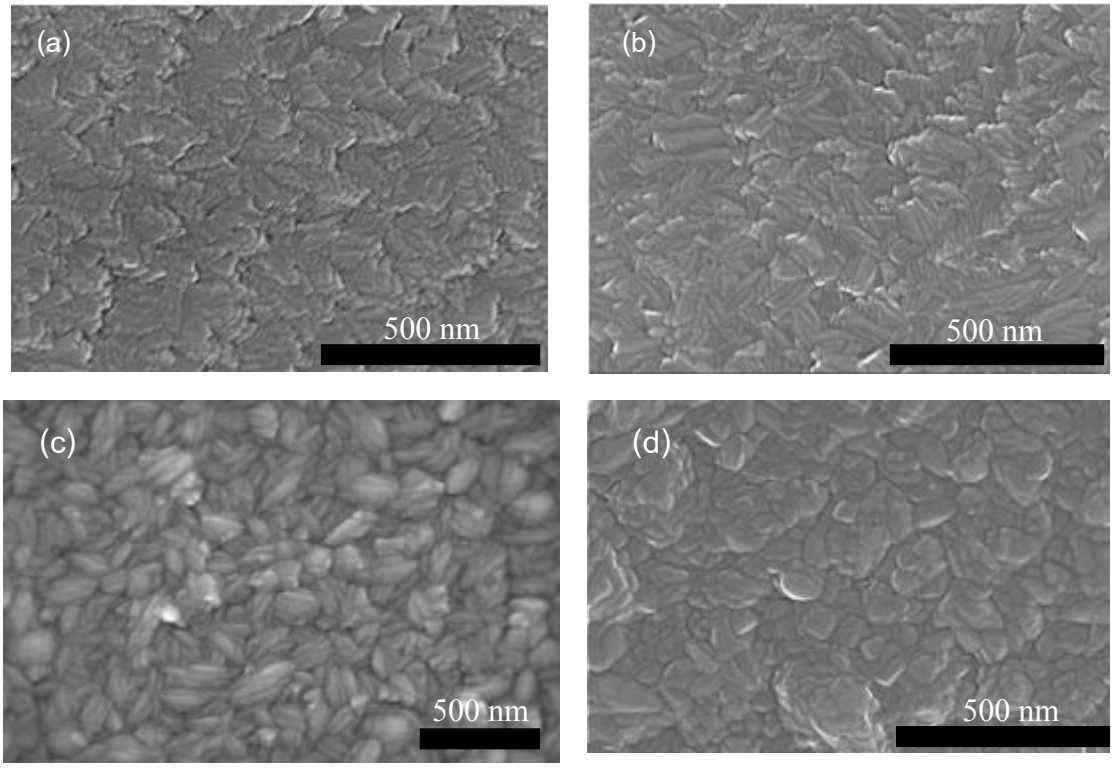

Figure 4.23 FE-SEM image of the films deposited under different sputtering gas and Er_2O_3 concentration, (a) 0.5mol% Er_2O_3: 8/2, (b) 1mol% Er_2O_3: 8/2, (c) 0.5mol% Er_2O_3: 10/0 (d) 1mol% Er_2O_3: 10/0.

4.3.2.2 Scanning Probe Microscope (SPM)

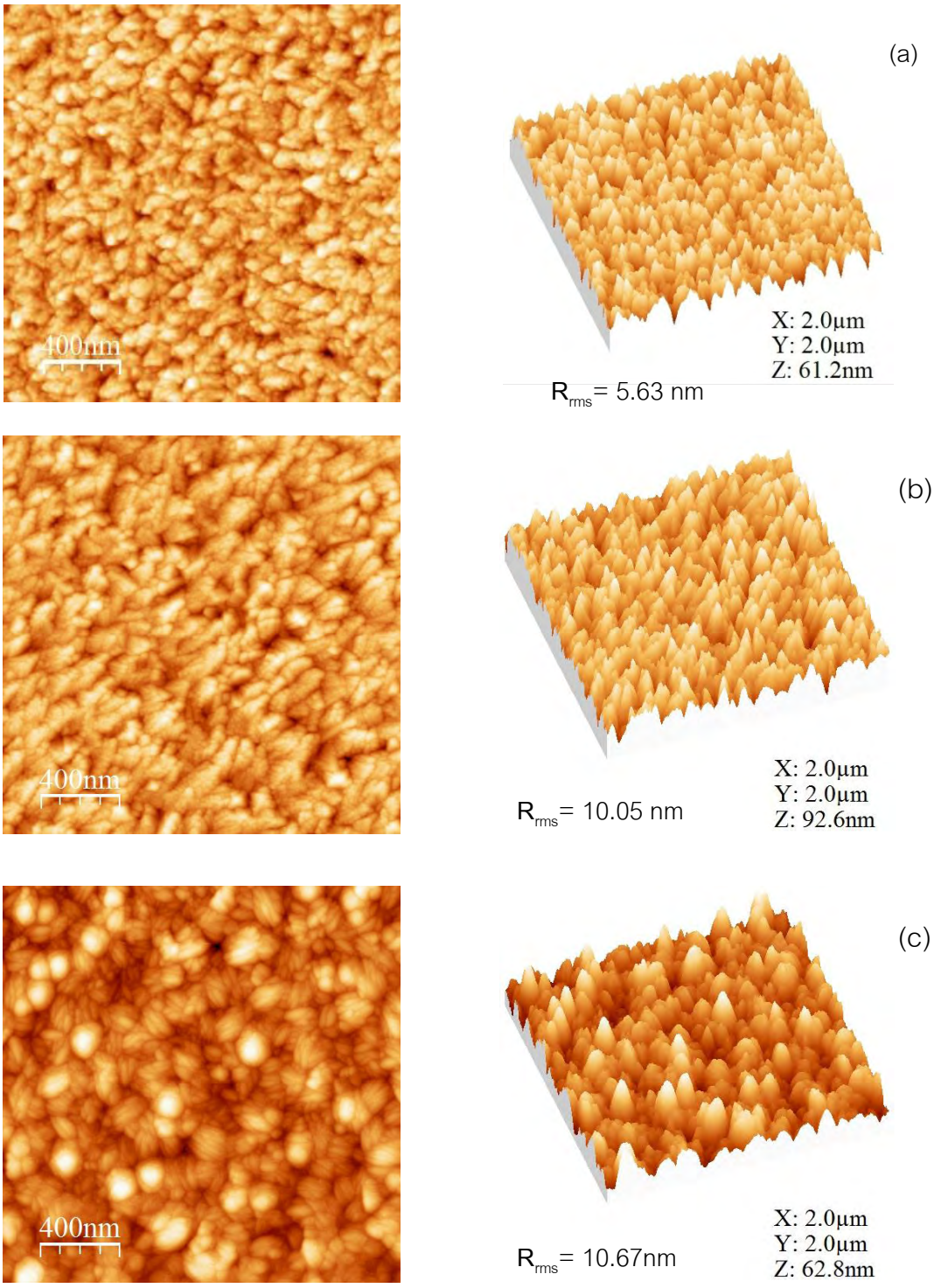

Figure 4.24 Two-dimensional and three-dimensional SPM images of (a) pure TiO_2 , (b) 0.5 mol% Er_2O_3-doped TiO_2 and (c) 1 mol% Er_2O_3-doped TiO_2 films prepared on glass substrate under Ar/O_2 at 8/2, heated at 500 ^{o}C and total sputtering pressure3 Pa.

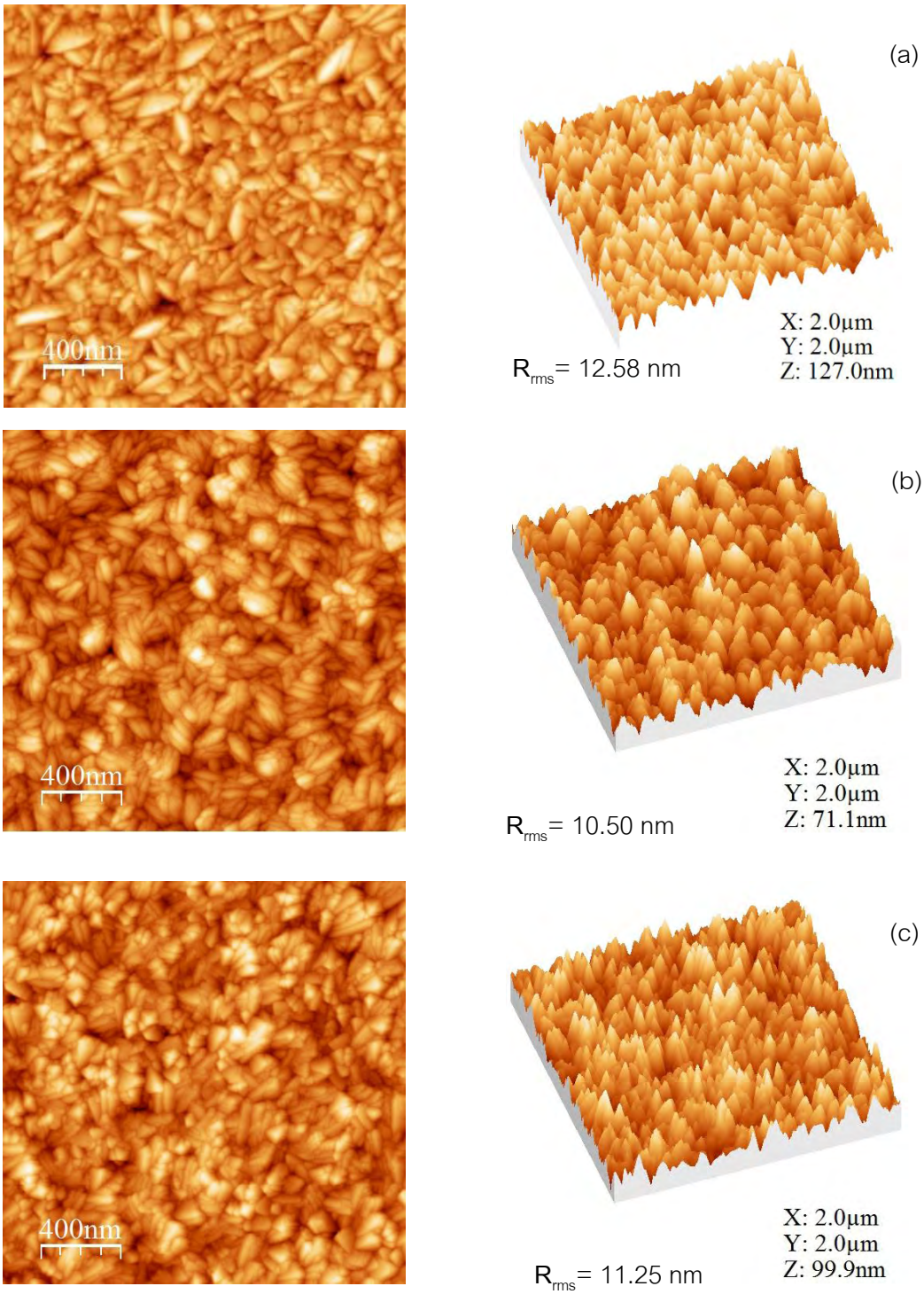

Figure 4.25 Two-dimensional and three-dimensional SPM images of (a)TiO_2 (b) 0.5mol% Er_2O_3-TiO_2 (c) 1mol% Er_2O_3-TiO_2 films prepared on glass substrate under pure Ar, heated at 500 ^{o}C and total sputtering pressure 3 Pa.

Fig 4.24 shows SPM images of Er_2O_3-doped TiO_2 thin films prepared on glass substrate under different Er_2O_3 concentrations at Ar/O_2 of 8/2. It was found that the surface roughness (R_{rms}) of films are 5.63, 10.05 and 10.67 nm for pure TiO_2, 0.5 and 1 mol%Er_2O_3-doped TiO_2 target, respectively. It was noticed that the surface roughness of films drastically increased when doping with Er_2O_3. But it cannot show the difference between doping with 0.5 and 1 mol% Er_2O_3. While, the films prepared under pure Ar gas as shown in fig 4.25 have surface roughness (R_{rms}) approximately 12.58, 10.50 and 11.25 nm for pure TiO_2, 0.5 and 1 mol%Er_2O_3-doped TiO_2 target, respectively. From the results, it was found that the surface roughness of TiO_2 films had not significantly affect by Er_2O_3 doping when sputtered under pure Ar gas. It can be assumed that surface roughness values are almost no different between doped and undoped films.

4.3.3 Optical properties

This part shows effects of Er_2O_3-doping on optical properties of TiO_2 films, which consisted of Transmittance and optical band gab energy characterized by UV-vis spectroscopy and “Tauc’s plot” method.

4.3.3.1 Transmittance

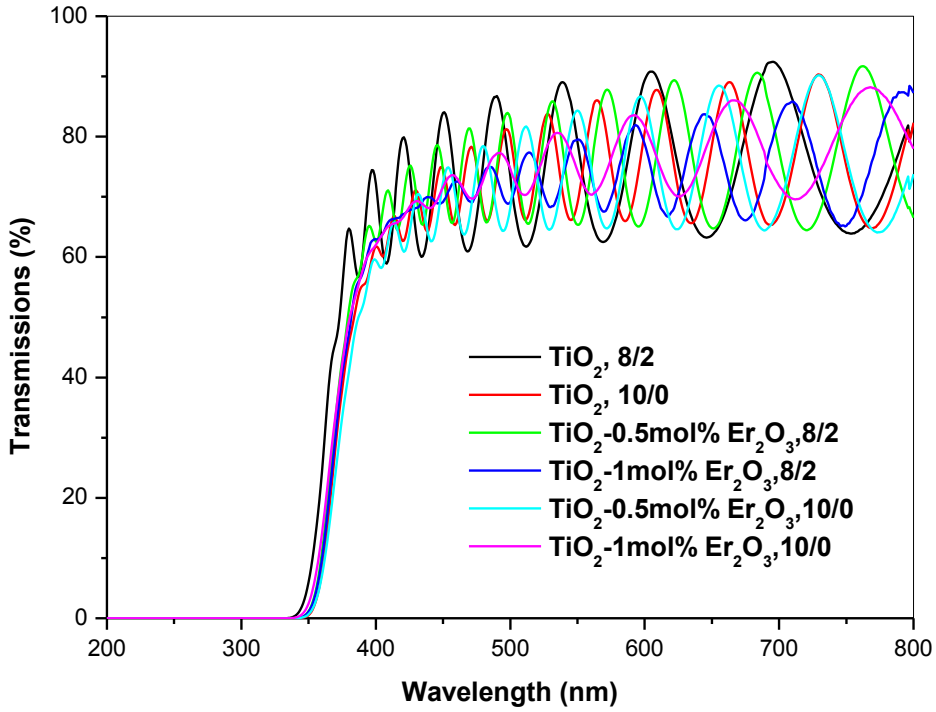

Figure 4.26 Transmittance spectra of TiO_2 and Er_2O_3-doped TiO_2 films prepared under different sputtering gas and doping amount of Er_2O_3 at total sputtering pressure 3 Pa.

The transmittance spectra of Er_2O_3-doped TiO_2 thin films deposited under various Er_2O_3 concentrations and sputtering gas were shown in fig 4.26. It was seen that all spectra show the normal light interference pattern in visible region. In addition, the interference pattern depends on the films thickness. The Er_2O_3-doped TiO_2 films deposited under all of different target concentrations and sputtering gas have high transparency as the average transmittance of films in visible region shown in fig 4.26 is about 70-80 %. While the films prepared by doping with Er_2O_3 displayed clearly drop in the transmittance of film with slightly red shifted into the longer wavelength. A decrease in optical transmittance is resulted from the increase an adsorption in the visible region.

It was suggested that, the sputtering gas and Er_2O_3 doping had played an important role on the transparency together with the shift of absorption edge of films.

4.3.3.2 Optical band gap energy

Optical transmission spectra of Er_2O_3-doped TiO_2 films measured at room temperature with an excitation wavelength of 200-800 nm by a UV-vis spectrophotometer were shown in fig.4-26. Determination of the absorption edge or energy band gap has been described in chapter 3. The tangential line at high α region of the $h\nu$ *vs* $(\alpha E)^{1/2}$ curve is extrapolated to intercept the $h\nu$ axis as shown in fig.4-27. This intercept value is defined as the energy band gap.

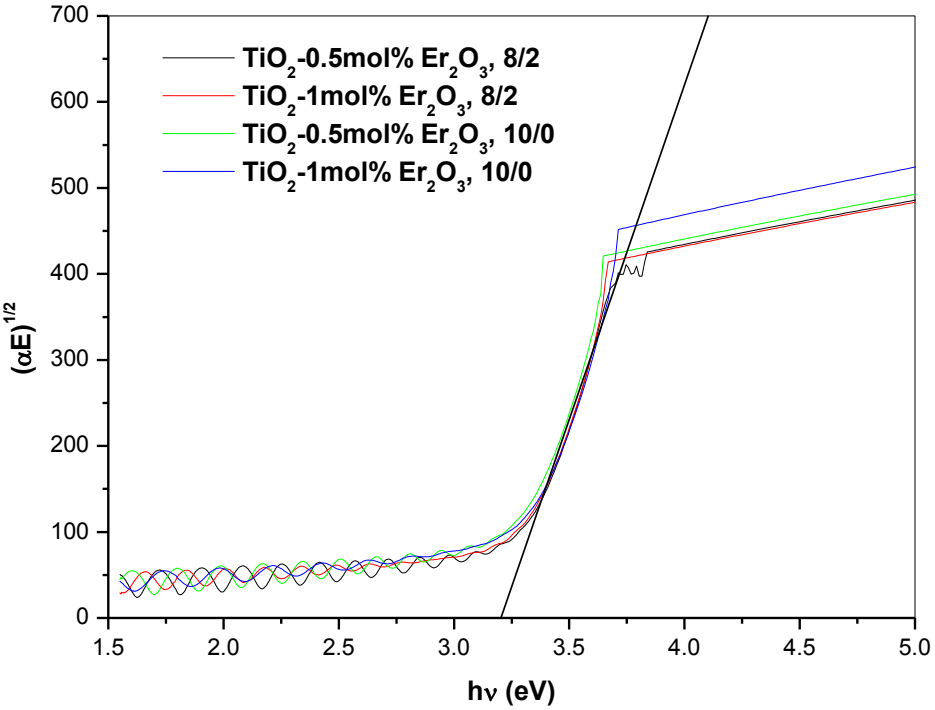

Figure 4.27 Graphs of $(\alpha E)^{1/2}$ versus photon energy, E ($h\nu$) of Er_2O_3-doped TiO_2 films.

The energy band gap values of Er_2O_3 –doped TiO_2 thin films prepared under difference Er_2O_3 concentration and Ar/O_2 gas were shown in Table 4.3. The energy band gap of TiO_2 in this work is about 3.19±.0.01 eV corresponding to the general TiO_2 anatase (3.2 eV). It was obtained that the energy band gap value of films prepared under mixture of Ar/O_2 gas are lower than that of films prepared under pure Ar gas.

Moreover, the energy band gap values of Er_2O_3-doped TiO_2 films decreased as the concentrations of Er_2O_3 increased.

Table 4.3 Band gab energy values (E_{bg}) of TiO_2 and Er_2O_3-doped TiO_2 films

Target	Concentrations (mol%)	Ar/O_2 ratio	Pressure (Pa)	E_{bg} (eV)
TiO_2	-	10/0	3	3.20±0.01
		8/2	3	3.19±0.01
TiO_2-Er_2O_3	0.5	10/0	3	3.18±0.02
		8/2	3	3.17±0.01
	1	10/0	3	3.17±0.02
		8/2	3	3.15±0.02

4.3.4 Photocatalytic activity

This section shows effects of sputtering Ar/O_2 gas and amount Er_2O_3 doping on photocatalytic activcity of TiO_2 film displayed by kinetic energy, *k*. Determination of the kinetic energy (k) has been described in chapter 3.

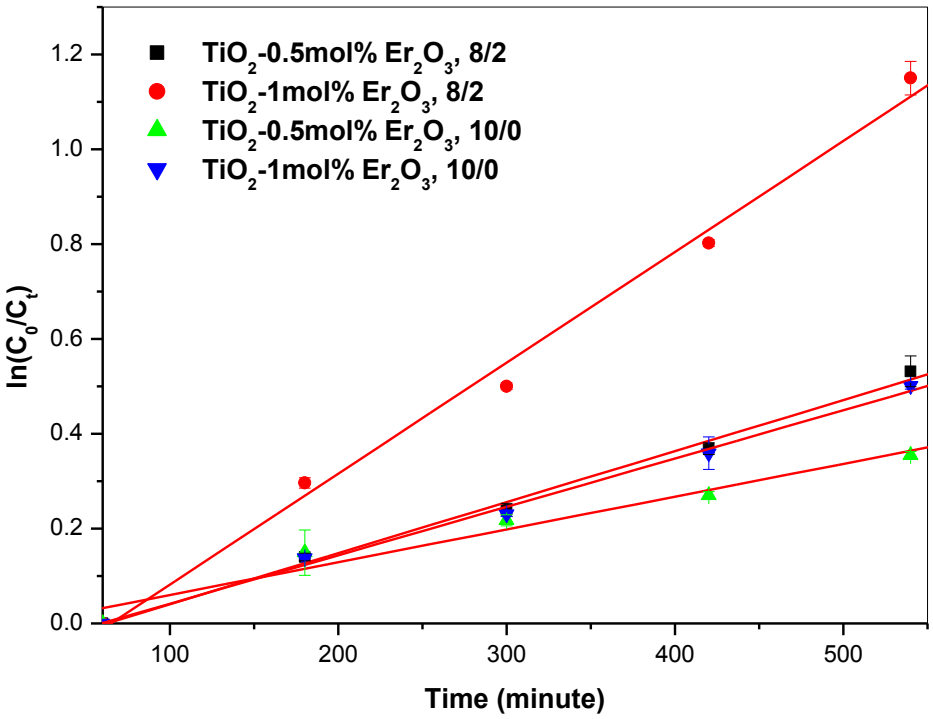

Figure 4.28 Photocatalytic degradation of methylene blue solution as a function of UV irradiation time of Er_2O_3-doped TiO_2 films prepared under different sputtering gas (Ar/O_2) and concentrations of Er_2O_3. (■) 0.5mol%Er_2O_3-10/0, (●) 1mol%Er_2O_3-10/0, (▲) 0.5mol%Er_2O_3-8/2 and (▼) 1mol%Er_2O_3-8/2.

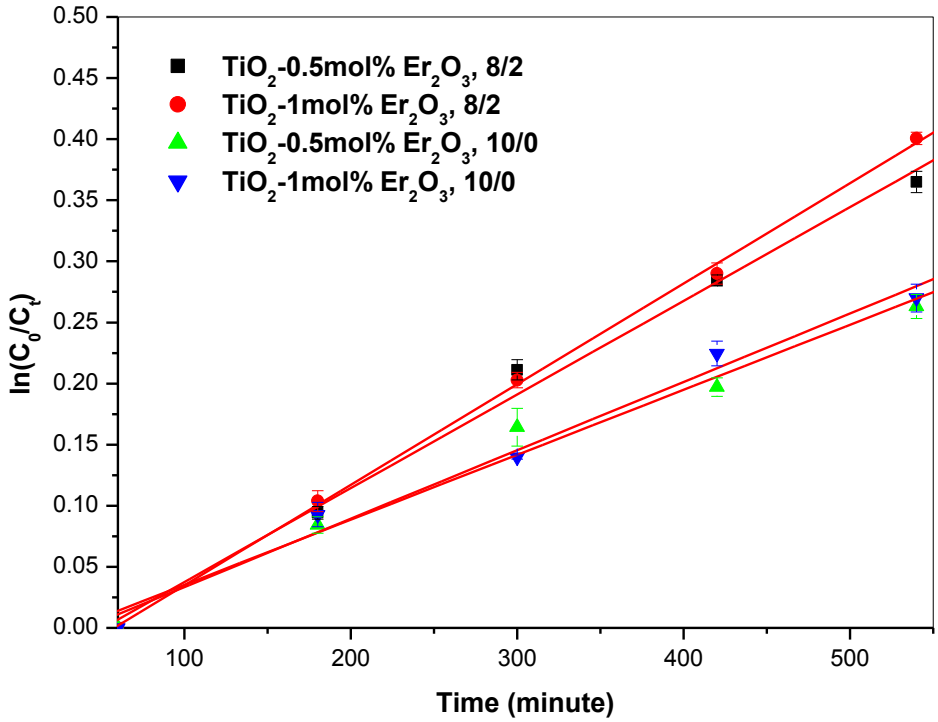

Figure 4.29 Photocatalytic degradation of methylene blue solution as a function of fluorescent irradiation time of Er_2O_3-doped TiO_2 films prepared under different sputtering gas (Ar/O_2) and concentrations of Er_2O_3. (■) 0.5mol%Yb_2O_3-10/0, (●) 1mol%Yb_2O_3-10/0, (▲) 0.5mol%Yb_2O_3-8/2 and (▼) 1mol%Yb_2O_3-8/2.

The results of photocatalytic activity under UV and fluorescent irradiation of films prepared from different targets and sputtering gas show that the efficiency of Er_2O_3 -doped TiO_2 films prepared under gas mixture (Ar/O_2:8/2) was higher than that of film prepared under pure Ar gas as shown in fig. 4.28 and 4.29. The efficiency of films prepared under Ar/O_2 (8/2) was strongly affected by concentration of Er_2O_3, in that higher amount of Er_2O_3 doping resulting in higher photocatalytic activity. While, the doping amount of Er_2O_3 had less effect on photocatalytic efficiency of films prepared under pure Ar gas.

Table 4.4 Kinetic energy of the Er_2O_3-doped TiO_2 thin films under UV and fluorescent irradiation.

Target	Concentrations (mol%)	Ar/O_2 ratio	Pressure	k under UV irradiation	k under Fluorescent irradiation
TiO_2-Er_2O_3	0.5	10/0	3	6.89 **X**10^{-4}	5.32 **X**10^{-4}
		8/2	3	10.67 **X**10^{-4}	7.69 **X**10^{-4}
	1	10/0	3	9.96 **X**10^{-4}	5.59 **X**10^{-4}
		8/2	3	23.1 **X**10^{-4}	8.23 **X**10^{-4}

CHAPTER V

CONCLUSION AND RECOMMEDATION

5.1 Conclusions

1. TiO_2 and Yb_2O_3/Er_2O_3-doped TiO_2 films showing photocatalytic activity under UV and fluorescent irradiation of methylene blue solution have been successfully fabricated by means of RF-magnetron sputtering method

2. The total sputtering pressure had played an important role on the surface morphology of TiO_2 deposited films. At high pressure (3 Pa), the film displayed porous structure with higher surface roughness resulted in higher photocatalytic activity. The sputtering gas, with and without O_2 flow, had shown an effect on the surface morphology and optical property of deposited films, which in turn had an influence on their photocatalytic activity. The film prepared under pure Ar had finer grain structure with higher surface roughness, resulting in higher photocatalytic activity than that of film prepared under gas mixture of Ar/O_2 (8/2).

3. The crystallinity and surface roughness of Yb_2O_3/Er_2O_3- doped TiO_2 films are significantly affected by sputtered gas. The doped TiO_2 films prepared under mixture of Ar/O_2 (8/2) gas had fine grain structure with high surface roughness, resulting in high photocatalytic activity.

4. The absorption thresholds for the Yb_2O_3/Er_2O_3 doped films slightly shifted to longer wavelength compared with the TiO_2 films which was attributed to the decrease in its energy band gap. The increasing in the amount of Yb_2O_3/Er_2O_3 dopant from 0.5 to 1 mol% resulted in the increasing in photocatalytic activity under UV and fluorescent light irradiation.

5. From this study, doping TiO_2 with Yb_2O_3 or Er_2O_3 did not show an improvement in photocatalytic activity of TiO_2 films. The optimal conditions for doping film should be carried out.

5.2 Recommendations

The recommendations for further study should be carried on finding optimal doping concentration and surface modification of TiO_2 to enhance its photocatalysis efficiency by reducing recombination of photo generated electrons and holes and to improve its photocatalytic activity under UV and Fluorescent irradiation.

REFERENCES

[1] Fujishima, A., Rao, T. N., and Tryk, D. A. Titanium dioxide photocatalysis. Journal of Photochemistry and Photobiology C: Photochemistry Reviews 1 (2000): 1-21.

[2] Anpo, M., and Takeuchi, M. The design and development of highly reactive titanium oxide photocatalysts operating under visible light irradiation. Journal of Catalysis 216 (2003): 505-516.

[3] Zhao, G., Kozuka, H., and Yoko, T. Effects of the incorporation of silver and gold nanoparticles on the photoanodic properties of rose bengal sensitized TiO_2 film electrodes prepared by sol-gel method. Solar Energy Materials and Solar Cells 46 (1997): 219-231.

[4] Martin, N., Rousselot, C., Rondot, D., Palmino, F., and Mercier, R. Microstructure modification of amorphous titanium oxide thin films during annealing treatment. Thin Solid Films 300 (1997): 113-121.

[5] Lapostolle, F., Billard, A., Stebut, J. v. Structurermechanical properties relationship of titanium-oxygen coatings reactively sputter-depositedq. Surface and Coatings Technology 135 (2000): 1-7.

[6] Martin, N., Rousselot, C., Savall, C., and Palmino, F. Characterizations of titanium oxide films prepared by radio frequency magnetron sputtering. Thin Solid Films 287 (1996): 154-163.

[7] Murakami, N., Chiyoya, T., Tsubota, T., and Ohno, T. Switching redox site of photocatalytic reaction on titanium(IV) oxide particles modified with transition-metal ion controlled by irradiation wavelength. Applied Catalysis A: General 348 (2008): 148-152.

[8] Carneiro, J. O., et al. Study of the deposition parameters and Fe-dopant effect in the photocatalytic activity of TiO_2 films prepared by dc reactive magnetron sputtering. Vacuum 78 (2005): 37-46.

[9] Bellardita, M., Addamo, M., Di Paola, A., and Palmisano, L. Photocatalytic behaviour of metal-loaded TiO2 aqueous dispersions and films. Chemical Physics 339 (2007): 94-103.

[10] Liang, C. H., Li, F. B., Liu, C. S., Lu, H. L., and Wang, X. G. The enhancement of adsorption and photocatalytic activity of rare earth ions doped TiO_2 for the degradation of Orange I. Dyes and Pigments 76 (2008): 477-484.

[11] Liang, C. H., et al. The effect of erbium on the adsorption and photodegradation of orange I in aqueous Er3+-TiO_2 suspension. Journal of Hazardous Materials 138 (2006): 471-478.

[12] Fujishima, A., Hashimoto, K., and Wanatabe, T. TiO_2 Photocatalyst Fundamentals and Application. Tokyo, Japan: BKC Inc., 1999.

[13] Pholporthon .S, Life cycle assessment of synthesizing titanium dioxide nanoparticles. The Degree of Master of Engineering Program, Department of Chemical Engineering Faculty of Engineering Chulalongkorn University, 2006.

[14] Wold, A. Photocatalytic Properties of $Ti0_2$. Chem. Mater 5 (1993): 280-283.

[15] Chutiphunphinyo .U, Synthesis of nanosized anatase particles from commercial rutile powder. The Degree of Master of Science Program, Department of Materials Science Faculty of Science Chulalongkorn University, 2007.

[16] Miao, l., Tanemura, S., Kondo, Y., and Iwata, M. Microstructure and bactericidal ability of photocatalytic TiO_2 thin films prepared by rf helicon magnetron sputtering. Applied Surface Science 238 (2004): 125-131.

[17] Fujishima, A, and Zhang, X., Titanium dioxide photocatalysis: present situation and future approaches. C.R. Chimie, 9 (2006): 750-760

[18] Seethawong, T. Titanium dioxide[Online]. 2008. Available from: http://www.vcharkarn.com/varticle/27809 [2010, September 15].

[19] Dangsranoi .P, Photocatalytic oxidation of organic compounds in wastewater. The Degree of Master of Science, Program Department of Chemical Technology Faculty of Science Chulalongkorn University, 2005.

[20] Mori, K., Photo-Functionalized Materials Using Nanoparticles: Photocatalysis. J. Soc. Powder Technology, 41 (2004): 750-756.

[21] Kosasang, O. Proton conductivity in Y-doped Barium Ziconate for intermediate temperature direct ethanol fuel cell. Master's Thesis, Department of Materials Science Faculty of Science, Thailand, Chulalongkorn University, 2009.

[22] Vossen, J. L., and Kern, W. Thin Films Process II. United Kingdom: ACDEMIC PRESS, INC., 1991.

[23] Spencer, R. Sputter deposition of thin film[Online]. 2002. Available from: http://www.alacritas-consulting.com [2010, October 3]

[24] Zeman, R., and Takabayashi, S. Effect of total and oxygen partial pressures on structure of photocatalytic TiO_2 films sputtered on unheated substrate. Surface & Coatings Technology 153 (2002): 93-99.

[25] Yamagishi, M., Kuriki, S., Song, P. K., and Shigesato, Y. Thin film TiO_2 photocatalyst deposited by reactive magnetron sputtering. Thin Solid Films 442 (2003): 227-231

[26] Zeman, P., and Takabayashi, S. Nano-scaled photocatalytic TiO_2 thin films prepared by magnetron sputtering. Thin Solid Films 433 (2003): 57-62.

[27] Takamura, K., Abe, Y., and Sasaki, K. Influence of oxygen flow ratio on the oxidation of Ti target and the formation process of TiO_2 films by reactive sputtering. Vacuum 74 (2004): 397-401.

[28] Kim, S. C., Heo, M. C., and Hahn, S. H. Photocatalytic Activity of Pd-Doped TiO_2 Thin Films by Using a RF Magnetron Co-Sputtering Method. Journal of the Korean Physical Society 47 (2005): 700-704.

[29] Meng, F., and Sun, Z. A mechanism for enhanced hydrophilicity of silver nanoparticles modified TiO_2 thin films deposited by RF magnetron sputtering. Applied Surface Science 255 (2009): 6715-6720.

[30] Paola, A. D., et al. Preparation of Sm-loaded brookite TiO_2 photocatalysts. Catalysis Today (2011).

[31] Stengl, V., Bakardjieva, S., and Murafa, N. Preparation and photocatalytic activity of rare earth doped TiO_2 nanoparticles. Materials Chemistry and Physics 114 (2009): 217-226.

[32] Chen, W., Hua, D., ying, T. J., and mei, Z. J. Photocatalytic activity enhancing for TiO_2 photocatalyst by doping with La. Transactions of Nonferrous Metals Society of China 16 (2006): s728-s731.

[33] Jiang, H. Q., Wang, P., Guo, X. L., and Xian, H. Z. Preparation and characterization of low-amount Yb^{3+}-doped TiO_2 photocatalyst. Russian Chemical Bulletin 55 (2006): 1743-1747.

[34] Pal, M., Pal, U., Gonzalez, R. S., Mora, E. S., and Santiago, P. Synthesis and Photocatalytic Activity of Yb Doped TiO_2 Nanoparticles under Visible Light. Journal of Nano Research 5 (2009): 193-200.

[35] Yang, Y., et al. Electrospun Er:TiO_2 nanofibrous films as effcient photocatalysts under solar simulated light. Materials Letters 64 (2010).

[36] Manos, D. Lab Equipment and Apparatus - Surface Characterization Lab II (L121[Online]. 2005. Available from: http://www.jlab.org/ARC/WM/121/NewDektak.html [2010, December 10]

[37] PAWLEY, J. The Development of Field-Emission Scanning Electron Microscopy for Imaging Biological Surfaces. Scanning 19 (1997): 324-336.

[38] Kalinin, S. V., Gruverman, A., Scanning Probe Microscopy of Functional Materials: Nanoscale Imaging and Spectroscopy, in USA, Spri-nger, 2010.

[39] Dios, A. C. d. Introduction to the U-2001 UV/Visible Spectrophotometer[Online]. 1996-2008. Available from: http://bouman.chem.georgetown.edu/S00/handout/spectrometer.html [2011, January 20]

[40] Mardare, D., Tasca, M., Delibas, M., and Rusu, G. I. On the structural properties and optical transmittance of TiO_2 r.f. sputtered thin films. Applied Surface Science 156 (2000): 200-206.

[41] Meng, F., Song, X., and Sun, Z. Photocatalytic activity of TiO_2 thin films deposited by RF magnetron sputtering. Vacuum 83 (2009): 1147-1151.

[42] Wang, T. M., Zheng, S. K., Hao, W. C., and Wang, C. Studies on photocatalytic activity and transmittance spectra of TiO_2 thin films prepared by r.f. magnetron sputtering method. Surface & Coatings Technology 155 (2002): 141-145.

[43] Wang, S. F., Hsu, Y. F., and Lee, Y. S. Microstructural evolution and optical properties of doped TiO_2 films prepared by RF magnetron sputtering. Ceramics International 32 (2006): 121-125.

[44] Hossain, M. F., Biswas, S., Takahashi, T., Kubota, Y., and Fujishima, A. Influence of direct current power on the photocatalytic activity of facing target sputtered TiO_2 thin films. Thin Solid Films 517 (2008): 1091-1095.

[45] Goodge, J. Electron probe micro-analyzer (EPMA)[Online]. 2007. Available from: http://serc.carleton.edu/research_education/geochemsheets/techniques/EPMA.html [2011, January 20]

[46] Lee, D. Y., Lee, J. R., Kim, D. G., Lee, G. H., and Song, P. K. Study of Ga-Doped ZnO films deposited on PET substrates by DC magnetron sputtering. Journal of Ceramic Processing Research 9 (2008): 638-642.

[47] KON, M., SONG, P. K., MITSUI, A., and SHIGESATO, Y. Crystallinity of Gallium-Doped Zinc Oxide Films Deposited by DC Magnetron Sputtering Using Ar, Ne or Kr Gas. The Japan Society of Applied Physics 41 (2002): 6174-6179.

[48] FUKAMI, T., NARUOKA, T., MOMOSE, T., and BAMBA, N. Effects of Sputtering Atmosphere Oxygen Pressure on Photocatalytic Phenomena in Anatase Films. The Japan Society of Applied Physics 41 (2002): L794-L796.

[49] Lin, Z., Lv, L., and Qiu, J. Effect of Ar/O_2 gas flow ratio on photocatalytic activity of TiO_2 films prepared by DC magnetron sputtering. (2007): 272-273.

[50] NOGUCHI, D., KAWAMATA, Y., and NAGATOMO, T. Effects of Sputtered High-Energy Particles on the Structure and Photocatalytic Performance of TiO_2 Films Prepared by a DC Reactive Sputtering Method. Japanese Journal of Applied Physics 43 (2004): 4351-4355.

APPENDICES

APPENDIX A

Electron Probe Micro-Analysis (EPMA)

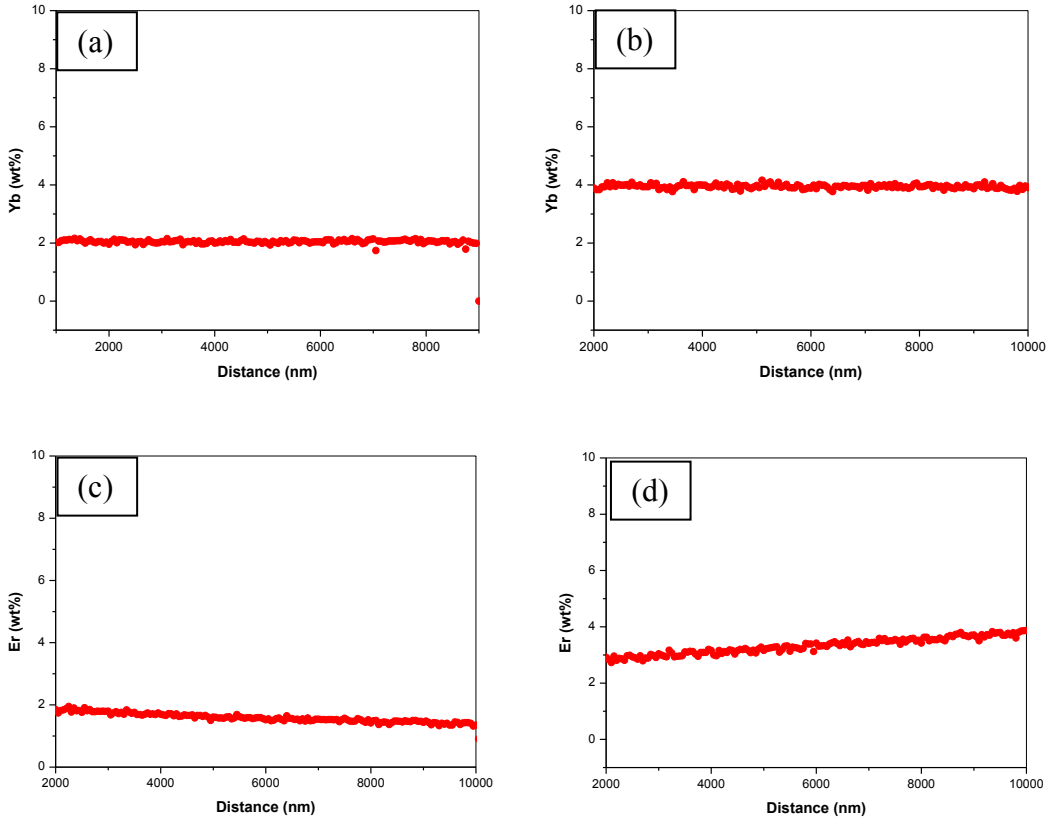

Figure A:1 The Electron Probe Micro-Analysis (EPMA) of sputtred films. (a) TiO_2-0.5 mol% Yb_2O_3 (b) TiO_2-1 mol% Yb_2O_3 (c) TiO_2-0.5 mol% Er_2O_3 (d) TiO_2-1 mol% Er_2O_3 target.

APPENDIX B

JCPDS

B:1 JCPDS of Anatase phase (JCPDS No. 211272)

00-021-1272 Quality = *

Wavelength=0.7093

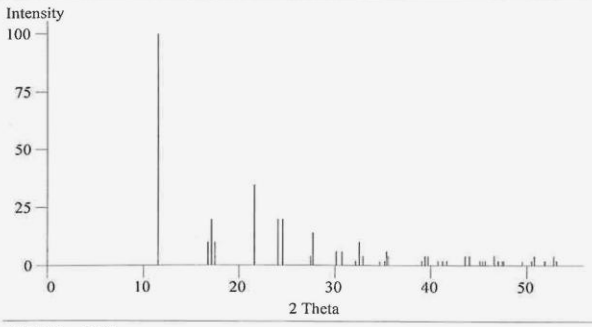

dÅ	2θ	Int	h	k	l
3.5200	11.5651	100	1	0	1
2.4310	16.7772	10	1	0	3
2.3780	17.1539	20	0	0	4
2.3320	17.4949	10	1	1	2
1.8920	21.6077	35	2	0	0
1.6999	24.0842	20	1	0	5
1.6665	24.5743	20	2	1	1
1.4930	27.4830	4	2	1	3
1.4808	27.7139	14	2	0	4
1.3641	30.1387	6	1	1	6
1.3378	30.7457	6	2	2	0
1.2795	32.1838	<2	1	0	7
1.2649	32.5655	10	2	1	5
1.2509	32.9403	4	3	0	1
1.1894	34.6961	<2	0	0	8
1.1725	35.2124	2	3	0	3
1.1664	35.4027	6	2	2	4
1.1608	35.5792	4	3	1	2
1.0600	39.0935	2	2	1	7
1.0517	39.4147	4	3	0	5
1.0436	39.7334	4	3	2	1
1.0182	40.7681	2	1	0	9
1.0070	41.2420	2	2	0	8
0.9967	41.6879	2	3	2	3
0.9555	43.5752	4	3	1	6
0.9464	44.0160	4	4	0	0
0.9246	45.1101	<2	3	0	7
0.9192	45.3899	2	3	2	5
0.9138	45.6732	2	4	1	1
0.8966	46.6005	4	2	1	9
0.8890	47.0228	2	2	2	8
0.8819	47.4245	<2	4	1	3
0.8793	47.5733	2	4	0	4
0.8464	49.5442	2	4	2	0
0.8308	50.5392	<2	3	2	7
0.8268	50.8010	4	4	1	5
0.8102	51.9185	2	3	0	9
0.7974	52.8157	4	4	2	4
0.7928	53.1461	2	0	0	12

Formula TiO_2

Name Titanium Oxide

Mineral Name Anatase, syn

Also Called anatase

Rad. λ Filter d-sp

Cut off Int. I/Icor. 3.3

Ref. Natl. Bur. Stand. (U.S.) Monogr. 25, 7, 82 (1969)

Camera Diameter

Author's Parameters:

Sys. Tetragonal S.G. $I4_1/amd(141)$ Aspect

a 3.7852 b c 9.5139 A C 2.5134

α β γ Z 4

Volume 136.31 mp

Ref. Ibid.

Dx 3.893 Dm SS/FOM: $F30=75(.012,35)$

R-factor: Error:

ICDD Calculated Parameters: S.G. $I4_1/amd(141)$

Cell Parameters:

a 3.785 b 3.785 c 9.514 A C 2.5136

α 90 β 90 γ 90 Z 4

Volume 136.31 Molecular Weight 79.9

Reduced Cell:

a 3.785 b 3.785 c 5.458 Volume 68.16

α 110.29 β 110.29 γ 90

CAS Number

Pearson tI12.00

Mineral Classification

Zeolite Classification

Additional Patterns: See PDF 01-071-1166. Validated by calculated pattern. Color: Colorless. General Comments: Pattern reviewed by Holzer, J., McCarthy, G., North Dakota State Univ, Fargo, North Dakota, USA, ICDD Grant-in-Aid (1990). Agrees well with experimental and calculated patterns. Polymorphism/Phase Transition: Anatase and another polymorph, brookite (orthorhombic), are converted to rutile (tetragonal) by heating above 700 C. Sample Source or Locality: Sample obtained from National Lead Co., South Amboy, New Jersey, USA. Temperature of Data Collection: Pattern taken at 298 K. Unit Cell Data Source: Powder Diffraction. Ti O2 type.

APPENDIX C

Table C:1 The films thickness of TiO_2 and Yb_2O_3/Er_2O_3-doped TiO_2

Target	Ar/O_2	Presure (Pa)	Films thickness (μm) (Average)	STDEV
TiO_2	10/0	3	1.08	± 0.08
		1	1.12	±0.03
	8/2	3	0.94	±0.04
		1	1.06	±0.05
TiO_2-0.5mol% Yb_2O_3	10/0	3	1.04	±0.09
		1	1.21	±0.01
	8/2	3	1.05	±0.05
		1	1.26	±0.05
TiO_2-1mol% Yb_2O_3	10/0	3	1.01	±0.03
		1	1.24	±0.05
	8/2	3	1.07	±0.04
		1	1.13	±0.02
TiO_2-0.5mol% Er_2O_3	10/0	3	1.03	±0.10
		1	1.23	±0.04
	8/2	3	1.05	±0.09
		1	1.10	±0.03
TiO_2-1mol% Er_2O_3	10/0	3	1.02	±0.05
		1	1.25	±0.04
	8/2	3	1.07	±0.07
		1	1.13	±0.02

APPENDIX D

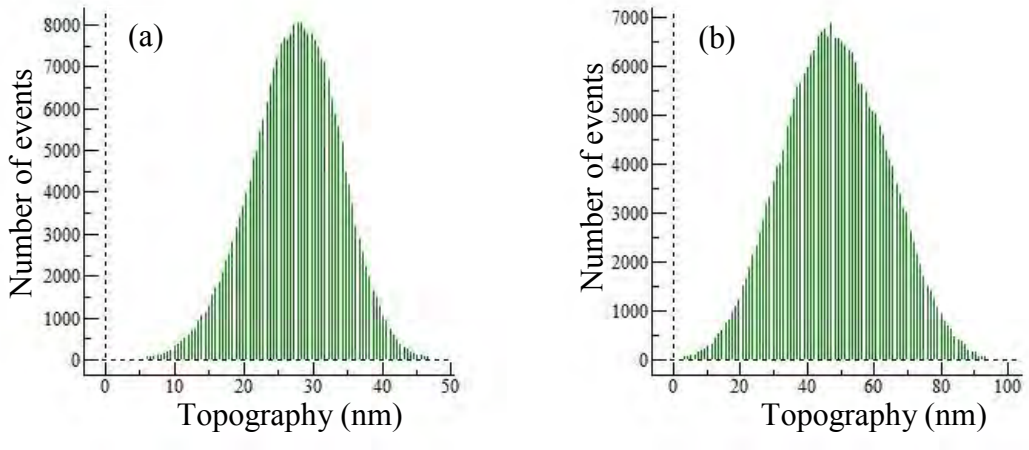

Figure:D-1 Histogram of surface roughness of TiO_2 thin films (a) 8/2 (b) 10/0

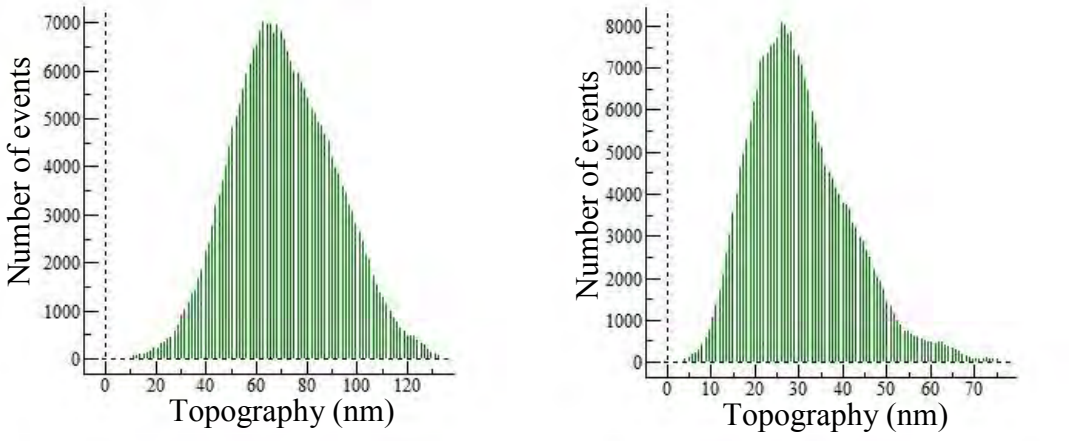

(a) 0.5mol%Yb_2O_3-doped TiO_2; 8/2 (b) 1mol%Yb_2O_3-doped TiO_2; 8/2

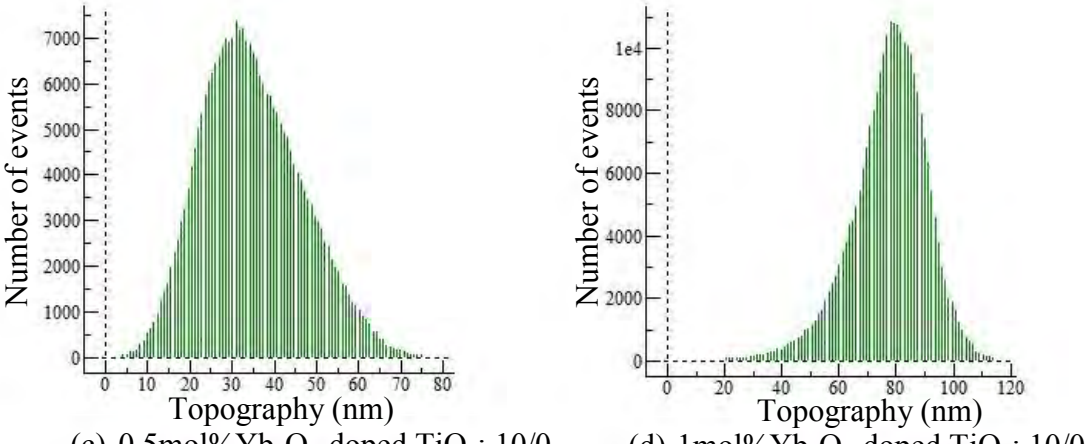

(c) 0.5mol%Yb_2O_3-doped TiO_2; 10/0 (d) 1mol%Yb_2O_3-doped TiO_2; 10/0

Figure:D-2 Histogram of surface roughness of Yb_2O_3-doped TiO_2 thin films

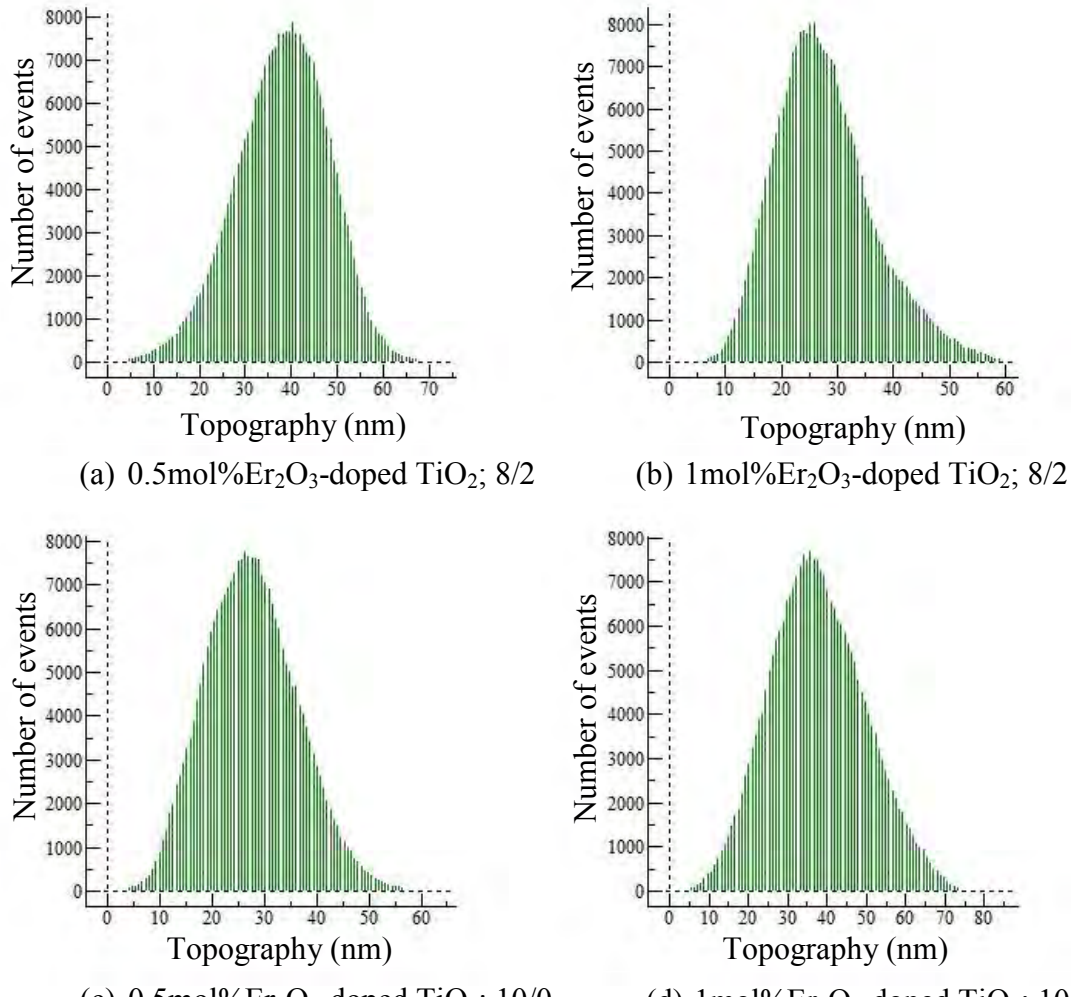

(a) 0.5mol%Er_2O_3-doped TiO_2; 8/2 (b) 1mol%Er_2O_3-doped TiO_2; 8/2

(c) 0.5mol%Er_2O_3-doped TiO_2; 10/0 (d) 1mol%Er_2O_3-doped TiO_2; 10/0

Figure:D-3 Histogram of surface roughness of Er_2O_3-doped TiO_2 thin films

VITA

Mr. Suthin Yuenyaw was born on March 19, 1985 in Khonkaen, Thailand. He has obtained the Bachelor Degree of Science in Physics from Khon Kaen University in 2007. He continued a further study in Master's degree in the field of Ceramic Technology at Chulalongkorn University and graduated in 2010.

Conference Presentations

S. Yuenyaw, K. Saito, E.H. Sekiya and P. Sudjaridworakun, "**Effect of sputtering gas on properties of Yb_2O_3-doped TiO_2 films prepared by RF magnetron sputtering**" Pure and Applied Chemistry International Conference (PACCON 2011), Miracle Grand Hotel, Bangkok, Thailand, January 5 – 7, 2011. (Oral)

S. Yuenyaw, K. Saito, E.H. Sekiya and P. Sudjaridworakun, "**Preparation and characterizations of Yb-doped TiO_2 photocatalyst films prepared by RF magnetron sputtering process**", The 3rd International Congress on Ceramics Congress (ICC3), Osaka, Japan, November 14-18, 2010. (Oral)

S. Yuenyaw, K. Saito, E.H. Sekiya and P. Sudjaridworakun, "**Influence of deposition parameter on the photocatalytic activity of TiO_2 films prepared by RF magnetron sputtering**", The 2nd Thailand-Japan International Academic Conference (TJIA 2009), Kyoto, Japan, November 20, 2009. (Poster)

Publications

S. Yuenyaw, K. Saito, E.H. Sekiya and P. Sudjaridworakun, "**Effect of sputtering gas on properties of Yb_2O_3-doped TiO_2 films prepared by RF magnetron sputtering**" Pure and Applied Chemistry International Conference (PACCON 2011), Miracle Grand Hotel, Bangkok, Thailand, January 5 – 7, 2011.(Proceeding)

S. Yuenyaw, K. Saito, E.H. Sekiya and P. Sudjaridworakun, "**Influence of deposition parameter on the photocatalytic activity of TiO_2 films prepared by RF magnetron sputtering**", The 2nd Thailand-Japan International Academic Conference (TJIA 2009), Kyoto, Japan, November 20, 2009. pp 103-104.(Proceeding)